THE UNIVERSITY OF ALBERTA

Investigations of the Chemistry of Silicate Melts: Kinetics, Structure, and Redox Equilibria

by

John Todd Dunn

A THESIS

SUBMITTED TO THE FACULTY OF GRADUATE STUDIES AND RESEARCH

IN PARTIAL FULFILMENT OF THE REQUIREMENTS FOR THE DEGREE

OF DOCTOR OF PHILOSOPHY

DEPARTMENT OF GEOLOGY

EDMONTON, ALBERTA

Spring 1983

THE UNIVERSITY OF ALBERTA

RELEASE FORM

NAME OF AUTHOR John Todd Dunn

TITLE OF THESIS Investigations of the Chemistry of Silicate Melts: Kinetics, Structure, and Redox Equilibria

DEGREE FOR WHICH THESIS WAS PRESENTED DOCTOR OF PHILOSOPHY

YEAR THIS DEGREE GRANTED Spring 1983

Permission is hereby granted to THE UNIVERSITY OF ALBERTA LIBRARY to reproduce single copies of this thesis and to lend or sell such copies for private, scholarly or scientific research purposes only.

The author reserves other publication rights, and neither the thesis nor extensive extracts from it may be printed or otherwise reproduced without the author's written permission.

(SIGNED) John T. Dunn

PERMANENT ADDRESS:

P.O. Box 398

Napavine, WA 98565

USA

DATED January 31 1983

THE UNIVERSITY OF ALBERTA

FACULTY OF GRADUATE STUDIES AND RESEARCH

The undersigned certify that they have read, and recommend to the Faculty of Graduate Studies and Research, for acceptance, a thesis entitled Investigations of the Chemistry of Silicate Melts: Kinetics, Structure, and Redox Equilibria submitted by John Todd Dunn in partial fulfilment of the requirements for the degree of DOCTOR OF PHILOSOPHY.

.....

Supervisor

.....

.....

.....

.....

External Examiner

Date.....January 27, 1983.....

Abstract

The results of investigations of the diffusion of oxygen in silicate melts, the structure of melts, and the redox equilibria in silicate melts are presented in this thesis. Five separate investigations were undertaken, all of which were directed toward gaining an understanding of the chemistry of silicate melts, and in particular the role played by oxygen in those melts.

The diffusion of oxygen was investigated in six different melt compositions. Three of the compositions were in the synthetic system diopside-anorthite. Oxygen diffusion was measured in those melts at one bar pressure by means of isotopic exchange. The diffusivities determined are similar in magnitude to divalent cation diffusivities and obey the compensation law for the diffusion of divalent cations in silicate melts. Those observations suggest that there is a significant contribution to the diffusivity of oxygen from a "cation-like" diffusion mechanism. Eyring model calculations, using the oxygen diffusion data and melt viscosity data from the literature, suggest that the size of the average diffusing species is similar to that of the SiO_4^{4-} anion.

The diffusion of oxygen was also measured in three basaltic melts (an olivine nephelinite, an alkali basalt, and a tholeiitic basalt) at various temperatures and pressures up to 21 kilobars. The diffusivities were determined by monitoring the rate of reduction of Fe^{3+} to

Fe^{2+} in the melts. The oxygen diffusivities measured are approximately the same as, or slightly greater than, divalent cation diffusivities in basaltic liquids. The diffusivity of oxygen shows an abrupt decrease in all three melts at approximately the same pressure as the change in the liquidus phase from olivine to pyroxene. The decreases in oxygen diffusivity are interpreted as being related to decreases in the proportion of O^{2-} anion in the melts during reactions which decrease the proportion of olivine building units and increase the proportion of pyroxene building units in the melt. The results suggest that oxygen diffuses principally as the O^{2-} anion in basaltic melts.

The structure of lead orthosilicate melts was investigated as a function of the thermal history of the melt by means of infrared spectroscopy. The melts were observed to become increasingly polymerized with decreasing rate of cooling and with increasing duration of isothermal soaking. The presence of silicate anions larger than SiO_4^{4-} in the melts was demonstrated, which requires that O^{2-} anions also be present. The proportion of O^{2-} anions in Pb_2SiO_4 melts depends on the thermal history. Therefore, the ratio of non-bridging oxygens to tetrahedral cations (NBO/T) also depends on thermal history.

The study of the structure of Pb_2SiO_4 melts provides direct evidence of the presence of O^{2-} anions in an orthosilicate melt. That result when combined with the implications of the diffusion studies suggests that O^{2-}

anions are present in much more polymerized melts and that the proportion of those anions in a given melt depends on the thermal history of the melt. That suggestion requires that melt models which do not incorporate O^{2-} anions be reassessed.

The two investigations of iron redox equilibria in basaltic melts provide an improved predictive equation for the oxidation of iron in natural melts and a model process which may account for the presence of reduced phases (graphite and Fe^{o}) in quenched rocks which are apparently too oxidized to allow those phases.

Acknowledgements

I wish to thank Dr. Chris Scarfe for inspiring my initial interest in silicate melts. I am grateful for his continued support and belief in me at times when I was sure nothing would ever go right again. I am greatly indebted to Dr. Karlis Muehlenbachs for getting me started in diffusion. The study of oxygen diffusion in the system diopside-anorthite would not have been possible without the many oxygen isotopic analyses Dr. Muehlenbachs did for me.

I wish to thank Dr. John Bertie, Dr. Fred Longstaffe, and Dr. Bruce Nesbitt for their advice and for serving on my committee. I am also indebted to Dr. Stewart McCallum for letting me do the controlled cooling rate experiments in his lab at the University of Washington. Dr. Dave Harris is thanked for doing the two water analyses reported in chapter 3. Finally, I wish to thank Dr. Toshi Fujii for always having the answer, no matter what question was asked.

Table of Contents

Chapter — Page

Abstract iv

Acknowledgements vii

List of Figures xi

List of Tables xiii

I. Introduction 1

A. Introductory remarks 1

B. Rationale behind the research 2

Oxygen diffusion in silicate melts 3

Effect of thermal history on melt structure 5

Iron oxidation state and oxygen activity in melts 6

II. Oxygen Diffusion in Three Silicate Melts along the Join Diopside-Anorthite 9

A. Introduction 9

B. Experimental methods 10

C. Results 16

D. Discussion 22

Compensation law 28

Comparison with the Eyring model 29

E. Conclusion 32

III. Oxygen Diffusion in Basaltic Liquids at Elevated Pressures 34

A. Introduction 34

B. Experimental 36

C. Results and Discussion 46

D. Conclusions 63

IV. The Effect of Thermal History on the Structure of Pb_2SiO_4 Melts 65

A. Introduction 65

B. Experimental 69

C. Results 73

Series one 74

Series two 74

Series three 77

Series four 79

D. Discussion 82

Series one 91

Series two, three, and four 93

E. Conclusions 97

V. The Oxidation State of Iron in Silicate Melts: New Data for Basaltic Melts 98

A. Introduction 98

B. Experimental and Analytical 99

C. Results and discussion 103

D. Applications 109

E. Conclusion 114

VI. Oxygen Activity in an Alkali Basalt as a Function of Temperature 116

A. Introduction 116

B. Experimental procedure 117

C. Results and discussion 121

D. Petrologic implications 128

E. Conclusion 130

VII. Conclusion 131

A. Summary of conclusions 131

B. Concluding remarks 133

Bibliography 134

List of Figures

1. Arrhenius plots for the composition 1, 2, and 3 data..18
2. Arrhenius plot of the composition 2 oxygen diffusion results.....21
3. Oxygen diffusion results from this study plus previous data for silicate melts.....26
4. Compensation law plot for oxygen diffusion in silicate melts.....30
5. Schematic drawing of a 1/2" piston-cylinder sample assembly.....42
6. Plot of logfO_2 *versus* P showing the position of various oxygen fugacity buffer curves.....44
7. 12 kilobar oxygen diffusion data for nephelinite and tholeiite.....49
8. 12 kilobar oxygen diffusion data for alkali basalt....50
9. 1350°C polybaric oxygen diffusivity for the nephelinite including liquidus phase equilibria.....52
10. 1400°C polybaric oxygen diffusivity for the alkali basalt including liquidus phase equilibria.....54
11. 1350°C polybaric oxygen diffusion data for 1921 Kilauea tholeiite including liquidus phase equilibria.....55
12. Infrared spectra of vitreous Pb_2SiO_4 and vitreous Fe_2SiO_4.....68
13. Infrared spectra of the series one experiments.....75
14. Infrared spectra of the series two experiments.....76
15. Infrared spectra of the series three experiments.....78
16. Infrared spectra of the series four experiments.....80

17. Smoothed infrared spectra of crystalline analogs of small silicate anions.....88
18. Infrared spectrum of vitreous SiO_2.....89
19. Synthetic and real infrared spectra of Pb_2SiO_4 melt...94
20. Calculated time required for equilibration in iron oxidation state experiments.....101
21. $ln(Fe^{3+}/Fe^{2+})$ *versus* 1/T for silicate melts at low oxygen fugacity.....111
22. $ln(Fe^{3+}/Fe^{2+})$ *versus* $\log fO_2$ for melts at 1250°C.....112
23. Experimental configuration for oxygen activity measurements in basaltic liquids.....118
24. Oxygen activity probe output as a function of time during heating and cooling.....122
25. Oxygen activity versus 1/T for a basalt melt.....123

List of Tables

1. Oxygen diffusion data for silicate melts.....10
2. Melt compositions used and other parameters.....13
3. Experimental conditions and results.....17
4. Calculated λ parameters for O^{2-} and SiO_4^{4-} as the diffusing species.....29
5. Composition of starting materials.....36
6. Volatile content of alkali basalt before and after a high pressure experiment.....44
7. Summary of experimental conditions and results.....47
8. Arrhenius parameters for the isobaric oxygen diffusion data.....51
9. Arrhenius parameters for the isothermal oxygen diffusion data.....58
10. Analyses of starting materials and experimental products.....70
11. Summary of experimental conditions and procedures.....73
12. Summary of experimental conditions and results.....104
13. Results of multiple regression analyses.....108
14. Variables ranked according to relative effectiveness.110
15. Composition of starting material for oxygen activity measurements.....119
16. Oxygen activities determined after apparent stabilization of the oxygen probe *emf*.....124

I. Introduction

A. Introductory remarks

Geologists and geochemists have been studying silicate melts for most of the twentieth century. Those studies have progressed from determinations of phase equilibria and physical properties in simple synthetic systems (e.g. Bowen, 1913 and 1915; Kozu and Kani, 1935) to investigations of melt structure (e.g. Taylor and Brown, 1979; Mysen *et al.*, 1980d; and de Jong and Brown, 1980) and the thermochemistry of silicate melts (e.g. Carmichael *et al.*, 1977; Richet and Bottinga, 1980; and Weill *et al.*, 1980). A present emphasis in the study of silicate melts is the study of kinetic phenomena (e.g. Watson, 1979; Kirkpatrick *et al.*, 1981; and Karsten *et al.*, 1982). Such studies have provided a great deal of information about the crystallization, structure and chemistry of silicate melts. However, one aspect of the study of silicate melts that has received comparatively little attention is the role played by oxygen in silicate melts.

This thesis is an attempt to fill some of the gaps in our knowledge of the behavior of oxygen in silicate melts. To that end, five more or less independent investigations were undertaken. The results of these researches are presented in chapters 2 through 6 of this thesis. Each of chapters 2 through 6 is written as an independent paper and has its own introduction and conclusions. Therefore, while

this chapter briefly describes the rationale for the study as a whole and to some extent for the individual chapters, the detailed rationale for each study is left to the beginning of that chapter. Similarly, the concluding chapter (chapter 7) is principally a summary of the individual conclusions of chapters 2 through 6.

B. Rationale behind the research

Oxygen, together with silicon and aluminum, constitutes the structural framework of all silicate melts. Oxygen accounts for more than 90% of the volume in all geological silicate melts. Furthermore, the coordination polyhedra of all the cations in a silicate melt are formed by oxygen. Highly charged cations (principally Si^{4+} and Al^{3+}) are bound to oxygen "anions" to form the silicate (or aluminosilicate) anionic units which define the structure of the melt. Other, less highly charged cations (e.g. Mg^{2+}, Ca^{2+}, Fe^{2+}, Na^{+}, and K^{+}) occupy the interstitial "sites" between the anionic units. There may also be oxygen anions (O^{2-}) occupying the interstitial "sites" as Bockris *et al.* (1948) suggested on the basis of their electrical conductivity data. However, the models presented by some workers (Mysen *et al.*, 1980a, 1980b, 1980c, 1980d, and 1981) do not allow for oxygen anions in melts with NBO/T (ratio of non-bridging oxygens to tetrahedral cations) of less than 3. Conversely, the models of melt structure presented by other workers (e.g. Masson *et al.*, 1970; Hess, 1971, 1975, and 1977; and Smart and

Glasser, 1978) require the presence of O^{2-} anions in all melts. That difference in interpretation is significant and must be resolved if the structure and chemistry of silicate melts are to be understood.

Oxygen, because it accounts for most of the volume in silicate melts, is in a unique position relative to the other constituent elements of silicate melts. The chemical and kinetic behavior of oxygen certainly affects the behavior of all other components in the melt. Consequently, investigations of the chemistry and kinetic behavior (diffusion) of oxygen in melts can provide a great deal of information about the overall chemistry and structure of those melts.

Oxygen diffusion in silicate melts

Comparison of the diffusivity of oxygen with the diffusivities of cations can provide an indirect assessment of the structural role of oxygen in melts. If oxygen diffusion is of the same magnitude as cation diffusivity it may be concluded that the mechanism of oxygen diffusion is similar to that for cations (i.e. oxygen diffuses as a free anion - O^{2-}). Similarly, if the magnitude of oxygen diffusion is close to that of the tetrahedral cations (Si^{4+} and Al^{3+}), oxygen diffusion may be linked to tetrahedral cation diffusion. In other words, oxygen diffuses by the movement of silicate (or aluminosilicate) anionic units. That implies that the oxygen in the melt is dominantly bound to the tetrahedral cations.

Oishi *et al.* (1975) and Yinnon and Cooper (1980) have observed that oxygen diffusion in silicate melts is inversely proportional to the viscosity of the melt. If that correlation is valid, models, such as that due to Eyring (Glasstone *et al.*, 1941), may be used to model the diffusing species from the combined oxygen diffusion and viscosity data.

Chapter 2 presents the results of a study of the diffusivity of oxygen in three melts along the join diopside ($CaMgSi_2O_6$) - anorthite ($CaAl_2Si_2O_8$) at one atmosphere total pressure. That system was selected for the investigation because the melts become increasingly polymerized as the anorthite composition is approached. In addition, there are good viscosity data for the system (Scarfe *et al.*, 1980). Thus, the system diopside-anorthite is ideal for an investigation of the relationships among melt structure, viscosity, and oxygen diffusivity.

Pressure can have a considerable effect on the structure of silicate melts, as has been illustrated by many workers (e.g. Waff, 1975; Kushiro *et al.*, 1976; Fujii and Kushiro, 1977; Scarfe *et al.*, 1979; Mysen *et al.*, 1980d; and Tyburczy and Waff, 1983). Because of the special position of oxygen in silicate melts (referred to above), the variation, if any, of the diffusivity of oxygen with increasing pressure should provide considerable information about the variation of the structure of silicate melts with pressure.

Chapter 3 is a study of the effect of pressure on oxygen diffusivity for three basaltic melts. The melts investigated are natural rock melts and were chosen because viscosity and phase equilibrium data were available for those or very similar compositions. Consequently, the study allows a further investigation of the apparent correlation between oxygen diffusivity and viscous flow. The study also investigates the possibility that oxygen diffusivity may reflect structural transformations in the melt as a function of pressure, which are suggested either theoretically (Waff, 1975), or by changes in the liquidus mineralogy observed for basaltic liquids (e.g. Takahashi, 1980).

Effect of thermal history on melt structure

Gotz *et al.* (1980) and Kirkpatrick *et al.* (1981) have shown that different phases can be made to crystallize from a given melt composition by varying the thermal history of the melt. Such changes imply that the structure of the melt depends on the thermal history. Therefore, an investigation of the effect of thermal history on the structure of a suitably chosen melt could provide some very useful information about the structure of the melt and could also yield some valuable insights into the role of oxygen.

Orthosilicates define an end member as far as the structures of geologically significant silicate melts are concerned. The other end member is SiO_2 melt. All geological melts fall between those two extremes. Indeed, the models put forth by Mysen and co-workers (Mysen *et al.*, 1980a,

1980b, 1980c, 1980d, 1981 and 1982b) utilize the orthosilicates as the low silica endmember. Mysen *et al.* (1982b) propose that melts with NBO/T greater than 3 contain only SiO_4^{4-} monomers, $Si_2O_7^{6-}$ dimers, and O^{2-} anions. If NBO/T is fixed for a given melt composition (as Mysen *et al.*, 1982b argue) then the relative proportions of those anions will also be fixed. The result is that the structure of the melt should be invariant. On the other hand, if NBO/T varies with variations in the thermal history of the melt then the relative proportions of the various anionic species may also change as a function of thermal history. Such a melt could contain a diverse assembly of silicate anions in contrast to the relatively simple melt envisioned by Mysen *et al.* (1982b) and would certainly have different physical properties. In any event, an orthosilicate composition melt is not likely to have a large fraction of highly polymerized silicate anions and it should be possible to identify the contributions of the various anions to the infrared spectrum of the melt. Therefore, an orthosilicate melt appears to be a good choice for an investigation of the effect of themal history on silicate melt structure. Chapter 4 reports the results of an investigation of the effect of thermal history on the structure of lead orthosilicate melts.

Iron oxidation state and oxygen activity in melts

Chapters 5 and 6 are principally concerned with applications of the oxygen diffusion data to petrologic problems. Both chapters deal with the oxidation state of

iron in silicate melts. Chapter 5 is a study of the relationship of the oxidation state of iron in melts to temperature, oxygen fugacity, and bulk composition. That study developed as an outgrowth of chapter 3, where it was necessary to determine the equilibrium oxidation state of iron in three melts at a given temperature and oxygen fugacity. Oxygen diffusion data were used to determine the required time to equilibrate the melts. Those calculations pointed out the likelihood that much of the iron oxidation state data in the literature were not equilibrium data. Consequently, the study reported in chapter 5 developed as an attempt to expand the data base for the oxidation state of iron in melts with new equilibrium data. Chapter 5 presents new iron oxidation state data for basaltic liquids and develops and discusses a predictive model.

Chapter 6 presents the results of a study of the interrelationship of redox reactions involving iron in a basaltic melt and the diffusion kinetics of oxygen. Loh *et al.* (1981) have shown that the oxygen activity in melts containing polyvalent cations varies greatly with changes of temperature. They ascribe the changes in oxygen activity to rapid redox reactions involving the polyvalent cations. The effects they observed are principally kinetic and are due to the difference in the rates of cationic redox reactions (fast) and oxygen diffusion in the melt (slow). Chapter 6 presents the results of a study of the feasibility of using an oxygen activity probe (Arculus and Delano, 1981) to

directly monitor the activity of oxygen in a basaltic melt during heating and cooling.

II. Oxygen Diffusion in Three Silicate Melts along the Join Diopside-Anorthite

A. Introduction

Oxygen self-diffusion in silicate melts and glasses has recently been a very active area of research. Table 1 summarizes the bulk of the recent work for silicate melts. The reasons for this activity are quite numerous, but are centered around the fact that oxygen is the major constituent of silicates. Consequently, studies of the kinetic behavior of oxygen may yield a great deal of information about the structure and chemistry of silicate melts.

In an attempt to systematically investigate the relationships between oxygen self-diffusion and melt composition, the diffusivity of oxygen has been measured in three melts along the join diopside-anorthite. Those compositions (Table 2) were chosen because samples were available upon which Scarfe *et al*. (1980) have made viscosity measurements. This allowed an investigation of the validity of the Eyring model relating the activation energies of oxygen diffusion and viscous flow. Such a study is suggested by the close correspondence of the experimental data of Yinnon and Cooper (1980) and the Eyring equation model values for oxygen diffusion coefficients in a soda-lime-silica melt.

Table 1. Oxygen diffusion data for silicate melts.

Composition (wt%)	T°C	D_o (cm^2/s)	E (kcal)	Ref.
Na_2OCaOSiO_2	1000-1300	4.2×10^{1}	53	1
25K_2O75SiO_2	850-1000	4×10^{1}	62	2a
36K_2O64SiO_2	700-1000	2.4×10^{-1}	46	2b
Basalt	1280-1540	2.0×10^{4}	90	3
Basalt	1160-1360	5.9×10^{1}	54	10a
Andesite	1260-1360	6.0×10^{1}	60	10b
40CaO20$Al_2O_3$40SiO_2	1275-1435	4.7×10^{5}	85	4
40CaO20$Al_2O_3$40SiO_2	1320-1540	1.8×10^{1}	54	5a
40CaO20$Al_2O_3$40SiO_2	1000-1450	4.5×10^{0}	33	6a
45CaO15$Al_2O_3$40SiO_2	1000-1450	4.5×10^{0}	33	6b
25CaO10$Al_2O_3$65SiO_2	1000-1450	4.5×10^{0}	34	6c
16Na_2O12CaO72SiO_2	800-1470	4.5×10^{-2}	38	5b
20Na_2O80SiO_2	1061-1395	7.9×10^{-2}	44	5c
37K_2O63SiO_2	820- 902	1.7×10^{1}	60	7
7K_2O68PbO25SiO_2	578- 678	3.2×10^{0}	72	8
97PbO3SiO_2	1000-1400	8.3×10^{0}	24	6d
94PbO6SiO_2	1000-1400	8.3×10^{0}	25	6e
90PbO10SiO_2	1000-1400	8.3×10^{0}	26	6f
Na_2OCaOMgOSiO_2	700-1083	6.3×10^{-2}	50	9a
20K_2O20SrO60SiO_2	680-1121	8.5×10^{-2}	52	9b

References: 1. Doremus (1960), 2. May *et al.* (1974), 3. Muehlenbachs and Kushiro (1974), 4. Koros and King (1962), 5. Oishi *et al.* (1975), 6. Sasabe and Goto (1974), 7. deBerg and Lauder (1980), 8. deBerg and Lauder (1978), 9. Yinnon and Cooper (1980), 10. Wendlandt (1980)

B. Experimental methods

The method used in this study to measure oxygen diffusivity is that of Muehlenbachs and Kushiro (1974). The method involves exchange of oxygen between a spherical sample of known oxygen isotopic composition with an "infinite" reservoir of gas, also of known oxygen isotopic

composition. After the exchange experiment the entire sample is analyzed for its oxygen isotopic composition. This configuration and analytical method allow the solution of the diffusion equation (Jost, 1960):

$$(\delta^{18}Of-\delta^{18}Og)/(\delta^{18}Oi-\delta^{18}Og)=6\pi^{-2}\sum_{n}n^{-2}\exp(-n^2\pi^2Dt/r^2) \quad (1)$$

where $\delta^{18}Of$ is the isotopic composition of the sample after the exchange experiment, $\delta^{18}Oi$ is the isotopic composition of the starting material, $\delta^{18}Og$ is the isotopic composition of the sample upon equilibration with the gas, t is the duration of the experiment, r is the radius of the sample, and D is the diffusion coefficient. The application of equation 1 to calculate diffusion coefficients is based on several assumptions including: 1) That volume diffusion of oxygen is the rate limiting process; and 2) That convection does not occur within the sample.

The results of this study confirm the observations of Oishi *et al.* (1975) that volume diffusion of oxygen is the rate-limiting process in long duration experiments but may not be in short duration runs, as discussed below.

The assumption of non-convection within the sample was tested theoretically. Rayleigh numbers were calculated for the worst case experiments (highest temperature) for each composition and found to be much less than one. As a Rayleigh number of greater than 657.5 is required for convection to occur (Chandrasekhar, 1961), it is concluded

that convection did not occur in the melts used.

Equation 1 is a series expansion. Consequently, it is important to know how many terms are required for convergence. If enough terms are not used too small a diffusion coefficient will result. The critical parameter in determining the required number of terms is the product Dt (diffusion coefficient times the experimental duration). As Dt increases the number of terms required for convergence decreases. A small exchange fraction requires many more terms than does a large exchange fraction. To alleviate this problem a computer program was used to fit equation 1 to the data for each experiment. That program adds terms until the diffusion coefficient converges within 0.1%. The minimum number of terms used was arbitrarily taken as 100.

The starting materials were aliquots of the same glasses used by Scarfe *et al*. (1980). In order to increase the accuracy of determination of the exchange fractions, the starting glasses were enriched in ^{18}O by hydrothermal exchange with ^{18}O enriched water. The glasses were finely crushed, sealed into Pt capsules with an aliquot of ^{18}O enriched water, and exchanged at 800°C and 1 kilobar pressure. The exchanges were carried out for at least seven days. The resulting hydrated glasses were finely ground and fused for 1-2 hours at 1450°C in an Ar atmosphere. The glasses were then reground and fused for an additional hour at 1450°C in argon. The resultant glasses were coarsely crushed and stored at 25°C.

Table 2. Melt compositions used (theoretical values, wt. %) and other parameters.

	C1	C2	C3
SiO_2	55.49	50.33	48.11
Al_2O_3	---	15.39	21.99
CaO	25.90	23.49	22.46
MgO	18.61	10.79	7.44
E'(kcal)	39.2	52.3	51.9
T°C(liq)	1391	1274	1388
$\delta^{18}O$(i)(‰)	-25.8	-62.3	-73.2
$\delta^{18}O$(g)(‰)	+23.5		

E is the activation energy for viscous flow. Both E and T(liq) are taken from Scarfe *et al.* (1980).

All experiments were done on spheres of glass (10-70 mg) suspended on weighed loops of 250 micrometer Pt wire. The glass spheres were made by placing chips of the starting glass on the wire loops and thoroughly fusing them with an oxy-acetylene torch to yield a bubble-free sphere. The torch fusion time was held to a minimum (always less than 30 seconds) at the lowest temperature required to melt the sample, that temperature was always below 1760°C (the melting point of Pt). A reducing flame was used for the fusion to minimize oxygen exchange between the sample and air. For each of the starting compositions, a sphere prepared in this manner was analyzed for its oxygen isotopic composition. Two spheres were analyzed for composition 3 and

found to have oxygen isotopic compositions within 0.3‰ of one another. It was concluded that the sample preparation did not appreciably alter the isotopic composition of the starting material. That conclusion is further supported by the similarity of the results of isothermal experiments in which spheres of different radius were used (Table 3 and fig. 1). Thus, those compositions were taken as the initial isotopic compositions ($\delta^{18}O_i$) and are given in Table 2. Several samples of the exchange gas were collected both before and after passing through the furnace. Isotopic analyses of the gas samples were within 0.2‰ of each other. The mean of those values (+23.5‰) was taken as $\delta^{18}O_g$ (Table 2). The sphere-loop combinations were weighed and the resultant sample mass was used in conjunction with melt densities (calculated using the method of Bottinga *et al.*, 1982) to compute the sample radii. Radii are estimated to be accurate within ±2%. The samples were also weighed after the experiments. A change in sample weight greater than 2% was taken as cause to reject the experiment.

The experiments were done in an electrically heated vertical tube furnace equipped with a gas-tight alumina muffle tube. Before each experiment, the furnace was set to the run temperature and allowed to equilibrate. The sample was then introduced into the cold zone of the furnace (temperature less than 220°C) and the furnace was sealed. The flow of exchange gas (oxygen) was started and the system was left to allow the furnace atmosphere to be purged of

air. After 30 minutes the sample was lowered into the hot zone of the furnace, thus initiating the experiment. At the end of the experiment the sample was removed from the furnace and placed in a stream of cool air. The samples cooled to ambient temperature (25°C) within 20-30 seconds. The samples were stored at 110°C until oxygen isotope analysis. As it is necessary to show that the diffusion coefficients are independent of experimental duration, the lengths of replicate experiments at each temperature were varied by a factor of at least 1.5 and up to 17.

Oxygen extraction was done by the BrF_5 technique (Clayton and Mayeda, 1963). The extracted oxygen was reacted with carbon to form CO_2, and analyzed on an isotope ratio mass spectrometer (micromass 602). The isotopic composition of the sample is given as:

$$\delta^{18}O = 1000(\{(^{18}O/^{16}O)_{smp}/(^{18}O/^{16}O)_{std}\}-1) \text{ ‰} \qquad (2)$$

and is reported relative to a laboratory standard. The isotopic analyses are considered to be accurate within 0.1‰ except as noted below. As the bulk compositions of the samples were known the theoretical yield of oxygen was calculated and used as an indicator of the quality of the oxygen extractions (Table 3). The oxygen yields were determined by transferring the CO_2 (produced by reaction of the oxygen with carbon) into a known volume and measuring the pressure. The yields ranged from 24 to 105%. Because of

the greater than 100% yields observed yields as low as 93.4% were accepted. The isotopic compositions of the samples are summarized in Table 3.

The isotopic analyses and the radius calculations are the primary identifiable sources of experimental error. A possible source of error in the isotopic analysis of samples which are significantly different from the standard used is leakage of gas between the sample and standard portions of the mass spectrometer. Gas leakage causes the sample to appear to be closer to the standard than is actually the case. Furthermore, the error increases as the difference between the sample and standard increases. In the worst case encountered in this study a gas leak of 1% would result in a 0.7‰ error. Therefore, it is possible that there may be errors as large as 1.0‰ for the more depleted samples analyzed in this study. Taking an error of 1‰ in the isotopic analyses and propogating it through eqn. 1 yields a worst case error in logD of approximately 0.5. The maximum scatter in replicate analyses is approximately 0.5 logD units which supports the error analysis. However, the leak rate for the mass spectrometer used is generally assumed to so small as to be negligible (k. Muehlenbachs, *pers. comm.*).

C. Results

The experimental results are summarized in Table 3 and shown graphically in figure 1. Most rate processes in silicate melts are exponentially related to the inverse of

Table 3. Experimental conditions and results.

No.	T°C	Time (sec)	^{18}O (‰)	r(cm)	-logD (cm^2/s)	yield (%)
1.1	1396	5400	-11.6	0.172	7.32	96.7
1.2	1397	12060	3.1	0.153	7.05	94.8
1.3[2]	1398	7200	-5.6	0.172	7.10	80.9
1.4	1431	12000	16.5	0.110	6.83	99.4
1.5	1437	9860	14.8	0.122	6.83	95.3
1.6	1438	12960	13.5	0.132	6.82	101.6
1.7	1440	7200	14.6	0.137	6.49	96.6
1.8	1473	3600	-4.2	0.156	6.82	96.5
1.9	1473	5400	2.1	0.149	6.77	96.8
1.10	1473	8100	15.3	0.097	6.82	98.4
2.1[1]	1282	3600	-56.3	0.131	8.64	97.7
2.2	1297	61200	12.8	0.109	7.50	104.3
2.3	1298	33180	4.6	0.127	7.29	n.d.
2.4[1]	1300	3600	-58.2	0.192	8.64	93.8
2.5	1357	29640	9.2	0.114	7.24	104.2
2.6[1]	1361	3600	-54.5	0.192	8.64	98.7
2.7	1419	14400	18.8	0.115	6.65	103.0
2.8[1]	1420	3660	-47.1	0.157	7.68	98.4
2.9	1473	8400	8.6	0.120	6.66	101.1
2.10	1475	3600	-29.6	0.158	6.95	99.0
3.1[2]	1386	10800	-29.3	0.109	7.61	26.3
3.2	1388	7500	-35.4	0.090	7.73	101.6
3.3	1388	7500	-43.2	0.107	7.80	95.7
3.4	1395	12780	-30.1	0.112	7.64	101.0
3.5	1395	14640	-27.6	0.116	7.61	95.8
3.6[2]	1430	15780	-26.2	0.159	7.34	86.7
3.7[2]	1430	90360	20.5	0.132	7.24	73.0
3.8	1473	3600	-43.3	0.116	7.42	105.2
3.9	1474	5400	-40.8	0.127	7.44	99.4
3.10[2]	1474	7620	-18.7	0.115	7.14	84.3

[1] - Rejected due to surface effects (see text).
[2] - Rejected due to poor oxygen yield.

Figure 1. Arrhenius plots for the composition 1 (C1), 2 (C2), and 3 (C3) oxygen diffusion data. The equations of the regression lines are given in the text as equations 4, 5, and 6, respectively.

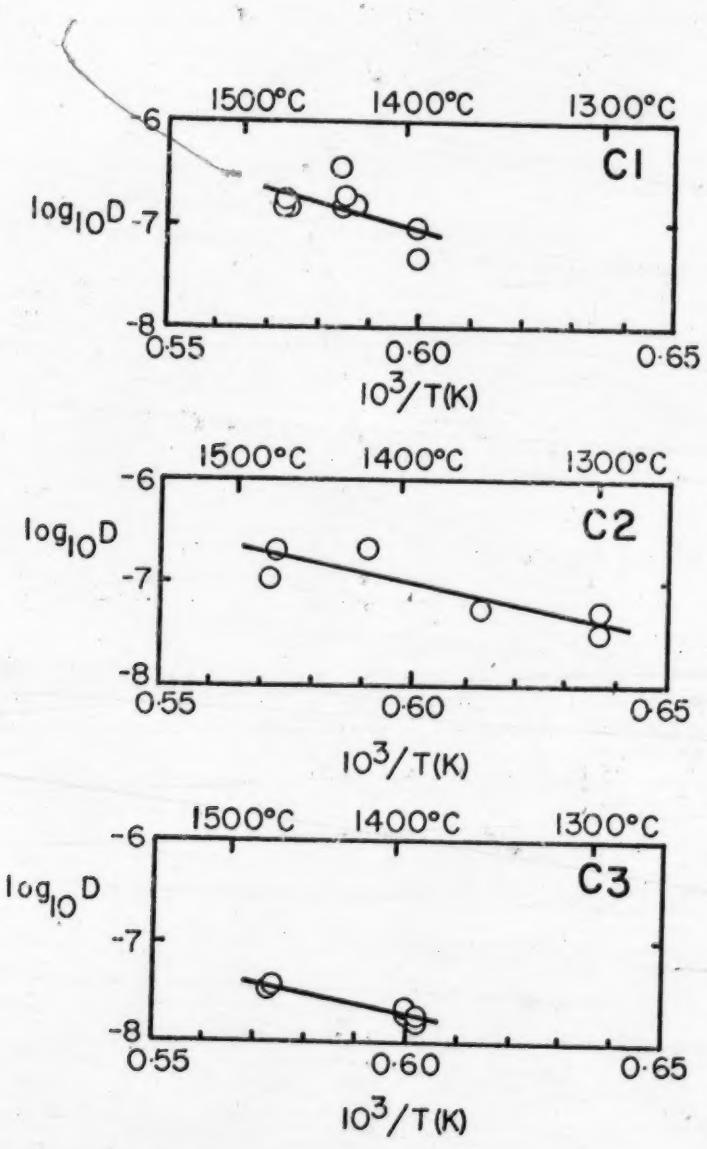

the absolute temperature. Such a relationship is termed an Arrhenius equation and is given for the case of diffusion by equation 3:

$$D = D_o \exp(-E/RT) \qquad (3)$$

where D is the diffusion coefficient, D_o is the Arrhenius frequency factor, E is the Arrhenius activation energy, R is the gas constant, and T is the absolute temperature. The data for the three compositions can be fit to Arrhenius equations to give Arrhenius activation energies for oxygen diffusion. The resultant equations (shown as solid lines in figure 1) are:

$$D=(1.64 \times 10^{1})\exp((-63000)/RT)\ (cm^2/sec) \qquad r^2=0.39 \qquad (4)$$

$$D=(1.35 \times 10^{-1})\exp((-47000)/RT)\ (cm^2/sec) \qquad r^2=0.75 \qquad (5)$$

$$D=(1.29 \times 10^{-2})\exp((-44000)/RT)\ (cm^2/sec) \qquad r^2=0.86 \qquad (6)$$

for compositions 1, 2, and 3, respectively. The activation energies are 63±20 kcal for composition 1, 47±9 kcal for composition 2, and 44±6 kcal for composition 3. The errors quoted are calculated from the regression analyses using the method of Birge (1932). The activation energies for compositions 1 and 3 are based on data from all of the experiments not rejected due to low oxygen yield, but the

activation energy for composition 2 is not. The composition 2 experiments form two trends which intersect only at 1782°C (fig 2.). These two data sets may be delineated in terms of experimental duration, the value of Dt, or exchange fraction. The experiments having a longer duration, a higher value of Dt, or a higher exchange fraction fall into the upper set while those experiments of short duration, small exchange fraction, or lower Dt value fall into the lower set. It is apparent, where only a small fraction of oxygen was exchanged, that some process other than volume diffusion is the rate-limiting process. Hofmann and Magaritz (1977) noted that a critical value of Dt had to be exceeded to decrease errors from competing transport processes. The composition 2 data indicate that the critical value of Dt is approximately 1×10^{-4} cm² for the experimental configuration used in this study. Samples having smaller Dt values were rejected (Table 3).

That experiments having higher exchange fractions give similar D values regardless of the experimental duration indicates that the competing process is itself of short duration. The competing process is most likely the establishment of a surface equilibrium between the sample and the furnace atmosphere.

The normal test in diffusion studies for surface effects is to plot the product of the diffusion coefficient and the experimental duration (Dt) versus the experimental duration (t) for each set of isothermal experiments. If

Figure 2. Arrhenius plot for the composition 2 oxygen diffusion results. Experiments having Dt values less than 1×10^{-4} are shown as circles and those having larger Dt values are shown as hexagons.

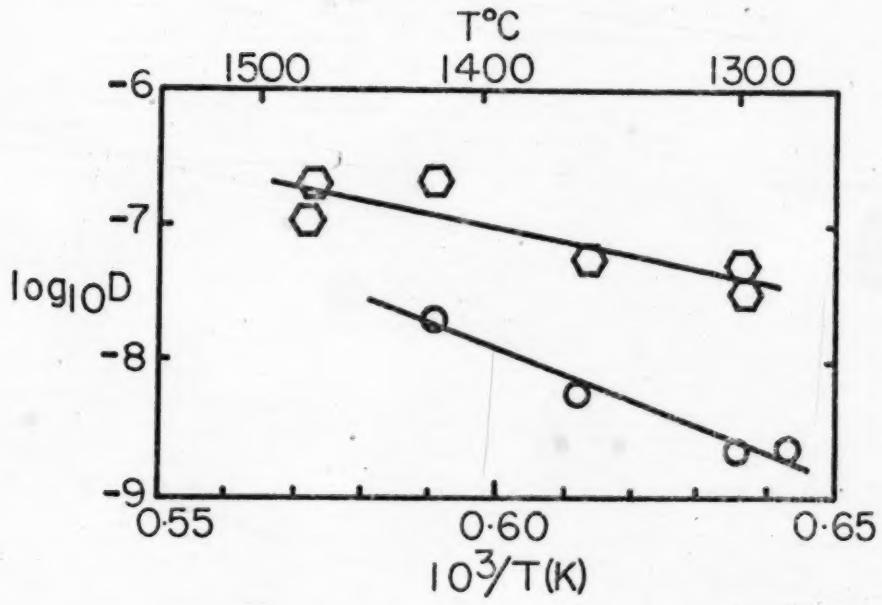

there are no surface or other competing effects, such a plot will be linear and will pass through the origin. In addition D was plotted against experimental duration (t) for each isothermal series of experiments. The plots for composition 2 show that volume diffusion is not the rate limiting process for the low Dt experiments. Therefore, those experiments were rejected. While the plots for compositions 1 and 3 show some variation from the ideal, the absolute variation in the D values is not systematic and is always small (less than 0.3 $\log_{10}$ units). Consequently, all of the data were used for compositions 1 and 3 as noted above.

D. Discussion

Table 1 summarizes the bulk of the previous oxygen diffusion measurements for silicate melts. The results of this study may be compared to those data either from the point of view of activation energy, or on the basis of the absolute magnitude of the measured diffusivity. Before making a comparison on the basis of activation energies, it is desirable to consider the physical meaning of the Arrhenius activation energy.

Mechanisms of oxygen diffusion in silicate melts have been and continue to be enigmatic. It is, however, essential that some understanding of the mechanism of oxygen diffusion in melts be achieved. Without such an understanding the physical meaning of the Arrhenius activation energy for diffusion remains abstruse.

Among the mechanisms which have been proposed are: diffusion of free oxygen anions, diffusion by combined Si-O bond rupture and free anion movement, diffusion by oxygen transfer during reactions among large silicate anions (with or without free oxygen anions), and diffusion via rotation and translation of large silicate anions without bond rupture. Mechanisms involving bond rupture have been suggested in studies where large activation energies have been determined (Muehlenbachs and Kushiro, 1974; Koros and King, 1962), thereby relating the activation energy to the strength of the Si-O bond. Oxygen diffusion via free oxygen anion movement has been proposed by those workers whose studies yielded low activation energies (Sasabe and Goto, 1974 and Wendlandt, 1980). In those cases, the activation energy is associated with the energy required to move a free oxygen anion from one "site" to another. Studies in which intermediate activation energies were determined tend to support diffusion via combined mechanisms (c.f. deBerg and Lauder, 1978 & 1980).

The Arrhenius activation energies for oxygen diffusion determined in this study (C-1: 63 kcal/mole, C-2: 47 kcal/mole, and C-3: 44 kcal/mole) are of the same order of magnitude as those determined by Doremus (1960), May *et al.* (1974), Oishi *et al.* (1975), Wendlandt (1980), deBerg and Lauder (1978 & 1980), and Yinnon and Cooper (1980) for oxygen diffusion in other silicate melts. However, the activation energies measured in this study are considerably

smaller than those determined by Muehlenbachs and Kushiro (1974) and Koros and King (1962) for oxygen diffusion in natural basalt and $CaO-Al_2O_3-SiO_2$ melts, respectively, and are greater than those determined by Sasabe and Goto (1974) for a variety of silicate melts.

The activation energies determined by Muehlenbachs and Kushiro (1974) and Wendlandt (1980) for basalt melts are very different (90 and 54 kcal/mole, respectively). The 90 kcal/mole reported by Muehlenbachs and Kushiro (1974) is the largest Arrhenius activation energy for oxygen diffusion in a silicate melt yet determined. The only similar value is that reported by Koros and King (1962) for a $CaO-Al_2O_3-SiO_2$ melt (85 kcal/mole). However, the result of Koros and King (1962) is questionable as Oishi *et al.* (1975) have reported an activation energy of 54 kcal/mole for oxygen diffusion in a melt of the same composition. Sasabe and Goto (1974) have also studied the same melt composition as Oishi *et al.* (1975) and Koros and King (1962) and report an activation energy of 33 kcal/mole. However, Sasabe and Goto (1974) did their measurements via oxygen ion electrode and as Tran and Brungs (1980a&b) have shown, such methods are fraught with difficulties. In addition the results of Sasabe and Goto (1974) fall well off the trend defined by all other oxygen diffusion measurements on a compensation law plot (fig. 4) which is discussed below.

The other basis for comparison is the magnitude of the diffusion coefficients. Figure 3 is an Arrhenius plot of the

results of this study and the data summarized in Table 1. The data define a range of oxygen diffusivities spanning approximately 2.5 orders of magnitude at a given temperature. The only data which fall outside that range are those of Sasabe and Goto (1974) which are from two to three orders of magnitude greater than the rest of the oxygen data and do not even plot within the range of fig. 3. The scatter in the data combines with the paucity of the results to make it impossible to derive any correlation between melt composition and oxygen diffusivity.

Notwithstanding this lack of a correlation, fig. 3 is useful in showing that Arrhenius activation energies are not neccessarily a good basis for comparison of diffusion data. The results of Oishi *et al.* (1975) and Koros and King (1962) for CaO-Al_2O_3-SiO_2 melts illustrate this well. Figure 3 shows that the results of those two studies are similar when the actual magnitudes of the diffusion coefficients are compared, even though their activation energies are very different.

The actual magnitudes of oxygen diffusion coefficients (Tables 1 & 3) are similar to those of various divalent cations (see fig. 3). In some melts oxygen has been reported to be the fastest moving species in the melt (Oishi *et al.*, 1975). However, the diffusivities measured in this study are less than those of divalent cations by up to an order of magnitude. Physical mobility must be related to the mechanism of diffusion. If oxygen moves as a free anion

Figure 3. Arrhenius plot showing the results of this study (C1, C2, & C3), previous oxygen diffusion measurements (numbers refer to reference numbers as given in Table 1), the field of divalent cation diffusivities as given by Hofmann (1980) and Watson (1981) (dotted box), and the silicon diffusion data of Towers and Chipman (1957) (dashed line).

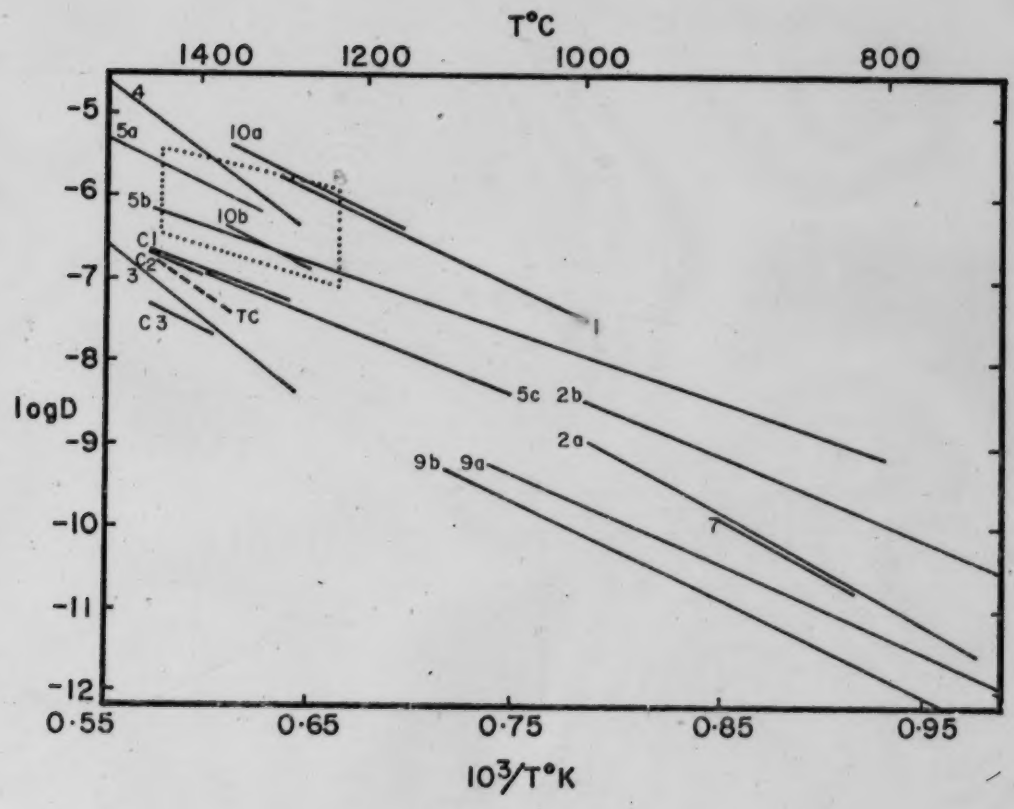

(O^{2-}) its rate of movement will be comparatively rapid like that of a cation of similar size and absolute charge. Similarly, if oxygen diffuses via bulk translation and rotation of large silicate anions, its mobility is expected to be small compared to divalent cations. As oxygen mobility is generally similar to, or slightly less than divalent cation mobility, oxygen may diffuse by a combination of the mechanisms discussed above. The results of this study bracket the silicon diffusion data of Towers and Chipman (1957). This may be taken as contradictory to the conclusion about oxygen diffusion mechanisms. However, the results of Oishi *et al.* (1975), Koros and King (1962), and Towers and Chipman (1957) when taken in conjunction with the results of Yinnon and Cooper (1980), show that comparisons between the relative mobilities of oxygen and cations for compositionally diverse melts are not necessarily valid.

Thus, the measured oxygen diffusivity may be thought of as representing a weighted average of the contributions from the various mechanisms. This hypothesis may be extended to provide an explanation for the slope changes observed in plots of lnD versus 1/T (Yinnon and Cooper, 1980; deBerg and Lauder, 1978 & 1980; and Oishi *et al.*, 1975), by postulating that such slope changes represent zones of transition from the dominance of one mechanism to another. This hypothesis is also compatible with the fact that the slope changes in lnD vs 1/T plots are generally at or near the glass transition temperature, where the translational degrees of

freedom in the system are lost with decreasing temperature.

Compensation law

Winchell (1969) and Winchell and Norman (1969) have proposed that all ionic diffusivities in silicate melts and glasses become similar at approximately 1497°C. This conclusion is based on the observation of a linear relationship between the log of the Arrhenius frequency factor and the Arrhenius activation energy ($\log_{10}D_o$ and E, respectively: see equation 3). Hofmann (1980) has expanded the data base used by Winchell (1969) and Winchell and Norman (1969) and reports the relationship:

$$\log_{10}D_o = 1.08 \times 10^{-4}E - 5.50 \qquad (7)$$

where D_o is in cm^2/sec and E is in cal/mole-deg. The frequency factors and activation energies determined in this study are within experimental error of the line represented by equation 7, when the errors inherent in equation 7 are considered. The oxygen diffusion results of this study along with those in Table 1 (excluding Sasabe and Goto, 1974) define a line essentially identical to Hofmann's result (figure 4) with the equation:

$$\log_{10}D_o = 1.27 \times 10^{-4}E - 6.52 \qquad r^2=0.76 \qquad (8)$$

From equation 8 a critical temperature of 1448°C can be calculated. That temperature is in reasonable agreement with

Table 4. Calculated λ_1 and $(\lambda_2\lambda_3)^{1/2}$ values for the diffusion of O^{2-} and SiO_4^{4-}.

	O^{2-}	SiO_4^{4-}
λ_1	7.13×10^{-8}cm	2.42×10^{-8}cm
$(\lambda_2\lambda_3)^{1/2}$	3.59×10^{-8}cm	6.63×10^{-8}cm

the critical temperatures calculated by Winchell (1969): 1234°C, Winchell and Norman (1969): 1504°C, and Hofmann (1980): 1770°C. Equations 7 and 8 and fig. 4 show that the trend of the oxygen diffusion data are compatible with the compensation law as proposed by Winchell (1969).

The work of Sasabe and Goto (1974) has been excluded from the compensation law calculation as their data fall well off the trend defined by all other oxygen diffusion data (fig. 4). This observation in conjunction with other considerations discussed above leads to the conclusion that the results of Sasabe and Goto (1974) may be in error.

Comparison with the Eyring model

Yinnon and Cooper (1980) and Oishi *et al.*, (1975) report good agreement between measured oxygen diffusion coefficients and those calculated using the Eyring equation (equation 9).

$$D = kT/\gamma\lambda \qquad (9)$$

Figure 4. Compensation law plot for oxygen diffusion. The results of this study (hexagons) and all previous oxygen diffusion data (circles) except those of Sasabe and Goto (1974) (triangles) are used to determine the compensation law equation for oxygen diffusion (solid line). The compensation law for cations as given by Hofmann (1980) is shown as a dashed line. The equations of the two lines are given in the text as equations 8 and 7, respectively.

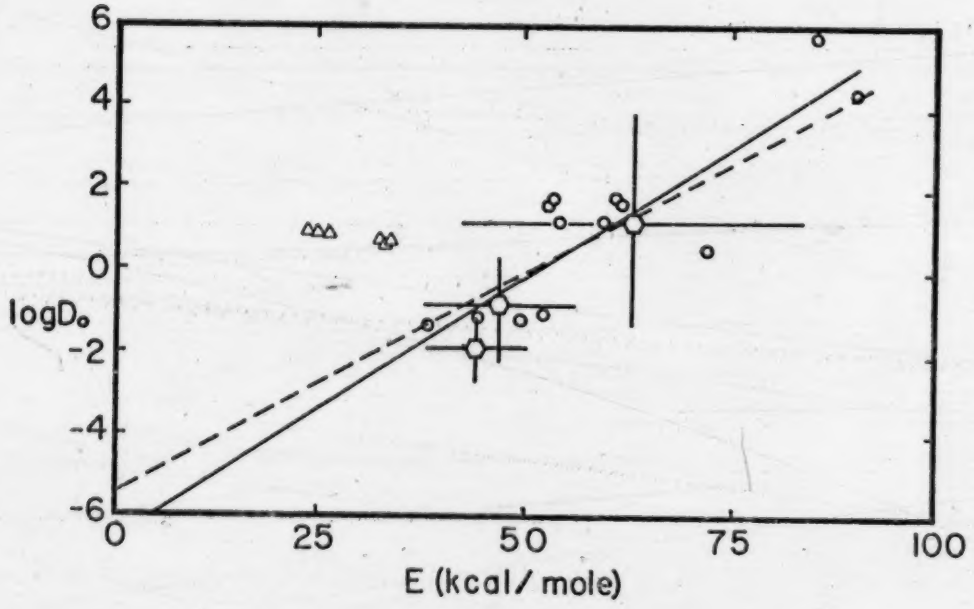

The parameters in equation 9 are the diffusion coefficient (D), the Boltzmann constant (k), the melt viscosity (η), the absolute temperature (T), and the characteristic particle translation distance (λ). D values were calculated from the viscosity data of Scarfe *et al.* (1980) and an assumed value of λ of 2.6 x 10^{-8}cm (the diameter of an oxygen anion). The calculated D values are larger than those measured by approximately an order of magnitude. This difference is considerably larger than that reported by either Yinnon and Cooper (1980) or Oishi *et al.* (1975).

The use of the Eyring model (equation 9) to model diffusion requires the assumption that the diffusing species is also the viscous flow unit. The failure of the Eyring model to adequately model the measured oxygen diffusivities of this study, when oxygen anion is taken as the viscous flow unit (λ =2.6x10^{-8}cm), implies either that O^{2-} is not the diffusing species or that O^{2-} is not the viscous flow unit. While compositions 1 and 2 have essentially identical oxygen diffusivities, the decrease in the magnitude of oxygen diffusivity between compositions 2 and 3 is as the Eyring model predicts. Also, if the value of λ in equation 9 is increased, Eyring model diffusivities can be brought into quite close agreement with the diffusivities measured in this study.

The form of the Eyring equation given in equation 9 has been simplified by an assumption about λ. Without that assumption the equation becomes (Glasstone *et al.*, 1941):

$$D = \lambda_1 kT/\eta\lambda_2\lambda_3 \qquad (10)$$

where λ_3 is the interatomic distance in the direction of transport and λ_1 and λ_2 are the interatomic distances perpendicular to the transport direction. The assumption that the product ($\lambda_1\lambda_2\lambda_3$) gives the effective volume of the diffusing species may be used in conjunction with the measured viscosity and diffusivity to compute values for λ_1 and $(\lambda_2\lambda_3)^{1/2}$. The results for composition 3 at 1400°C, assuming that the diffusing species is O^{2-} ($V=9.2\times10^{-24}cm^3$) and SiO_4 tetrahedral anion ($V=1\times10^{-23}cm^3$), are shown in Table 4. The value of λ_1 determined for the O^{2-} case is clearly too small to be realistic as it is smaller than the radius of O^{2-}. Whereas, the values determined for the SiO_4 case are more reasonable. This may be taken as implying a larger diffusion unit than O^{2-} anions. However, complete cation diffusion data for this melt composition are required to substantiate this supposition.

E. Conclusion

The results of this study are compatible with previous oxygen diffusion measurements for a diverse selection of silicate melts. However, there is a great deal of scatter in the data (fig. 3), which precludes the identification of any systematic trends or relationships between oxygen diffusivity and silicate melt composition. Some studies (Oishi *et al.*, 1975; Wendlandt, 1980, and this study) do

show a rough inverse relationship between oxygen diffusivity and the silica content of the melt. However, that correlation is far from conclusive.

The self-diffusion coefficients do not agree with the Eyring equation unless mean ionic jump distances (λ) considerably larger than the diameter of the oxygen anion are assumed. However, the sense of variation of the actual diffusivities is as the Eyring equation predicts. Fitting the data to the Eyring equation by varying the parameters allows an estimate of the size of the diffusing species to be made. For the compositions studied, the average size of the diffusing species is too large to be an oxygen anion but it is smaller than any of the silicate anions present in melts except the monomer (SiO_4^{4-}).

Consideration of the results of this study and the bulk of previous work shows that oxygen conforms to the compensation law for cationic diffusion in silicate melts and glasses. The range of oxygen diffusivities was also found to encompass the range of divalent cation diffusivities in silicate melts.

These results lead to the rather speculative conclusion that the diffusion of oxygen in silicate melts may involve a contribution from a cation-like diffusion mechanism as well as contributions from the diffusion of larger structural units in the melt.

III. Oxygen Diffusion in Basaltic Liquids at Elevated Pressures

A. Introduction

Measurements of component diffusivities have proven very useful in increasing our understanding of a variety of processes in silicate melts. Oxygen, however, is unique because it is the major component of all silicates. As such, the kinetic behavior of oxygen in silicate liquids strongly affects and may indeed control the kinetic and chemical behavior of the other components in the melt. In this respect, Dunn (1982) and Oishi *et al*,. (1982) have shown that oxygen diffusion data can be very useful in understanding the structure of silicate melts.

The data set for oxygen diffusion in silicate melts is quite restricted (Dunn, 1982). The bulk of the data is for simple systems which are of limited applicability to geological problems. With the exception of Muehlenbachs and Kushiro (1974), who report oxygen diffusion results for a basalt liquid, and Wendlandt (1980), who presents data for tholeiitic basalt and andesite melts, there are no oxygen diffusion data for rock melts. Unfortunately, their results for basalt liquids are significanlty different. While that difference probably reflects differences in experimental methods and melt composition, it is important that the difference be resolved.

All existing oxygen diffusion data have been determined at one atmosphere pressure. Oishi *et al.* (1975) have shown that oxygen diffusion in silicate melts is inversely related to the viscosity of those melts. Recent work on the pressure dependence of the viscosity of basaltic liquids has revealed that with increasing pressure the viscosities of those melts either remain essentially constant (olivine nephelinite - Scarfe, 1981), decrease slightly (1921 Kilauea tholeiite - Kushiro *et al.*, 1976), or decrease significantly (alkali basalt - Scarfe, 1981). Those results imply that oxygen diffusivity may increase with increasing pressure in contrast to the behavior of Ca (Watson, 1979) and CO_2 (Watson *et al.*, 1982) (the only other species whose diffusion has been studied as a function of pressure). Therefore, the diffusion of oxygen in a series of basaltic liquids was investigated as a function of pressure.

The compositions chosen for this study (Table 5) are an olivine nephelinite from Hamada, Japan, an alkali olivine basalt from Kettle River B.C., and 1921 Kilauea tholeiite. The three compositions were chosen because they increasingly approach silica saturation (nephelinite to tholeiite) and there are both viscosity and phase equilibrium data for these or similar compositions as a function of pressure. The three compositions allow an investigation of the effects of temperature, pressure, and bulk composition on oxygen diffusion in basaltic liquids.

Table 5. Composition of starting materials.

	C-11	KR-13	1921
SiO_2	37.77	49.63	48.08
TiO_2	2.75	2.43	2.97
Al_2O_3	12.00	14.63	12.11
MgO	9.29	5.91	11.30
CaO	12.59	9.38	9.44
FeO^1	2.08	2.26	2.44
$Fe_2O_3^2$	13.46	10.10	10.05
MnO	0.22	0.21	0.18
Na_2O	4.29	4.06	2.25
K_2O	2.17	1.25	0.51
P_2O_5	2.37	0.50	0.28
Total	98.99	100.36	99.68

[1] - Volumetric determination.
[2] - Determined by difference between probe FeO and FeO'.

B. Experimental

The experiments were done by reducing previously oxidized spheres of basalt glass in a solid media piston-cylinder apparatus (Boyd and England, 1960). The oxidation state of the samples was determined before and after the experiment by micro-titration (Wilson, 1960). The spheres of glass were packed with graphite powder into graphite capsules. In this experimental configuration, oxygen diffuses out of the spherical samples into an effectively infinite reservoir of graphite. Analysis of the entire sample after the experiment allows the solution of the diffusion equation given by Jost (1960) to apply:

$$\{FeO(f)-FeO(e)\}/\{FeO(i)-FeO(e)\}=6\pi^{-2}\sum_{n} n^{-2}EXP(-n^2\pi^2Dt/r^2) \quad (11)$$

where FeO(f) is the wt. % FeO in the sample after the experiment, FeO(i) is the initial wt. % FeO in the starting glass, FeO(e) is the equilibrium wt. % FeO in the sample, D is the diffusion coefficient, t is the experimental duration, and r is the radius of the sample.

Equation 11 is a series expansion and it is important to know how many terms are required for convergence. If enough terms are not used, too small a diffusion coefficient will result. The critical parameter in determining the required number of terms is the product of the diffusion coefficient and the experimental duration (Dt). As Dt increases the number of terms required for convergence decreases. To alleviate this problem a computer program using a large number of terms (≥999) was used to fit eqn. 11 to the data for each experiment using a convergence limit of 0.1%.

The approach used here measures the chemical diffusivity of oxygen rather than oxygen self-diffusion. That is because of the oxygen chemical potential gradient imposed by placing a highly oxidized sample into extremely reducing conditions (discussed below). The determination of oxygen diffusivity by monitoring the rate of reduction of iron in the sample requires that oxygen diffusion be the rate limiting process. That the reduction or oxidation of transition metal cations in silicate melts is rapid compared

to oxygen diffusion has been demonstrated by several workers. Semkow *et al*. (1982) have directly measured the rates of oxidation and reduction of Ni, Co, and Zn in diopside melts and found them to be fast compared to diffusion (The first order rate constants are on the order of 10^{-3} cm/sec at 1500°C). Loh *et al*. (1981) investigated the oxidation-reduction behavior of arsenic in soda-lime-silica melts using immersed oxygen fugacity probes. They found that immediate oxidation or reduction occurred on cooling and heating, respectively. The melts then equilibrated slowly by diffusion of oxygen into or out of the bulk melt. Similarly, Tran and Brungs (1980b) found that the rate of oxidative equilibration was greatly enhanced by stirring the melt, thus decreasing diffusive path lengths.

In addition to the arguments above, it is necessary to show that the diffusion coefficients are independent of either sample size, or experimental duration. Both tests were done in this study (Table 7), but the test of independence from sample size predominated due to the fact that two samples were generally run together in each experiment. The results (Table 7) show that the diffusion coefficients measured are, in most cases, independent of both time and sample size.

Dunn (1982) and Oishi *et al*. (1975) noted that the time required to establish surface equilibrium caused erroneous results in short duration oxygen diffusion experiments. Even

though the experiments done in this study were short (≤ 1 hr.), the establishment of surface equilibrium is not thought to be a problem because of the experimental design and procedure used in this study. After loading into the graphite capsules with graphite powder, and before heating, the samples were taken up to a pressure 3 to 5 kilobars above the run pressure. This overpressuring compresses the sample assembly, seats the thermocouple, and forces the sample into intimate contact with the graphite powder, thereby, assuring rapid attainment of surface equilibrium upon heating. After that step, the experiment was initiated by rapidly heating the sample to the run temperature (the time from 900°C to run T was generally less than 15 seconds). The experiments were terminated by shutting off the power. The water cooled apparatus quenched the charge at approximately 250°C per second. Several samples examined optically were completely glassy.

The starting glasses were prepared from rock powders by multiple fusion in air at 1350°C (nephelinite and tholeiite) or 1400°C (alkali basalt) in covered Pt crucibles. The samples were crushed between fusions. The homogeneity of the starting glasses was determined for the major elements by electron microprobe and for FeO by at least four replicate FeO analyses (Table 5).

The microprobe analyses were done on the University of Alberta ARL-SEMQ automated microprobe by wavelength dispersive methods. Data reduction was done by the method of

Bence and Albee (1968) using the alpha factors of Albee and Ray (1970). FeO analyses were done by the method of Wilson (1960). Samples for FeO analysis were weighed on either a Mettler M5 microbalance or a Cahn Gram electrobalance to a precision of ±5 micrograms. The titrations were done with a 10 microliter syringe. These procedures, when used with reagent solutions as described by Wilson (1960), allow a precision of ±0.01 wt. % FeO for a 10 milligram sample. To test the accuracy of the method 25 aliquots of BCR-1 (8.80 wt. % FeO; Flanagan, 1973) were analyzed and gave a value for FeO of 8.66±0.21 wt. %. Several batches of the reagent solutions were used over the course of this study. Those solutions were periodically standardized against each other as well as against the initial batch of ammonium vanadate solution. The FeO value reported here for BCR-1 indicates that the split had become slightly oxidized. However, as the FeO contents of the samples in this study need only be known relative to one another rather than absolutely, this does not cause a problem.

Spheres of the starting glasses were prepared either by directly grinding chips using a sphere grinder similar to that described by Bond (1951), or by gluing chips of glass onto loops of Pt wire and fusing the chips into roughly spherical shapes at either 1350°C or 1400°C in air (as noted above) and then grinding the spheroids into a final spherical shape. Several spheres prepared in the latter manner were analyzed for FeO and found to be

indistinguishable from the starting glasses. The latter method of making spheres was adopted due to the long times (10-15 days) required to grind irregular chips into good spheres. The sample spheres were ultrasonically cleaned, weighed, and measured with a micrometer (±0.01 millimeters) before use.

The experiments were done in a solid media piston-cylinder apparatus (Boyd and England, 1960) using both 1/2" (above 8 kbar) and 3/4" (8 kbar and below) assemblies. In order to ascertain that the results achieved with the 1/2" and 3/4" assemblies were the same, two runs were made for the nephelinite at 16 kbar. The first run (#67a and #67b Table 7) was done with a 3/4" assembly and the other (#111 Table 7) was done with a 1/2" assembly. The results for samples 67a and 111 are indistinguishable and the errors associated with all three results overlap. Temperatures were monitored with Pt-$Pt_{.7}Rh_{.3}$ thermocouples without any pressure correction. Temperatures are estimated to have an uncertainty of better than ±10°C. The pressure calibration was done for both types of assemblies by monitoring the melting point of NaCl by DTA. Pressures reported here have an uncertainty of ±0.5 kbar.

Generally, two samples with different radii were packed in graphite powder in a graphite capsule (fig. 5). The capsules were then heated to red heat for 1-2 minutes to drive off adsorbed water and final assembly was done before the capsule cooled. Samples run in this manner retain their

Figure 5. Schematic drawing of the 1/2" sample assembly showing the location of the samples. The 3/4" assembly is the same except that the graphite heater and the AlSiMag end plugs are tapered to reduce the temperature gradient in the 10mm long capsule (Kushiro, 1976).

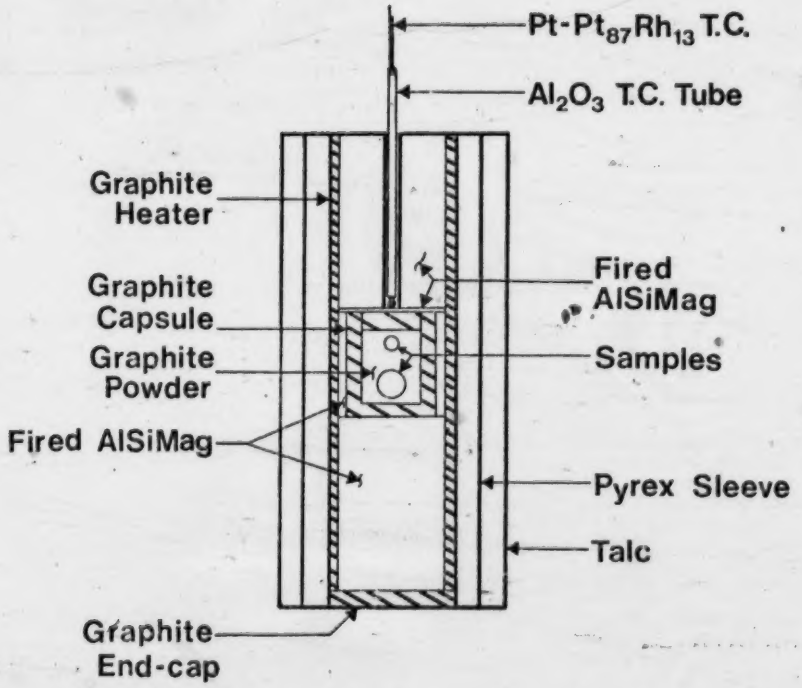

shape (no distortion was observed for any of the samples run in this study). The only difference in the samples after the experiments is that they are coated with graphite. The possibility that the graphite might affect the FeO analyses was tested by mixing equal weights of BCR-1 and graphite powder together and then analyzing for FeO. No interference from the graphite was observed. In all cases, the entire sample was analyzed for FeO without any pre-analytical treatment.

The experimental method described above assures that the system is on the C-CO-CO_2-O_2 buffer curve (French and Eugster, 1965). That buffer curve is approximately one log unit above Fe-FeO (Eugster and Wones, 1962) for the experimental conditions employed in this study. Furthermore, that curve is well below FeO-Fe_3O_4 (Ernst 1960 and Eugster and Wones, 1962). The relative positions of the three buffer curves are insensitive to changes in pressure and temperature (fig. 6). Thus, the equilibrium state of the iron in the samples is expected to be essentially 100% ferrous throughout the range of temperatures and pressures investigated. This was verified for each composition by doing a long duration run (minimum 4 hours) and analyzing the sample for both FeO and total iron (by atomic absorption). In all cases, total iron (as FeO) was indistinguishable from FeO. The total iron content (as FeO) of the samples was taken as FeO(e) for use in the diffusion calculation.

Table 6. Volatile contents of the alkali basalt starting material and alkali basalt run for two hours at 1350°C and 12 kilobars.

	#61	#74
H_2O'(wt. %)	≤0.06	≤0.06
CO_2(wt. %)	0.018±0.002	0.24±0.02

' - wt. % H_2O includes the total pressure of non-condensible gas (taken as H_2 and recalculated as H_2O) in addition to gas detected as water.
Analyst D. Harris using the method of Harris (1981).

Figure 6. Log of oxygen fugacity *versus* pressure showing the FeO-Fe_3O_4 (— · —), Fe-FeO (— · —), and C-CO-CO_2-O_2 (———) oxygen fugacity buffer curves at 1280°C (light lines) and at 1450°C (heavy lines).

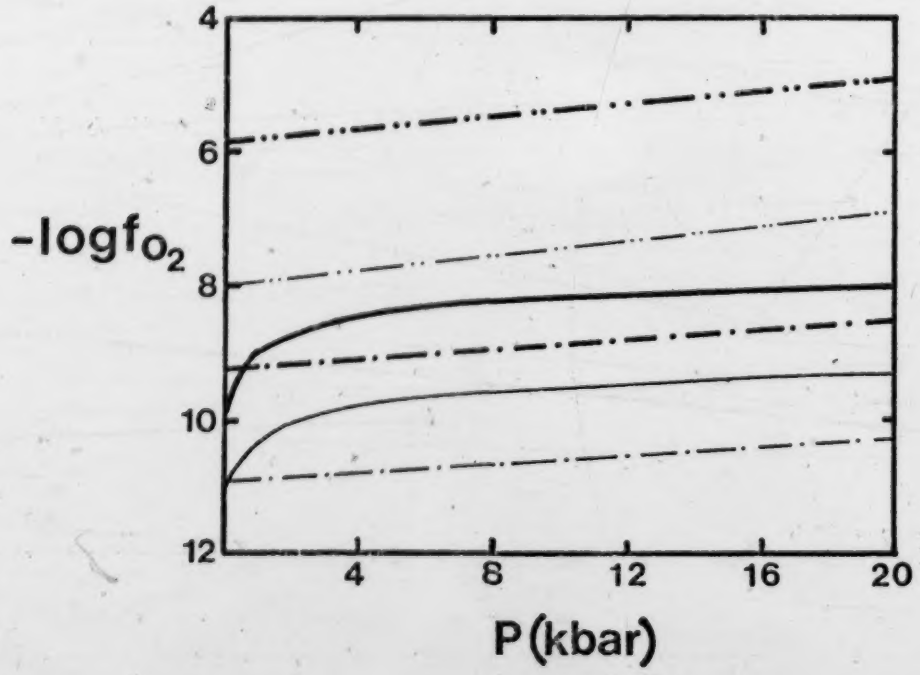

Considerable care was taken to assure that the samples were anhydrous. This was verified in two ways. In the first case a sample (#62 - Table 7) was packed into a Pt capsule with graphite powder. The capsule was then heated to red heat and welded shut. The sealed Pt capsule was loaded into a 1/2" assembly, surrounded by Fe_2O_3, and run. After the experiment, the iron oxide packing was examined both optically and by x-ray diffraction and found to consist only of Fe_2O_3, implying that hydrogen did not diffuse into the sample from the talc pressure medium. Furthermore, the diffusion coefficient determined from that experiment agrees with that determined in another experiment done in the normal fashion (#63 - Table 7). In the second case, the volatile contents of a chip of the alkali basalt starting material and a chip of alkali basalt run in the normal manner at 1350°C and 12 kbar for 2 hours were determined by the method of Harris (1981). The results of those measurements (Table 6) show that the starting material is essentially anhydrous and that it does not gain an appreciable amount of water in a two hour run (twice the duration of the longest diffusion experiment). However, table 7 shows that the CO_2 content of the glass increased from 0.018 wt. % to 0.24 wt. % during the 2 hour experiment. While Eggler and Rosenhauer (1978) and Eggler *et al.* (1979) have shown that dissolved CO_2 can affect melt structure, their results also show that considerably more than 0.2 wt. % are required to produce a measureable effect. Thus, the

effect of dissolved CO_2 has been neglected in this study.

The errors reported for the oxygen diffusion coefficients in Table 7 were calculated by propagating all of the errors due to the determination of FeO, sample mass, experimental duration, and sample radius through eqn. 11. Those errors are reported at the one standard deviation level.

C. Results and Discussion

The results of this study are summarized in Tables 7, 8, and 9 and in figures 7 through 11. The temperature dependence of oxygen diffusivity in silicate liquids is adequately described by an Arrhenius relationship (eqn. 12), where D is the diffusion coefficient, D_o is the Arrhenius frequency factor, E is the activation energy, R is the gas constant, and T is the absolute temperature.

$$D = D_o EXP(-E/RT) \qquad (12)$$

Arrhenius lines were determined isobarically for the nephelinite and the tholeiite at 12 kilobars (fig. 7) and for the alkali basalt at 4, 12, and 20 kilobars (fig. 8). The parameters for the regression lines shown in figures 7 and 8 are given in Table 8. The activation energies determined in this study span the range of previous determinations of activation energy for oxygen diffusion in natural rock melts (54 kcal (Wendlandt, 1980) to 90 kcal (Muehlenbachs and Kushiro, 1974)).

Table 7. Summary of experimental conditions and results.

No.	T°C	P(kbar)	t(min)	FeO(wt %)'	r(cm)	-logD (cm^2/sec)
Alkali basalt (KR-13)						
72a	1280	4	60	9.66±0.03	0.090	6.57±0.10
72b	1280	4	60	10.22±0.13	0.072	6.63±0.15
71a	1280	12	50	9.24±0.05	0.081	6.66±0.11
71b	1280	12	50	10.15±0.07	0.070	6.59±0.13
70a	1350	4	30	10.11±0.03	0.092	6.14±0.12
70b	1350	4	30	9.17±0.06	0.074	6.53±0.13
50	1350	12	30	10.76±0.04	0.077	6.21±0.07
58	1350	12	60	10.94±0.03	0.087	6.36±0.04
57	1350	12	240	11.74±0.05	0.076	≤6.70
59	1350	20	45	8.78±0.04	0.126	6.35±0.03
73a	1400	4	15	9.23±0.06	0.114	5.84±0.13
73b	1400	4	15	10.35±0.04	0.080	5.90±0.15
51	1400	12	120	>11.60	0.144	≤5.84
53	1400	12	30	11.06±0.04	0.125	5.74±0.06
55	1400	12	20	10.09±0.04	0.132	5.72±0.10
86a	1400	14	20	9.39±0.12	0.073	6.32±0.14
86b	1400	14	20	9.54±0.04	0.065	6.39±0.12
81a	1400	16	30	9.58±0.05	0.078	6.40±0.12
81b	1400	16	30	9.29±0.07	0.086	6.38±0.12
79a	1400	20	17	9.53±0.08	0.091	6.03±0.12
79b	1400	20	17	9.87±0.08	0.066	6.24±0.12
56	1450	12	10	8.80±0.04	0.163	5.48±0.07
77	1450	20	15	9.21±0.03	0.122	5.79±0.11
Nephelinite (C-11)						
85	1300	12	45	11.8±0.07	0.087	6.49±0.09
82a	1350	4	30	12.64±0.09	0.079	6.28±0.09
82b	1350	4	30	13.60±0.05	0.065	6.22±0.13
65a	1350	8	30	13.00±0.10	0.126	5.78±0.11
65b	1350	8	30	12.93±0.11	0.138	5.71±0.11
62	1350	12	30	12.73±0.10	0.095	6.08±0.10
63	1350	12	31	11.92±0.05	0.115	6.07±0.08
67a[2]	1350	16	30	12.85±0.14	0.101	6.01±0.12
67b[2]	1350	16	30	12.88±0.06	0.143	5.70±0.17
111[3]	1350	16	18	13.18±0.09	0.071	6.03±0.20
68a	1350	21	30	12.03±0.19	0.078	6.37±0.11
83	1450	12	10	12.11±0.05	0.096	5.70±0.10

Table 7. Summary of experimental conditions and results

1921 Kilauea tholeiite

No.	T°C	P(kbar)	t(min)	FeO(wt%)[1]	r(cm)	-logD (cm^2/sec)
88a	1300	12	120	10.63±0.05	0.096	≤6.43
88b	1300	12	120	10.94±0.05	0.076	≤6.40
89a	1300	12	30	10.03±0.03	0.086	6.14±0.06
89b	1300	12	30	10.25±0.05	0.078	6.16±0.05
112a	1350	4	15	10.03±0.03	0.112	5.61±0.05
112b	1350	4	15	10.14±0.01	0.108	5.61±0.04
113a	1350	6	13	10.21±0.02	0.101	5.59±0.05
113b	1350	6	13	10.47±0.02	0.088	5.61±0.06
114a	1350	8	15	9.85±0.05	0.097	5.78±0.05
114b	1350	8	15	10.29±0.04	0.078	5.84±0.06
90a	1350	12	20	9.97±0.10	0.095	5.89±0.06
90b	1350	12	20	10.80±0.03	0.072	5.80±0.10
109a	1350	16	30	10.08±0.03	0.110	5.91±0.04
109b	1350	16	30	10.35±0.02	0.100	5.91±0.04
108a	1350	20	30	10.14±0.02	0.101	5.97±0.04
108b	1350	20	30	10.42±0.02	0.092	5.96±0.05
105a	1400	12	20	10.24±0.01	0.110	5.69±0.04
105b	1400	12	20	10.24±0.02	0.090	5.86±0.05
87	1450	12	15	10.27±0.01	0.114	5.52±0.05
110	1450	12	10	9.92±0.03	0.114	5.45±0.05

1 - FeO is the wt. % FeO in the sample after the experiment.
2 - Experiment done in 3/4" assembly at 16 kilobars for comparison with experiment #111 (see note 3).
3 - Experiment done in 1/2" assembly at 16 kilobars for comparison with experiments 67a and 67b (see note 2).

Figure 7. Arrhenius plots of the 12 kbar data for the olivine nephelinite (a) and the tholeiite (b). The activation energies are 62±7 kcal for the olivine nephelinite and 51±4 kcal for the tholeiite.

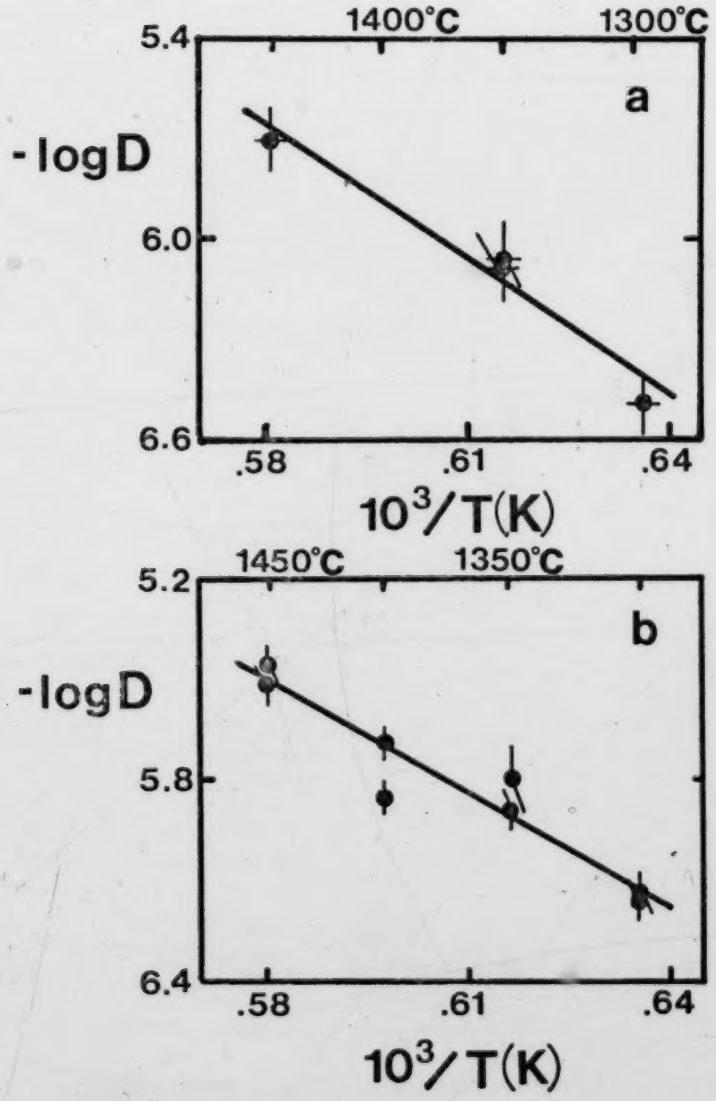

Figure 8. Arrhenius plots for the alkali basalt data at 4 kbar (a), 12 kbar (b), and 20 kbar (c). The activation energies are 70±7 kcal (4 kbar), 86±6 kcal (12 kbar), and 71±14 kcal (20 kbar).

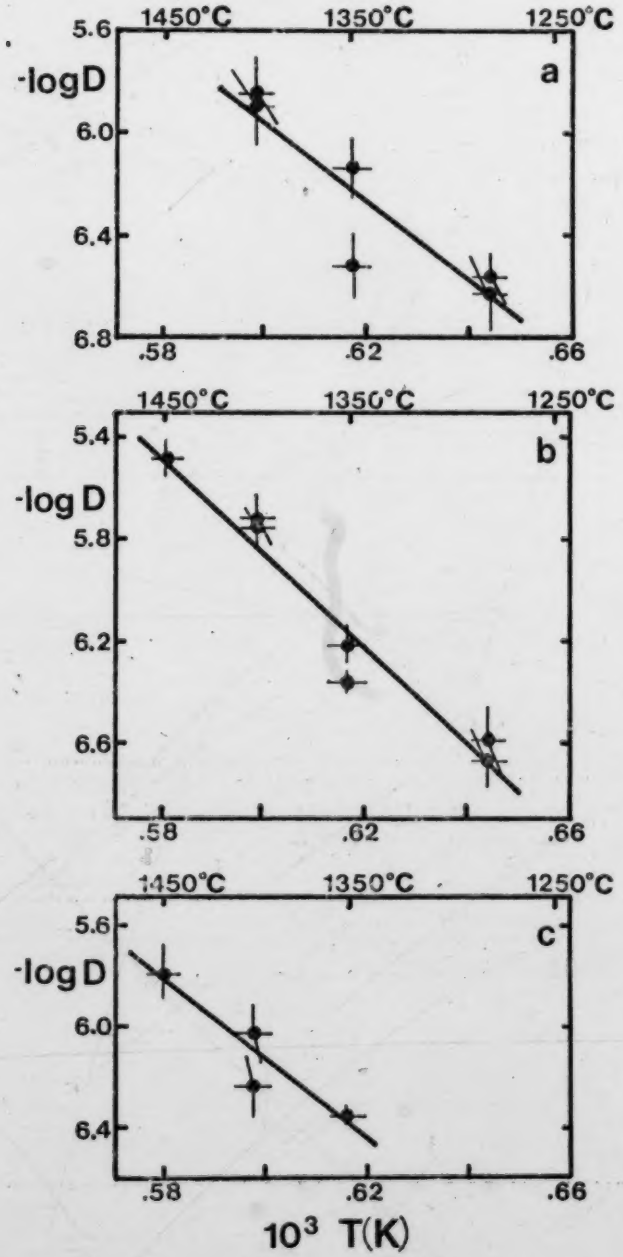

Table 8. Parameters for Arrhenius equations for the isobaric oxygen diffusion data.

Composition	P(kb)	$\log_{10} D_o$ (cm^2/sec)	E(kcal)	r^2
Nephelinite	12	2.23±0.97	62±7	0.94
Alkali basalt	4	3.21±2.51	70±7	0.81
Alkali basalt	12	5.45±0.81	86±6	0.95
Alkali basalt	20	3.23±1.87	71±14	0.85
Tholeiite	12	0.99±0.59	51±4	0.91

The parameters above were determined in each case by least squares analyses of the entire data set. Errors were calculated by the method of Birge (1932) and are reported at the one standard deviation level. r^2 is the correlation coefficient for the regression analysis.

The effect of pressure on oxygen diffusion in the three melts was investigated isothermally at 1350°C for the nephelinite (fig. 9) and the tholeiite (fig. 11) and at 1400°C for the alkali basalt (fig. 10). Figures 9, 10, and 11 show that the pressure dependence of oxygen diffusion in basaltic liquids is not simple. The olivine nephelinite (fig. 9) exhibits an increase in oxygen diffusivity with increasing pressure from 4 to 8 kilobars followed by an apparent sharp decrease between 8 and 12 kilobars. Above 8 kilobars the oxygen diffusivity continues to increase, but the pressure dependence is smaller. The tholeiite and the alkali basalt show sharp decreases in oxygen diffusivity with increasing pressure at 6-8 kilobars and 12-14 kilobars,

Figure 9. Isothermal (1350°C) polybaric diffusion data for the olivine nephelinite. The two lines yield activation volumes of -39±3 cm³ (4-8 kbar) and -4±2 cm³ (12-16 kbar). The preliminary phase liquidus phase relations for C-11 nephelinite (Shimada and Scarfe, unpublished) are also shown.

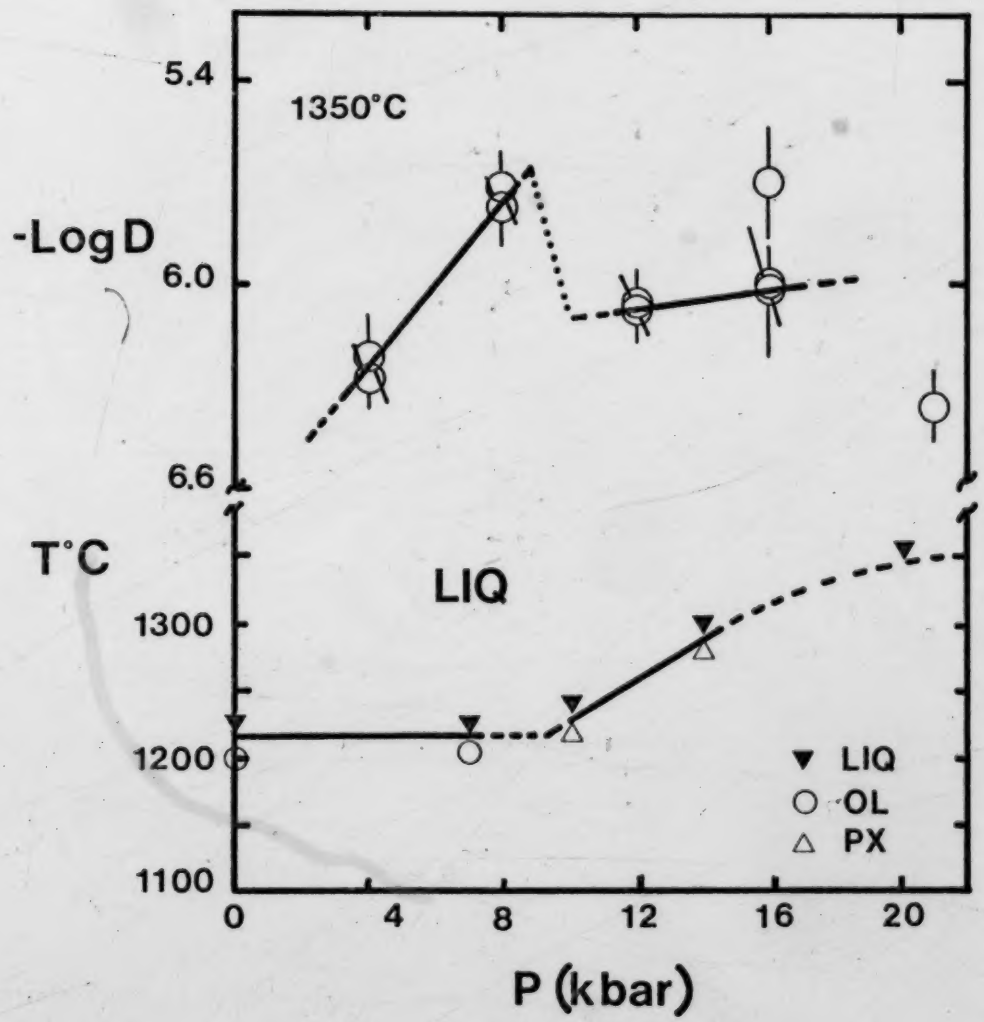

respectively (figures 11 and 10).

The pressures at which the decreases in diffusivity occur for the three melts correspond well to the pressures of the first occurrence of pyroxene as a liquidus phase. Except for the nephelinite, phase equilibrium data are not presently available for the actual melt compositions studied, but there are data available for compositionally similar melts. Figure 10 shows the liquidus relationships of an alkali-olivine basalt determined by Takahashi (1980) in addition to the oxygen diffusion data. Pyroxene first appears as a liquidus phase at approximately 13.5 kilobars in that basalt. Similarly, fig. 11 shows the liquidus phase relationships for 1959 Kilauea tholeiite (Fujii, unpublished). The correlation between the decrease in oxygen diffusivity and the first occurrence of pyroxene as a liquidus phase is even better than for the alkali basalt.

Except for the transition zones noted above the pressure dependence of the diffusivity of oxygen can be described by an Arrhenius relationship (eqn. 13):

$$D = D_0 \cdot EXP(-PV_a/RT) \qquad (13)$$

where D is the diffusion coefficient at the pressure of interest, D_0 is the zero pressure diffusion coefficient, P is the pressure, V_a is the activation volume, and R and T are the same as in eqn. 12. The solid lines in figures 9, 10, and 11 are least squares fits of eqn. 13 to the diffusion data. The activation volume for the high pressure portion of the nephelinite data does not include either the

Figure 10. Isothermal (1400°C) polybaric diffusion data for the alkali basalt. The two solid lines give activation volumes of -6±1 cm^3 (4-12 kbar) and -13±4 cm^3 (14 to 20 kbar). Also shown are the phase relationships for an alkali basalt reproduced from Takahashi (1980). The coincidence of the abrupt decrease in oxygen diffusivity with the first appearance of pyroxene as a liquidus phase is discussed in the text.

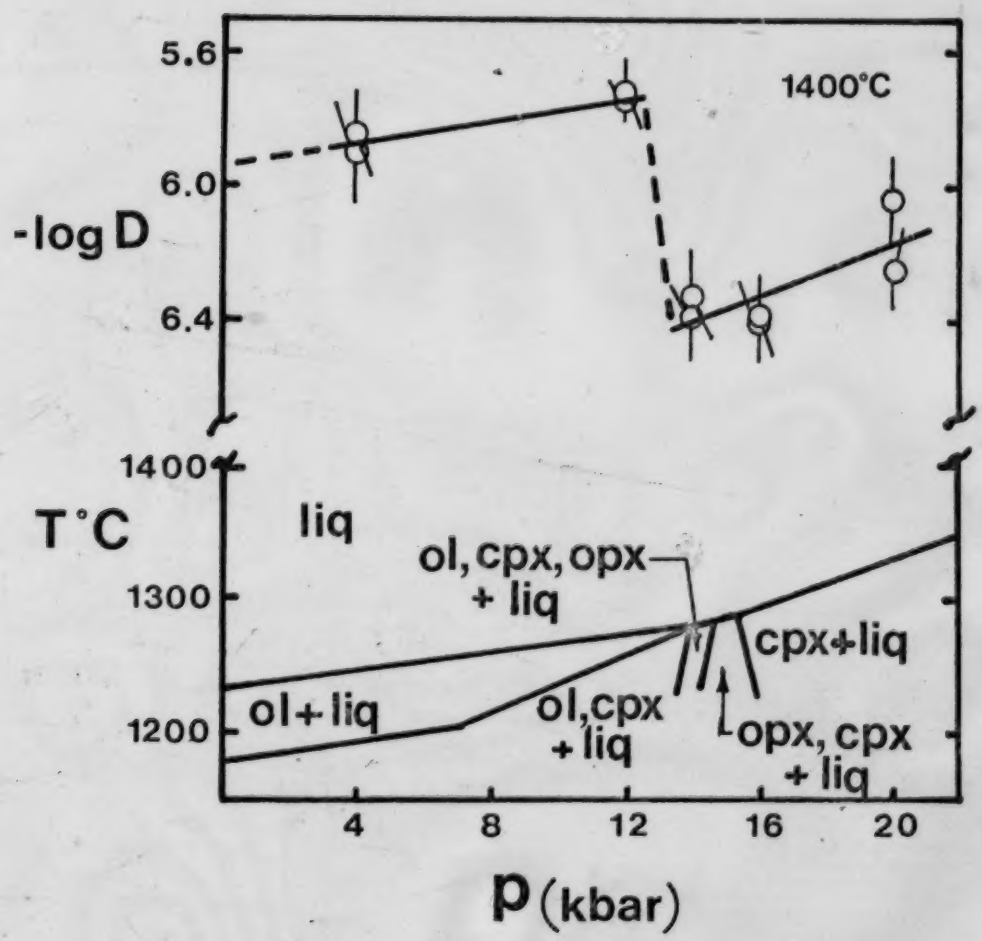

Figure 11. Isothermal (1350°C) polybaric diffusion data for the tholeiite. The two solid lines give activation volumes of -1.5±2 cm³ (4-6 kbar) and 4±1 cm³ (8-20 kbar). The phase relationships of 1959 Kilauea tholeiite (Fujii, unpublished) are also shown. The coincidence of the sharp decrease in oxygen diffusivity and the first appearance of clinopyroxene as a liquidus phase is discussed in the text.

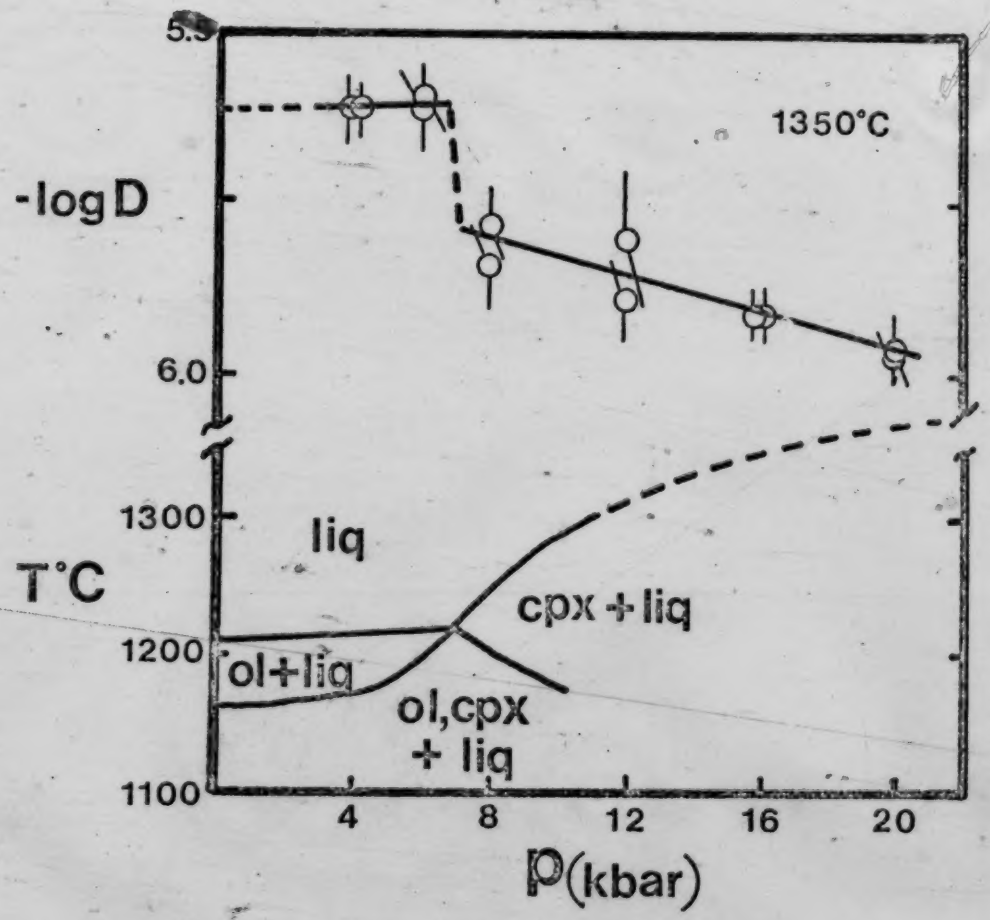

data point at 21 kilobars or the apparently erroneous point at 16 kilobars (fig. 9). The point at 21 kilobars was excluded because the preliminary liquidus curve for the nephelinite (fig. 9) shows 1350°C to be below the liquidus at 21 kilobars. The coefficients for those equations are given in table 9. It is of interest to note, except for the high pressure portion of the tholeiite data, that the activation volumes are negative.

Activation volumes for diffusion in melts have been interpreted as being related to the volume of the diffusing species (Hamann, 1965; Watson, 1979; and Watson *et al.*, 1982) and also to the sum of the volume of the diffusing species and the volume change during the jump from "site" to "site (jump volume) (e.g. Tyburczy and Waff, 1983). Both interpretations were developed principally to explain the positive activation energies observed for cation diffusion and neither of them provides an explanation for the negative activation volumes observed in this study.

Oxygen, because of its unique structural role in silicate melts, is unlikely to diffuse in strictly the same manner as do cations. Dunn (1982) speculates that oxygen diffuses by a combination of the movement of free oxygen anions (O^{2-}) and larger silicate anions. Furthermore, Dunn (1982) also suggests that with changing conditions the relative contributions from the different diffusing species may change due to changes in the relative proportions of those species. Koros and King (1962) and Muehlenbachs and

Kushiro (1974) propose that oxygen diffuses by transfer between different anionic units during reactions involving the breaking of Si-O bonds. The activation volumes to be expected from those mechanisms are quite different. The activation volume for Dunn's suggested mechanism is related to the average volume of the diffusing species, or when the proportions of the diffusing species change, to the sum of the average volume of the diffusing species and the change in the average volume due to changes in the proportions of species of different sizes. If oxygen diffuses by transfer during reactions among various anionic species, the activation volume may be related to the volume changes of the reactions.

The diffusion coefficients for oxygen determined in this study are approximately the same as the diffusion coefficients of divalent cations in basaltic liquids (see fig. 3, chapter 2). Therefore it seems reasonable to suggest that the principal diffusing species is the free oxygen anion (O^{2-}). With the exception of the value at 12 kilobars for the alkali basalt (Table 9), the activation energies determined in this study are too small to be associated with the rupture of either Si-O or Al-O bonds. Therefore, (with one exception) it is unlikely that there is a large contribution to the diffusivity of oxygen in the melts studied from a mechanism involving bond rupture. If, as Dunn (1982) suggests, the diffusion of oxygen is by the movement of O^{2-} and other silicate anionic units, then the observed

Table 9. Parameters for Arrhenius equations for the isothermal oxygen diffusion data.

Composition	T°C	P(kb)	$-\log_{10} D_o$ (cm^2/sec)	V_a(cm^3	r^2
Nephelinite	1350	4-8	6.75±0.05	-39±3	0.98
Nephelinite	1350	8-21	5.51±0.15	-4±2	0.92
Alkali basalt	1400	4-12	5.94±0.02	-6±1	0.91
Alkali basalt	1400	14-20	6.97±0.18	-13±4	0.61
Tholeiite	1350	4-6	5.63±0.10	-1.5±2	0.33
Tholeiite	1350	8-20	5.70±0.06	4±1	0.82

The parameters above were determined in each case by least squares analyses of the entire data set. Errors were calculated by the method of Birge (1932) and are reported at the one standard deviation level. r^2 is the correlation coefficient for the regression.

activation volumes can be related to the changes in the average volume of the diffusing species as the proportions of the diffusing species change with increasing pressure. Negative activation volumes then reflect a decrease in the average size of the diffusing species (an increase in O^{2-}). As smaller anions are expected to be more mobile than larger anions, such a change in anionic speciation is compatible with the observed increases of oxygen diffusivity. Similarly, the observed decreases in oxygen diffusivity (figs. 9, 10, and 11) can be explained by a decrease in the proportion of O^{2-}, which imparts a positive activation volume as is required for those changes. This model, while

it is compatible with the results, remains speculative because the identities, relative proportions, and partial molar volumes of the anionic species present in the melts studied are unknown.

The observed decreases in oxygen diffusivity (figs. 9, 10, and 11) imply that the melt undergoes a change of some sort at 8-12 kilobars for the nephelinite, at 12-14 kilobars for the alkali basalt and at 6-8 kilobars for the tholeiite. The observation that those pressures are close to the pressures where olivine is replaced by pyroxene as the liquidus phase (figs. 9, 10, and 11), implies that the change in the melt involves an increase in the activity of pyroxene building units (short chain anions) relative to the activity of olivine building units (monomers) for the two melts. Tyburczy and Waff (1983) have observed that the slope of the log of electrical conductivity *versus* pressure decreases sharply between 5 and 8 kilobars for a Hawaiian tholeiite melt. They postulate, on the basis of their data, that Hawaiian tholeiite melt undergoes a pressure induced depolymerization reaction in the pressure range 5-8 kilobars. The viscosities (Kushiro, 1976; Scarfe *et al.*, 1979 and Scarfe, 1981) and densities (Fujii and Kushiro, 1977; Scarfe *et al.*, 1979; and Kushiro, 1980) of basaltic melts do not show sharp changes at the same pressures as the observed changes in oxygen diffusivity. Therefore, the change that occurs at 8-12 kilobars for the nephelinite, 6-8 kilobars for Kilauea tholeiite and 12-14 kilobars for the

alkali basalt, does not involve either a large volume change, or a major depolymerization of the melt.

The pressure dependence of oxygen diffusion for the melts studied is sufficiently varied that no one model can adequately explain the entire data set. The diffusion coefficients determined for oxygen in this study are of the same order of magnitude as cation diffusivities in basaltic liquids (see fig. 3, chapter 2). Therefore, it seems reasonable to speculate that the principal diffusing species is the oxygen anion (O^{2-}). The abrupt decreases in oxygen diffusivity at approximately the pressures where olivine is replaced by pyroxene as the liquidus phase in the three melts are compatible with pressure induced depolymerization of the melt. Because of the lack of partial molar volume data for the anionic species it is not possible to write a specific depolymerization reaction. However, the changes in the phase equilibria suggest that, in addition to decreasing the oxygen diffusivity, the reaction that occurs also consumes small depolymerized anions (olivine building units) and produces larger, but still relatively depolymerized anions (pyroxene building units). Therefore, it is suggested that the reaction is not a simple depolymerization reaction. Rather, it may be a complex reaction in which large polymerized anions react with small depolymerized anions and oxygen anions to produce anions of intermediate degrees of polymerization. A hypothetical reaction, representative of that class of reactions is given in eqn. 14:

$$Si_2O_5^{2-} + SiO_4^{4-} + O^{2-} \rightleftharpoons Si_3O_{10}^{8-} \quad (14)$$

where $Si_2O_5^{2-}$ represents a sheet like structure and $Si_3O_{10}^{8-}$ represents a short chain structure. If reactions such as reaction 14 occur, they result in a net depolymerization of the melt while simultaneously decreasing the proportions of small relatively mobile oxygen bearing species. Thus, a reaction like reaction 14 can account for both the observed changes in phase equilibria and the changes in oxygen diffusivity.

As noted above, the melts studied are expected to show decreases in viscosity with increasing pressure. If oxygen diffusion is inversely related to viscosity as suggested by Oishi *et al.* (1975) and Dunn (1982) then the diffusivity should increase continuously with pressure for the three melts studied. The results of this study show that this is not the case and lead to the conclusion that the mechanisms of oxygen diffusion and viscous flow are not related for basaltic liquids.

The parameters in Table 8 can be used to define a compensation law for oxygen diffusion in basaltic liquids. The resultant line is given in eqn. 15:

$$\log_{10} D_o = 1.27 \times 10^{-4} E - 5.64 \qquad r^2 = 0.99 \quad (15)$$

Dunn (1982) has determined a compensation law for oxygen diffusion in a variety of simple silicate melts and three natural rock melts. Eqn. 15 is essentially the same as Dunn's compensation law and is also indistinguishable from the compensation law for cationic diffusion in silicate

melts given by Hofmann (1980). The compensation law result further supports the contention that oxygen diffuses principally as O^{2-}.

The compensation law results show that the activation energies determined in this study are reasonable in comparison with other oxygen diffusion results. The activation energy for the tholeiite (51±4 kcal) is indistinguishable from that reported by Wendlandt (1980) for a tholeiitic basalt (54 kcal). While the physical meaning of activation energies in liquids in not clear (Dunn, 1982), it is interesting to consider the variation in activation energy of the alkali basalt as a function of pressure. At 12 kilobars the activation energy for oxygen diffusion is considerably larger than at either 4 or 20 kilobars (Table 8). Twelve kilobars is very near the transition pressure for the alkali basalt (fig. 10). The increased activation energy at 12 kilobars (relative to 4 and 20 kilobars) suggests that the activation energy is related to structural transformations in the melt. Muehlenbachs and Kushiro (1974) argue, on the basis of their 90 kcal activation energy for oxygen diffusion in a basalt melt, that oxygen diffusion involves Si-O bond rupture. Similarly, the 86 kcal activation energy for the alkali basalt may reflect the occurrence of a reaction among the various anionic species at 12 kilobars pressure.

D. Conclusions

This study has shown that the pressure dependence of oxygen diffusivity in basaltic liquids is quite different from that shown by cations in simple silicate liquids (Watson, 1979; Watson and Bender, 1980). Variations in oxygen diffusion coefficients with pressure can be related to the liquidus phase mineralogy and by extension to the anionic constitution of the melt. As such, oxygen diffusion measurements provide a very sensitive probe into the variation of melt structure with pressure.

The data suggest that the principal diffusing species is the O^{2-} anion. The observed changes in the diffusivity with pressure can be attributed to changes in the relative proportions of O^{2-} and other small anionic species (SiO_4^{4-} etc.) during pressure induced reactions in the melt. While it is not possible to specifically identify those reactions, the correlation of the changes in diffusivity and liquidus phase equilibria suggest that with increasing pressure O^{2-} anions and olivine building units are consumed in reactions which produce pyroxene building units.

This study has shown that the diffusivity of oxygen in basaltic liquids is very sensitive to structural changes in the melt. Oxygen diffusion determinations indicated the presence of melt structure changes that do not show up in either the viscosity or density data. Therefore, oxygen diffusion measurements constitute one of the most sensitive probes into the variation of melt structure with pressure

presently available.

IV. The Effect of Thermal History on the Structure of Pb_2SiO_4 Melts

A. Introduction

Recent work on the effect of cooling rate on the crystallization of Pb_2SiO_4 melts (Gotz *et al.*, 1980) and $CaMgSi_2O_6$ melts (Kirkpatrick *et al.*, 1981) has shown that both the order and temperature of crystalline phase occurrence are dependent on the thermal history of the melt. Gotz *et al.* (1980) observed that different lead silicate phases crystallized from Pb_2SiO_4 melt depending on the thermal history of the melt. Similarly, Kirkpatrick *et al.* (1981) found that, depending on the cooling rate, either forsterite or diopside crystallized first from melts of diopside composition. In both cases, the phases which crystallized from melts with different thermal histories had different structures. The crystallization of structurally different phases from isochemical melts with different thermal histories implies that the structures of those melts depend on thermal history. Such differences may be due to changes in the relative proportions of the silicate anionic species in the melt without altering the anionic speciation (Mysen *et al.*, 1980d), or to changes in the anionic speciation of the melt (Gotz *et al.*, 1980).

This paper presents the results of a study of the effect of thermal history on lead orthosilicate (Pb_2SiO_4) melts. There are several reasons for choosing to study

Pb_2SiO_4 melts rather than more geologically significant compositions. Orthosilicate melts have a non-bridging oxygen to tetrahedral cation ratio (NBO/T) of 4 (Mysen *et al.*, 1980d). According to the anionic speciation equations of Mysen *et al.* (1982b), a melt with NBO/T = 4 should have SiO_4^{4-} monomers, $Si_2O_7^{6-}$ dimers and O^{2-} anions as its only anionic species. If NBO/T is fixed by the bulk composition of the melt, an orthosilicate melt should be isostructural under all conditions. The results of Gotz *et al.* (1980) suggest that this is not the case for Pb_2SiO_4 melts. If the structure of Pb_2SiO_4 melt varies as a function of thermal history, then NBO/T for that melt must also be a function of thermal history. Consequently, it is important to determine if and how the structure of Pb_2SiO_4 melt varies with thermal history.

Pb_2SiO_4 is virtually the only orthosilicate whose melt may be easily quenched to glass. More geologically meaningful orthosilicate melts (Mg_2SiO_4, Fe_2SiO_4, and Ca_2SiO_4) can only be quenched to glass with the aid of exotic rapid quenching techniques. For example, Kusabiraki and Shiraishi (1981) employed a splat quenching device to quench Fe_2SiO_4 to glass. It may be argued, because lead orhtosilicate melts are easily quenched to glass, that they are not representative of other less easily quenched orthosilicate melts. However, comparison of the infrared (IR) spectra of Pb_2SiO_4 glasses, prepared by rapid quenching after short duration fusions, with the IR spectrum of

Fe_2SiO_4 glass (Kusabiraki and Shiraishi, 1981) (fig. 12) shows that lead orthosilicate is representative of other orthosilicate melts. However, the principal Si-O stretching envelope is broader and shifted to slightly higher frequency for the Fe_2SiO_4 spectrum as compared to the Pb_2SiO_4 spectrum. As is discussed later, those differences imply that vitreous Fe_2SiO_4 may be more polymerized than vitreous Pb_2SiO_4. Thus, conclusions drawn from the study of lead orthosilicate melts may be extended to other orthosilicate compositions.

Infrared spectroscopy can be a very powerful probe into the structure of silicates (e.g. Billhardt, 1969; Furukawa *et al.*, 1978, 1979; Tarte, 1963). Billhardt (1969) has shown that IR spectroscopy is particularly sensitive to the vibrations of Si-O-Si bridging bonds. All silicate anions larger than the monomer (SiO_4^{4-}) have Si-O-Si bridges. Therefore, since the principal aim of this study was to determine if anionic units larger than either the monomer or the dimer are present in lead orthosilicate melts, IR spectroscopy was chosen as the structural probe for use in this study.

Due to the difficulty of taking IR spectra of high temperature silicate melts, glasses formed by rapid quenching of melts were investigated. Sweet and White (1969), Sharma *et al.* (1978), and Seifert *et al.* (1981) have all shown that glasses formed by rapid quenching of silicate melts are structurally representative of the melts from

Figure 12. Infrared spectra of a. vitreous Pb_2SiO_4 (Pb-1) and b. vitreous Fe_2SiO_4 (Kusubiraki and Shiraishi, 1981).

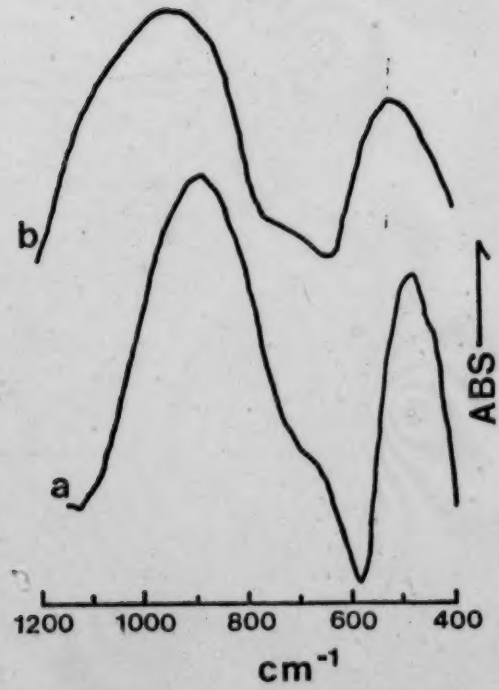

which they were quenched. However, their determinations were not for orthosilicate glasses and this study is dependent on the validity of the assumption that their results can be extended to orthosilicates. The need to work on glass was the final factor in the choice of Pb_2SiO_4 as the subject of this study.

B. Experimental

The Pb_2SiO_4 glasses were prepared by cooling at various rates though the temperature interval 850 to 700°C. Infrared spectra were taken of the glasses as described below. All experiments were done on aliquots of two 5 gram batches of Pb_2SiO_4 glass prepared from reagent grade PbO and $SiO_2.nH_2O$. Experiments Pb-1 through Pb-10 were done on aliquots of one batch and experiments Pb-11 through Pb-14 were done on splits of the second batch (Table 10). The reagents were dried to constant weight (PbO - 200°C and $SiO_2.nH_2O$ - 1400°C). After weighing, the reagents were thoroughly mixed by grinding under alcohol in an agate mortar. The resultant mixture was then put through three cycles of fusion followed by grinding. All fusions were done at 850°C and had a duration of two hours. Chips of the glass were analyzed via electron microprobe and found to be homogenous and on composition (Table 10).

The electron microprobe analyses were done on the University of Alberta ARL-EMX microprobe by both energy dispersive (EDA) and wavelength dispersive (WDA) methods.

Table 10. Analyses of starting materials and experimental products.

No.	SiO_2	PbO
Batch	11.81	88.19
Pb-1	11.90	88.10
Pb-5	11.92	88.08
Pb-6	11.90	88.10
Pb-7	11.81	88.19
Pb-8	11.88	88.12
Pb-9	11.79	88.21
Pb-10	11.92	88.08
Pb-11	10.66	89.34
Pb-12	10.99	89.01
Pb-13	11.01	88.99
Pb-14	10.84	89.16

Analyses were done on chips of glass by electron microprobe as described in the text. Analyses are normalized to 100.

Galena and quartz were used as standards for the EDA analyses and the data were reduced with the computer program EDATA2 (Smith and Gold, 1979). The glasses analyzed by EDA and a lead silicate glass standard (EPS-22) were used as the standards for the WDA analyses. The WDA data were reduced by hand using atomic number, absorption, and fluorescence corrections.

Approximately 200 milligram aliquots of the starting glass were placed in Pt envelopes which were crimped shut, but not sealed. The capsules were left open to air to retain the lead in the divalent state (Smart and Glasser, 1978).

All of the experiments were done in a Deltech vertical tube furnace. Temperatures were monitored by a Pt-$Pt_{.7}Rh_{.3}$ thermocouple placed within 1-2 mm of the sample. Thermocouples were calibrated against the melting point of Au. Cooling rates were controlled with a Love cooling rate controller. In all cases, samples were quenched by dropping the Pt envelopes directly from the furnace into water. The resultant quench rate is estimated to be in excess of 500°C/sec.

The experiments were done in four series. The first series of four experiments consisted of thirty minute fusions at four superliquidus temperatures (760, 850, 964, and 1100°C) followed by rapid quenching. The second series of three experiments involved a thirty minute fusion at 850°C, followed by controlled cooling at one of three rates (5.0, 0.7, or 0.1°C/min.) to 700°C and then rapid quenching. The third series of three experiments utilized the same fusion durations, temperatures, and cooling rates as the second series of experiments, but upon reaching 700°C the samples were held for 48 hours prior to quenching. The fourth series of four experiments involved a thirty minute fusion at 850°C, followed by cooling to 700°C at 0.1°C/min. The samples were then held for different times (6, 12, 24, and 36 hours) at 700°C prior to quenching. Experimental conditions are summarized in Table 11. There was no evidence of crystallization at 700°C. According to Gotz *et al.* (1980), larger degrees of undercooling are required for

nucleation and crystal growth. A chip of glass from each of the longer duration experiments was analyzed by electron microprobe to ascertain that the samples had not changed composition during the course of the experiments. The analyses of the samples are given in Table 10. The analyses of the experimental products are all within analytical precision of the theoretical composition. Experiments Pb-11 through Pb-14 are slightly lower in SiO_2 than Pb-1 through Pb-10, but the difference is not sufficient to acount for the structural changes noted below.

The IR spectra were taken at a resolution of 4 cm^{-1} on KBr discs, containing 1.0 wt. % glass, using a computer controlled Nicolet 7199 Fourier transform IR spectrometer in the transmission mode. Fifty scans of the 4000-400 cm^{-1} spectral region were collected and computer averaged for each sample. Such averaging enhances the signal to noise ratio by a factor of approximately 7 relative to a single scan of the spectrum. Replicate spectra were taken on several samples after rotating the KBr disc to assess the effect of finite sample particle size. No differences were observed between replicate spectra. The spectra were transformed from transmittance to absorbance prior to printing. As there are no features attributable to silicate anionic vibrations above approximately 1200 cm^{-1} , only the 400-1200 cm^{-1} portions of the spectra are reported here.

Table 11. Summary of experimental conditions and procedures.

#	T(i)°C	T(f)°C	t(i) (min)	Rate (deg/min)	t(f) (min)	t(t) (min)
Pb-1	760	760	30	---	---	30
Pb-2	850	850	30	---	---	30
Pb-3	964	964	30	---	---	30
Pb-4	1100	1100	30	---	---	30
Pb-5	850	700	30	5.0	0	60
Pb-6	850	700	30	0.7	0	245
Pb-7	850	700	30	0.1	0	1530
Pb-8	850	700	30	5.0	2880	3060
Pb-9	850	700	30	0.7	2880	3125
Pb-10	850	700	30	0.1	2880	4410
Pb-11	850	700	30	0.1	360	1890
Pb-12	850	700	30	0.1	720	2250
Pb-13	850	700	30	0.1	1440	2970
Pb-14	850	700	30	0.1	2160	3690

T(i) - Initial fusion temperature.
T(f) - Final experimental temperature.
t(i) - Initial fusion duration.
Rate - Cooling rate.
t(f) - Duration at final temperature.
t(t) - Overall length of experiment.

C. Results

The results of this study are in the form of IR spectra, as shown in figures 13-16 which represent the series 1-4 experiments, respectively. In all cases the spectra are characterized by two major bands. The first band, centered at 480 cm^{-1}, is of roughly gaussian shape, but shows a slight high frequency shoulder at 500-520 cm^{-1}. The other band, centered around 880 cm^{-1}, varies considerably in form. In all cases there is a definite low

frequency shoulder in the 630-680 cm^{-1} region. Details of the spectra for each series are given below. Vibrational mode assignments are discussed in a following section.

Series one

The spectra of the series one experiments are shown in fig. 13. It is apparent from fig. 13 that the spectra of glasses rapid quenched after short duration fusions at various superliquidus temperatures are essentially identical. This is in agreement with results obtained from similar experiments for glasses of diopside composition (Mysen and Virgo, 1980; Dunn - unpublished data). These spectra are also qualitatively indistinguishable from spectra of Pb_2SiO_4 glass reported by Furukawa *et al.* (1978) and Gotz *et al.* (1980).

As mentioned above, the spectra are dominated by two bands at 480 and 880 cm^{-1}. While the 480 cm^{-1} band is very nearly gaussian in shape (there is a slight high frequency asymmetry which implies a shoulder around 500 cm^{-1}), the 880 cm^{-1} band is definitely a composite band. The 880 cm^{-1} band has a high frequency shoulder (approximately 900 cm^{-1}) and a low frequency shoulder (approximately 800 cm^{-1}), both of which are indicated by slope changes. In addition, there is a more prominent shoulder on the low frequency side centered around 650 cm^{-1} .

Series two

Fig. 14 shows the results of the series two experiments (30 minute fusions at 850°C followed by controlled cooling

Figure 13. Infrared spectra of the series one experiments. The spectra are stacked in order of increasing fusion temperature (760°C - Pb-1; 850°C - Pb-2; 964°C - Pb-3; and 1100°C - Pb-4). Salient features discussed in the text are marked by arrows.

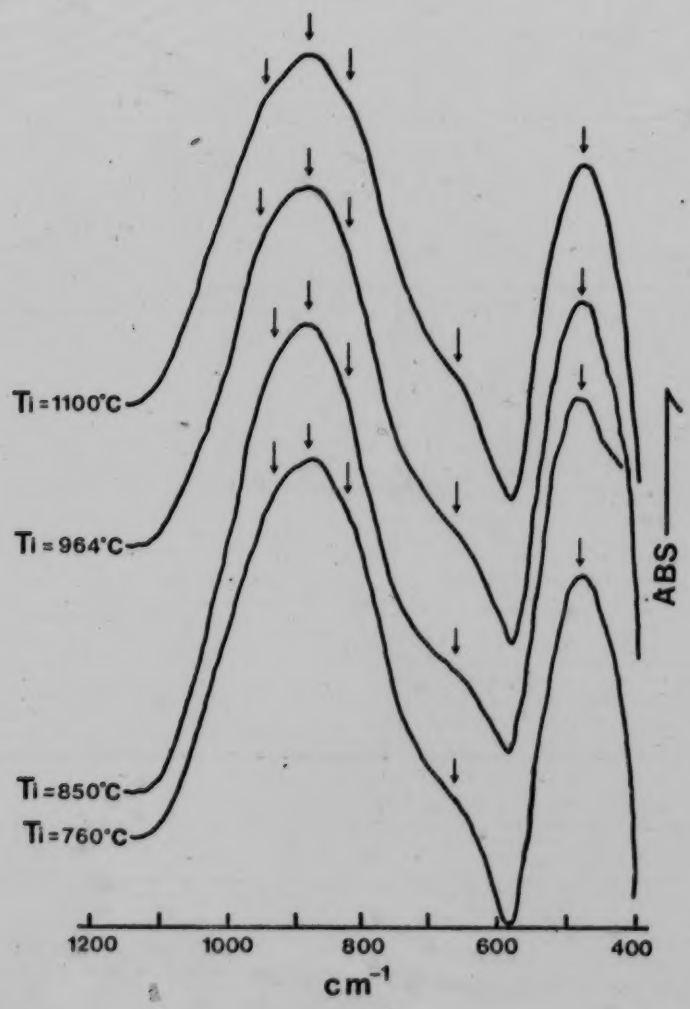

Figure 14. Infrared spectra of the series two experiments. Samples were cooled from 850 to 700°C at different cooling rates (5.0°C/min - Pb-5; 0.7°C/min - Pb-6; and 0.1°C/min - Pb-7). Salient features discussed in the text are marked by arrows.

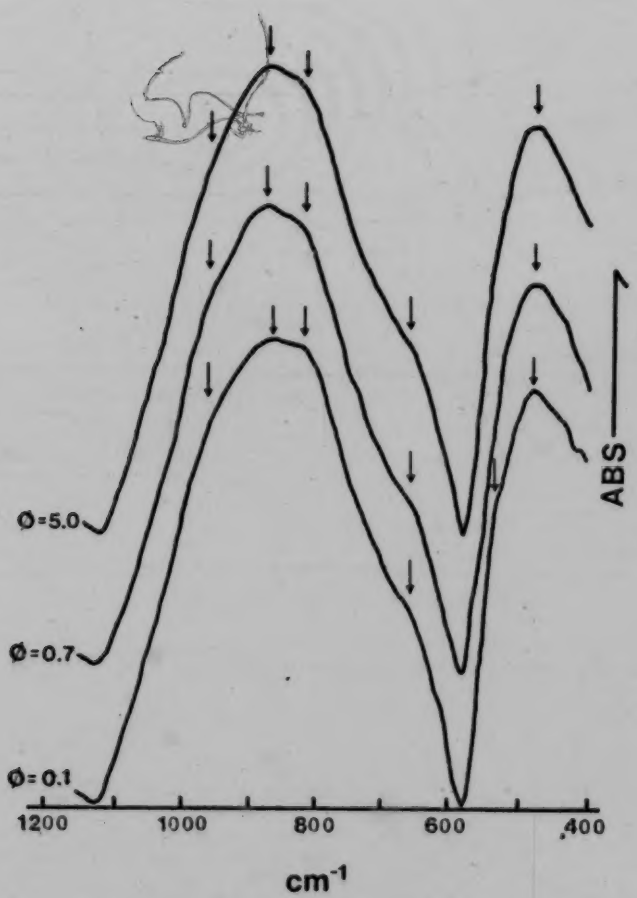

at various rates to 700°C and then rapid quenching). Qualitatively, the spectra are very similar to the series one results. However, there are notable differences. The 480 cm^{-1} band is very similar to that in the series one spectra, except that the high frequency shoulder is more pronounced in the spectrum of the sample cooled at 0.1°C per minute. The 880 cm^{-1} band is significantly different from that observed in the series one experiments and also varies systematically in form as a function of cooling rate. In general, the high frequency band is characterized by a maximum at 860-870 cm^{-1} , with definite low frequency shoulders centered at 800 and 650 cm^{-1} , as well as an asymmetry on the high frequency side. With decreasing cooling rate, the 800 cm^{-1} shoulder increases in intensity as does the high frequency asymmetry. The 650 cm^{-1} band shows no discernable dependence on cooling rate.

Series three

The results of the series three experiments (30 minute fusion at 850°C followed by controlled rate cooling at various rates to 700°C and then holding at 700°C for 48 hours prior to quenching) are shown in fig. 15. The spectra show three distinct morphologies. The spectrum of the sample cooled at 5°C/min is indistinguishable from both the series two experiment that has the same cooling rate and the series one experiments. Similarly, the 0.7°C/min spectrum is essentially identical to its series two counterpart. However, the 0.1°C/min experiment shows significant changes

Figure 15. Infrared spectra of the series three experiments. Samples were cooled from 850 to 700°C at different cooling rates (5.0°C/min - Pb-8; 0.7°C/min - Pb-9; and 0.1°C/min - Pb-10) and then held at 700°C for 48 hours. Salient features discussed in the text are marked with arrows.

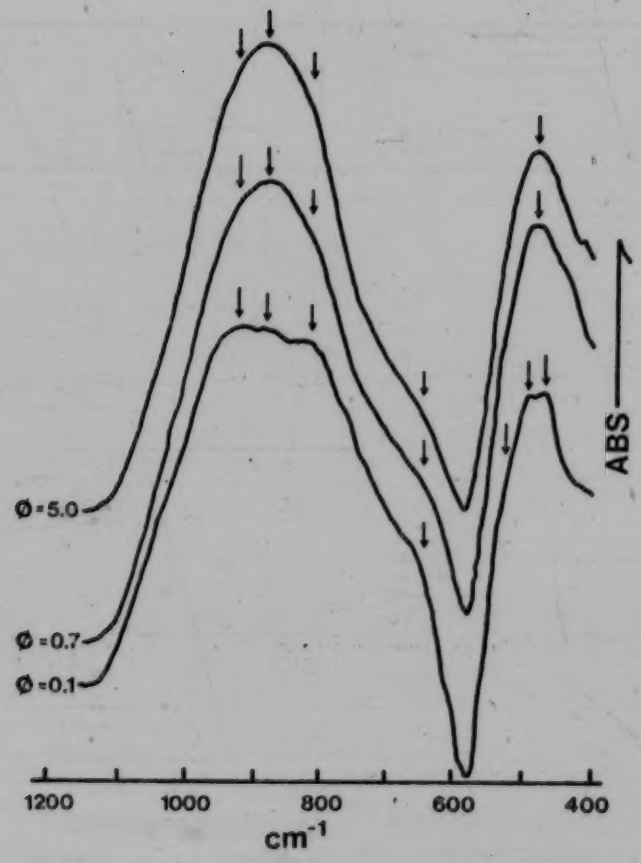

as a function of thermal soaking at 700°C relative to the corresponding series two experiment. The 480 cm^{-1} band in that spectrum shows two maxima (465 cm^{-1} and 485 cm^{-1}) and a definite shoulder at about 525 cm^{-1} . The largest differences are observed in the 880 cm^{-1} band. That band displays three distinct maxima at 920 cm^{-1} , 880 cm^{-1} , and 820 cm^{-1} . The shoulder at 650 cm^{-1} appears unchanged relative to other series 1, 2, and 3 spectra, except for experiment PB-10 where it is of increased intensity. In addition, the center of the band (determined at half maximum) is shifted to 856 cm^{-1} , approximately 20 cm^{-1} lower in frequency than observed for any other series 1, 2, or 3 experiments. It appears that thermal soaking at 700°C has no significant effect on melts cooled at 0.7°C/min or faster.

Series four

The results of the series four experiments (30 minute fusion at 850°C followed by cooling at 0.1°C/min to 700°C and then thermal soaking at 700°C for various times prior to quenching) and the series three experiment that was cooled at 0.1°C/min are shown in fig. 16. The spectra in fig. 16 are stacked in order of increasing thermal soaking time with the shortest soaking time (Pb-11: 6 hours) at the bottom and the longest soaking time experiment (Pb-10: 48 hours) at the top. With increasing soaking time the 480 cm^{-1} band shows an increase in the intensity of its high frequency shoulder (500-520 cm^{-1}). Similarly, the high frequency shoulder and

Figure 16. Infrared spectra of the series four experiments. Samples were cooled from 850 to 700°C at 0.1°C/min and then held at 700°C for varying times (6hr. - Pb-11; 12hr. - Pb-12; 24 hr. - Pb-13; 36hr. - Pb-14; and 48hr. - Pb-10). Salient features discussed in the text are marked by arrows.

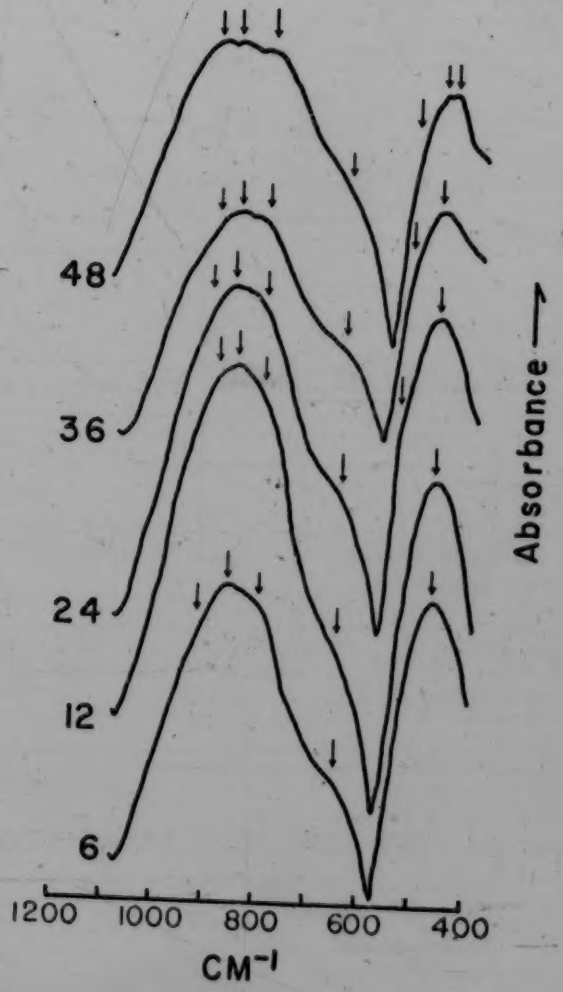

the 820 cm^{-1} shoulder in the 880 cm^{-1} band also increase in intensity with increasing soaking time. After 48 hours of thermal soaking both of those shoulders can be resolved as separate bands. In all cases the center of the 880 cm^{-1} band (determined at half maximum) is shifted approximately 20 cm^{-1} to 855-860 cm^{-1} . The 650 cm^{-1} shoulder increases slightly in intensity with increasing isothermal soaking time. In addition, the band width (full width at half maximum - FWHM) shows a continuous increase (from 270 cm^{-1} to 400 cm^{-1}) with increasing soaking time.

All of the series 2, 3, and 4 experiments had 700°C as their final temperature. The melting temperature of lead orthosilicate is approximately 740°C. Even though the samples were cooled to below the melting temperature and held at that temperature for considerable lengths of time, there was no evidence, either in the form of visible crystals, or as sharp crystalline bands in the IR spectra, that any crystallization occured.

In summary, the effects on the melt structure of slow cooling and isothermal soaking are similar. Both treatments result in an increase in the number of bands in the high frequency envelope, but the effect of isothermal soaking appears to be larger than that of slow cooling.

D. Discussion

Workers such as Gotz *et al.* (1980 and 1976), Furukawa *et al.* (1978), Smart and Glasser (1978), and Hess (1975) have argued on the basis of both spectroscopic and chromatographic evidence that Pb_2SiO_4 melts contain a diverse assemblage of silicate anions as well as Pb^{2+} and O^{2-} ions. Another possibility is that with increasing duration of heating, Pb_2SiO_4 melts begin to phase separate into PbO and SiO_2-rich regions. However, if such phase separation occurs, it is on a very small scale. Furukawa *et al* (1978) report no evidence of phase separation at a scale greater than 50 angstroms. The glasses prepared in this study are both optically and compositionally (microprobe) homogenous. Therefore, it is concluded that phase separation does not occur in Pb_2SiO_4 melts.

The silicate anions presumed to exist in Pb_2SiO_4 melts include SiO_4^{4-} (Furukawa, *et al.*, 1978; Smart and Glasser, 1978; and Gotz *et al.*, 1976), $Si_2O_7^{6-}$, $Si_3O_{10}^{8-}$, $Si_4O_{12}^{8-}$, and larger polysilicate anions (Smart and Glasser, 1978 and Gotz *et al.*, 1976). In addition, Worrell and Henshall (1978) and Furukawa *et al.* (1978) speculate as to the existence of Pb-O units. In as much as the Raman active bands of crystalline lead oxides occur at frequencies below 400 cm^{-1} (Worrell and Henshall, 1978), it seems unlikely that any IR active bands for Pb-O vibrations will fall within the spectral range (400-1200 cm^{-1}) examined in this study. Consequently, the vibrational modes of hypothetical lead

oxide will not be considered further. The contributions made by the various silicate anions to the IR spectrum of the melt may be estimated by considering the spectra of suitable crystalline analogs. Ideally, the crystalline phases used as analogs should have both the same metal cations as the melt and the appropriate anionic units. Therefore, lead silicate crystalline phases have been used wherever possible. The only exception is for the SiO_4^{4-} anion, for which there is no lead silicate crystalline analog.

The highest possible symmetry for an SiO_4^{4-} anion is tetrahedral. From the character table for tetrahedral molecules (e.g. Harris and Bertolucci, 1978) it can be seen that a tetrahedral SiO_4^{4-} ion has four normal modes of vibration (A_1, E, and $2F_2$). Those normal modes are ν_1, a totally symmetric Si-O stretching mode (A_1), ν_2, a doubly degenerate O-Si-O bending mode (E), ν_3, a triply degenerate antisymmetric Si-O stretching mode (F_2), and ν_4, a triply degenerate O-Si-O bending mode (F_2) (Nakamoto, 1978). All four of the normal modes are Raman active, but only ν_3 and ν_4 are IR active. The relative frequencies of the normal modes generally follow the rules ν_3 greater than ν_1 and ν_4 greater than ν_2 (Nakamoto, 1978). On the basis of Raman depolarization ratios, Furukawa *et al.* (1978) conclude that the ν_1 vibration of SiO_4^{4-} occurs at approximately 830 cm^{-1}. The IR spectra of olivine structure minerals can be used to determine the positions of the ν_3 and ν_4 bands. The SiO_4 tetrahedra in Co_2SiO_4 (Morimoto *et al.*, 1974) are less

distorted than for other olivines (Birle *et al.*, 1968), and this is illustrated by the smaller site splitting observed in the IR bands of Co_2SiO_4 than for forsterite, fayalite, and Ni_2SiO_4-forsterite solid solutions (Tarte, 1963). Additionally, the IR bands in olivines have been observed to shift to lower frequencies with increasing cation mass and radius (Tarte, 1963; Burns and Huggins, 1972). For those reasons, the IR spectrum of Co_2SiO_4 (Tarte, 1963) was used to determine the positions of the ν_3 and ν_4 bands of the SiO_4^{4-} anion. In Co_2SiO_4 those bands fall at 880 and 480 cm^{-1}, respectively. The ν_2 vibration is expected to fall below 480 cm^{-1}, based on the relative frequency rules noted above. Thus, in the 400-1200 cm^{-1} portion of the IR spectrum, a tetrahedral SiO_4^{4-} anion will only contribute two bands at approximately 880 and 480 cm^{-1}.

If the SiO_4^{4-} anion is distorted from tetrahedral symmetry, the degeneracies noted above will be split and all of the normal modes of vibration will become IR active. The IR spectrum of SiO_4^{4-} anion will then resemble those of the olivine minerals.

In the case of the dimer ($Si_2O_7^{6-}$) there are two crystalline phases which have been shown to contain $Si_2O_7^{6-}$ units. Billhardt (1969), Petter *et al.* (1971), and Smart and Glasser (1978) have shown that $Pb_3Si_2O_7$ contains pyrosilicate structural units. Similarly, Gotz *et al.* (1975b and 1976) and Smart and Glasser (1978) have shown that the phase L-Pb_2SiO_4 (using the nomenclature of Smart and

Glasser, 1978) also has pyrosilicate structural units. Because crystallographic data (Petter *et al.*, 1971) are available for $Pb_3Si_2O_7$, but not for L-Pb_2SiO_4, the former was used as the crystalline analog of the dimer. Infrared spectral data were taken from Billhardt (1969).

The dimer IR spectrum is of particular interest because the dimer possesses a non-linear Si-O-Si bridge. The spectrum, consequently includes the vibrational modes characteristic of that bridge. Normal coordinate analyses of other X_2Y_7 (Y_3X-Y-XY_3 type) ions (Brown and Ross, 1972) have shown that there are three normal modes attributable to the X-Y-X bridge. They are a symmetrical X-Y-X stretch, an antisymmetrical X-Y-X stretch, and an in-plane X-Y-X bending deformation. Wing and Callahan (1969) have shown that the antisymmetrical stretch lies to high frequency of the symmetrical stretch and that the separation is proportional to the X-Y-X bridging angle. Billhardt (1969) identifies a "characteristic" pyrosilicate band at 679 cm^{-1} in the IR spectrum of $Pb_3Si_2O_7$, which by analogy to $Na_4(P_2O_7)$ (Bues *et al.*, 1963) and Cl_2O_7 (Roziere *et al.*, 1973), is most likely due to the Si-O-Si symmetrical stretch. Billhardt (1969) also noted a strong negative linear correlation between metal cation size and the frequency of that vibrational mode. Similarly, the band at 822 cm^{-1} may be assigned to the Si-O-Si antisymmetrical stretching mode. The normal coordinate analyses and assignments of Brown and Ross (1972) show that the bending vibration lies to low frequency of

both the stretching modes (generally between 100 cm^{-1} and 300 cm^{-1}). Thus, it is not expected to appear in the spectra reported here.

The trimer provides a problem because there is no lead silicate crystalline phase containing $Si_3O_{10}^{8-}$ structural units for which crystallographic data are available. However, Smart and Glasser (1978) found that hexagonal $PbSiO_3$ contained $Si_3O_{10}^{8-}$ units. In addition Furukawa *et al.* (1978 and 1979) found from vibrational spectroscopy that hexagonal $PbSiO_3$ is not a chain silicate such as alamosite, which supports the chromatographic determination that the structural unit in hexagonal $PbSiO_3$ is the trimer. Thus, hexagonal $PbSiO_3$ was used as the crystalline analog of the trimer. Infrared spectral data were taken from Furukawa *et al.* (1978 and 1979).

The tetramer presents an additional problem because there are four structural isomers. Those are: chain, branched chain, three-membered ring with one branch, and four-membered ring. Smart and Glasser (1978) found that silicate glasses along the join $PbO-SiO_2$ contain tetramers in the form of four-membered rings ($Si_4O_{12}^{8-}$). As far as a crystalline analog is concerned, Gotz *et al.* (1975a and 1976), Smart and Glasser (1978), and Furukawa *et al.* (1979) all confirm that $H-Pb_2SiO_4$ (using the nomenclature of Smart and Glasser, 1978) contains $Si_4O_{12}^{8-}$ rings. Therefore, $H-Pb_2SiO_4$ was used as the crystalline analog of the tetramer. IR spectral data were taken from Furukawa *et al.*

(1979).

In a melt, the anionic units are not held rigidly as in a crystal. The anions will presumably undergo continuous deformation as a consequence of the dynamic melt environment. Thus, upon quenching to the glass state, the individual anions of a given species will exhibit a range of shapes clustered around some average structure. Such small differences will lead to broader IR bands than is the case for the crystalline analogs. Consequently, the crystal analog spectra described above were broadened and smoothed by fitting Gaussian curves to the bands. The method is described below in some detail. The "quasi-melt" spectra for the anionic units up to $Si_4O_{12}^{8-}$ are shown in fig. 17. Larger anionic units were not considered due to the large number of structural isomers possible for each case and because there currently are no data which allow a particular structure (or structures) to be chosen for a given polymer. However, qualitatively speaking, the IR spectra of such anions will tend to approach that of vitreous SiO_2 (fig. 18) with increasing anionic size.

The smoothed "quasi-melt" spectra in fig. 17, when taken in conjunction with the discussion above, show that the IR spectra of silicate anions may be divided into three principal regions. Those are: the O-Si-O bending region below about 600 cm^{-1}, the Si-O-Si stretching region between 600 and 830 cm^{-1}, and the Si-O stretching region above 830 cm^{-1}. Further, several trends are apparent. With increasing

Figure 17. Smoothed infrared spectra of the crystalline analogs of the monomer (M), dimer (D), trimer (T), and tetramer (Te).

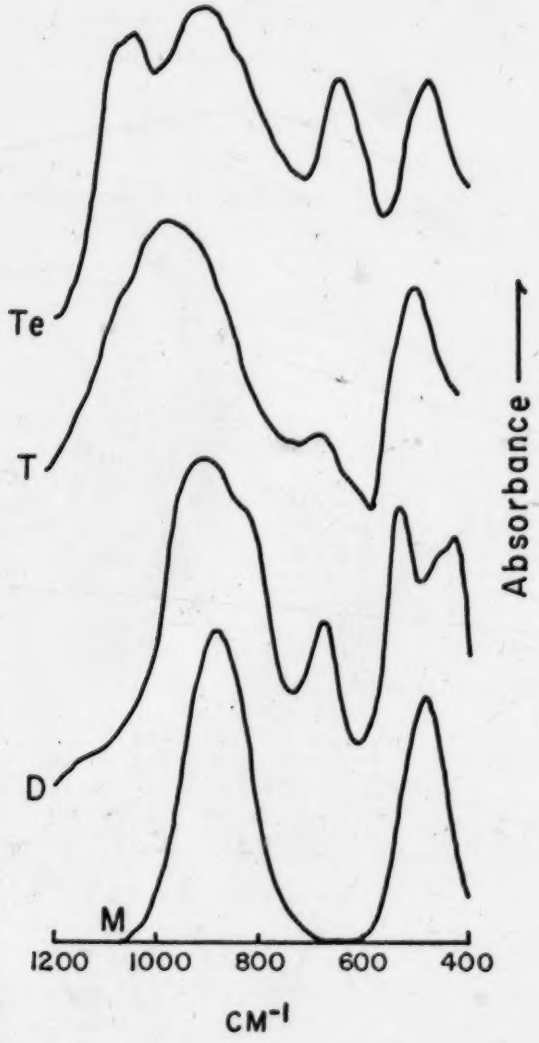

Figure 18. Infrared spectrum of vitreous SiO_2 from Ishikawa and Akagi (1978).

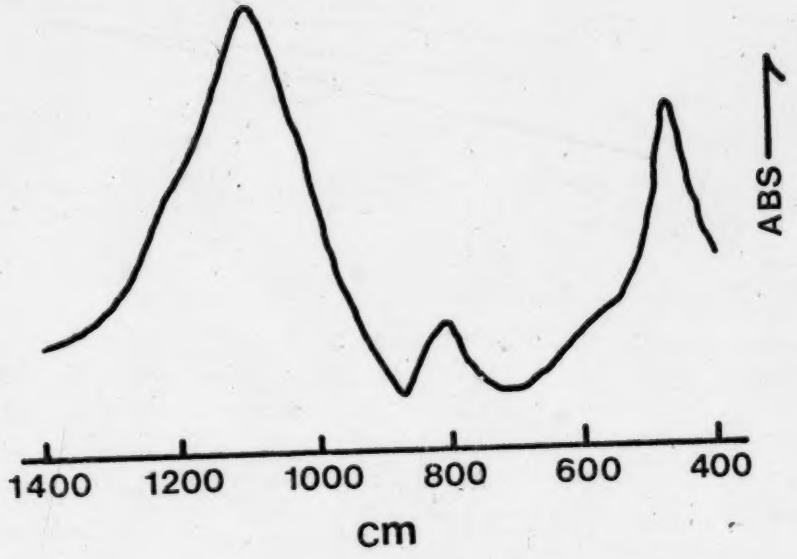

anionic size, the median of the Si-O stretching band shifts to higher frequency and the Si-O-Si stretching mode shifts to lower frequency. These features allow the qualitative interpretation of the IR spectra of silicate melts and glasses.

It is also possible to use the smoothed crystalline analog spectra (fig. 17) to qualitatively deconvolute the glass spectra. However, by simply examining the spectrum, it is possible to tell with reasonable certainty if there are contributions attributable to a particular anionic species. In order to do more than that by deconvolution methods, there must either be data about the relative intensities of the vibrational modes for different anionic species, or assumptions must be made about those intensities. This presupposes that the possible anionic species are known. Without such data, deconvolution relies on the assumption that the relative intensities of vibrational modes in the same class (Si-O stretches etc.) are the same for different anionic species. Deconvolution schemes currently in use for silicate glass spectra (e.g. Mysen *et al.*, 1982a) depend on a determination of the number of bands in a particular composite band. The bandwidths, intensities, and positions are then varied in order to minimize the difference between the real and synthetic spectra. While such methods have met with some success for Raman spectra of silicate glasses (Mysen *et al.*, 1980d and 1982a), the large number of IR active bands for even simple silicate anions (fig. 17)

significantly complicates the problem. Additionally, the results of spectral deconvolution by iteratively varying parameters (band width, intensity, and band position) and evaluating the goodness of fit by minimizing residuals are strongly dependent on the order in which the variables are changed. Because of these difficulties, the spectra presented in this paper were not deconvoluted. The interpretations presented here are based on inspection and comparison of the spectra with the crystalline analog spectra.

Series one

As was previously noted, the series one spectra are very similar and are treated as one. The 480 cm^{-1} band indicates that O-Si-O bending modes are present. There is no way of telling whether the oxygens involved in those modes are non-bridging oxygens (NBO) or are bridging oxygens (BO) between two silicons. The 880 cm^{-1} band, on the other hand, provides more information. The principal maximum in that band is most likely due to the antisymmetrical Si-O stretching mode of SiO_4^{4-} (ν_3). However, the presence of both low and high frequency shoulders in that band argues either for contributions from larger silicate anions, or for a deformed SiO_4^{4-} anion. The pronounced shoulder at approximately 650 cm^{-1} on the low side of the Si-O stretching envelope is in the Si-O-Si stretching region and thus indicates the presence of silicate anionic units larger than the monomer. The most likely candidate is the dimer

($Si_2O_7^{6-}$) which has bands at 680, 820 and 910 cm^{-1} (fig. 17). The spectra do not show other features which may be confidently assigned to particular anionic units, but that does not preclude the presence of small proportions of such units.

Smart and Glasser (1978) report, based on chromatographic resolution of trimethylsilyl derivatives of glass, that Pb_2SiO_4 glasses, prepared by short duration fusion and rapid quenching, contain 21% monomer, 30% dimer, 17% trimer, 7% ring tetramer, 2-3% ring hexamer, and 22-23% polysilicate (larger than hexamer) anions. In order to estimate the appearance of the IR spectrum of such a melt, a synthetic spectrum was constructed.

The synthetic spectrum was constructed by adding the digitized (% transmission) spectra of the crystalline analogs together in the proportions reported by Smart and Glasser (1978). Because the spectra of Pb_2SiO_4 glasses do not have any features above 1000 cm^{-1} which are attributable to the vibrations of silicate anions, only contributions from the monomer, dimer, trimer, and tetramer were included. The sum of the contributions was then transformed to absorbance and plotted. This procedure assumes that the maximum infrared activity of the strongest absorption for each of the anionic species is the same. The synthetic spectrum was smoothed and broadened by fitting Gaussian bands to the observed maxima. The band widths (FWHM) of the Gaussian curves were assigned according to the position of

the band. Bands below 600 cm^{-1} were assigned a band width of 100 cm^{-1}. Band widths of 200 and 160/200 cm^{-1} were used for bands between 600 and 800 cm^{-1} and above 800 cm^{-1}, respectively. The result, shown in fig. 19 along with one of the series one spectra (Pb-1; Table 11), is very similar to the series one spectrum, except that the series one spectrum has a more intense shoulder at approximately 650 cm^{-1}. That result, while not proving that higher order polymers are present in Pb_2SiO_4 melts, lends support to the results of Smart and Glasser (1978). The conclusion for the series one Pb_2SiO_4 melts is that both monomeric and dimeric anionic units are present and that small proportions of larger anionic units may also be present. That conclusion, in conjunction with mass balance considerations, requires that a sizeable fraction of the oxygen in Pb_2SiO_4 melts be present as the free anion (O^{2-}).

Series two, three, and four

These results show progressive changes in the IR spectra either as a consequence of decreasing cooling rate, or as a function of increasing isothermal soaking time. The sense of those changes is the same for all three series of experiments. The most polymerized melt is that from experiment PB-10 (Table 11 and figs. 15 and 16), which underwent both the slowest cooling and the longest isothermal soaking. The spectra of the other experiments are intermediate between those of series one and that of PB-10. Thus, a discussion of the PB-10 results serves to delineate

Figure 19. Synthetic infrared spectrum of Pb_2SiO_4 constructed by adding the infrared spectra of crystalline analogs of various silicate anions in the proportions determined by Smart and Glasser (1978). Both raw (a) and smoothed (b) spectra are shown. The smoothing parameters are given in the text. The infrared spectrum of glass from experiment Pb-1 is shown for comparison (c).

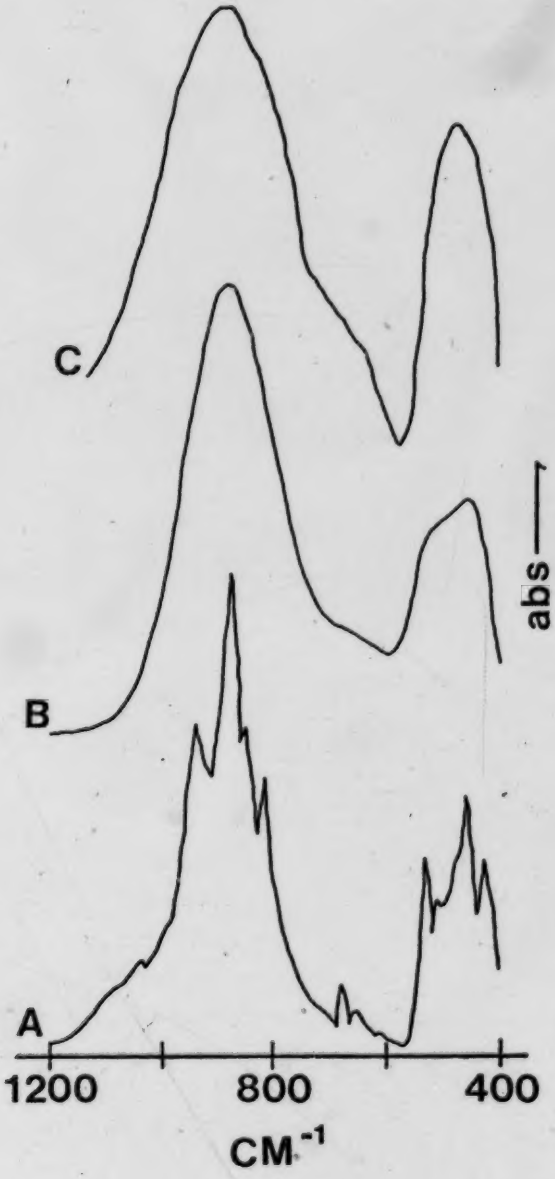

the entire series of progressive changes.

The IR spectrum of PB-10 includes identifiable bands at 465, 485, 820, 880, and 920 cm^{-1} . There are also definite shoulders at 525, 650, and at greater than 950 cm^{-1} . Furthermore, the band width (FWHM) of the Si-O stretching envelope is much greater than that of the series one spectra (400 cm^{-1} versus 270 cm^{-1}), and the mid-point of that envelope is shifted by 20-30 cm^{-1} to lower frequency. Those band positions and changes (relative to series one) are consistent with the presence of both monomer and dimer as well as some larger anionic units (the shoulder above 950 cm^{-1} implies at least the tetramer). The 650 cm^{-1} shoulder was also noted to have increased intensity relative to series one, which argues for an increasing contribution by larger anionic units.

Relative to the series one experiments, the spectrum of PB-10 shows decreasing contributions from the monomer coupled with increasing contributions from dimeric and larger silicate anions. These results show that both types of thermal treatment (slow cooling and isothermal soaking) lead to increasing polymerization of Pb_2SiO_4 melts (i.e. NBO/T decreases). Mass balance considerations require, as a corollary to that conclusion, that such thermal treatments also increase the proportion of free oxygen anions (O^{2-}) in Pb_2SiO_4 melts. It is possible to calculate the proportion of O^{2-} anion in the glass from the mass balance using the anionic proportions reported by Smart and Glasser (1978). If

the polysilicate reported by Smart and Glasser (1978) is assumed to be completely polymerized (SiO_2), the calculation yields 15% O^{2-}.

At this point it is necessary to consider the IR spectrum of vitreous fayalite and the interpretations reported by Kusabiraki and Shiraishi (1981). The IR spectrum of vitreous fayalite has strong bands centered at 508 and 933 cm^{-1} , as well as a weak band at 695 cm^{-1} . Additionally, the 933 cm^{-1} band has a pronounced high frequency shoulder above 1000 cm^{-1} . Kusabiraki and Shiraishi (1981) interpret that spectrum as being totally due to the vibrations of SiO_4^{4-} monomers. They assign the 695 cm^{-1} band to the symmetric Si-O stretching mode of tetrahedral SiO_4^{4-} (ν_1) and completely neglect the high frequency shoulder in the 933 cm^{-1} band. Their assignment of the 695 cm^{-1} band is incorrect. From the discussion of the crystal spectra above, it is clear that the 695 cm^{-1} band is within the Si-O-Si stretching region, not the Si-O stretching region. Furukawa *et al* (1978) report the ν_1 mode of tetrahedral SiO_4^{4-} at approximately 830 cm^{-1} . The position of the 695 cm^{-1} band is in very close accord with that predicted from the ionic radius of Fe^{2+} and the correlation noted by Billhardt (1969) between metal cation radius and the position of the Si-O-Si stretching band for various pyrosilicates. Similarly, the high frequency shoulder on the 933 cm^{-1} band is indicative of silicate anions at least as large as the tetramer. The IR spectrum of

vitreous fayalite is consistent with the interpretation that vitreous fayalite contains silicate anions larger than SiO_4^{4-}. However, the low intensity of the Si-O-Si stretching band (695 cm^{-1}) implies that the dominant anionic species is the monomer.

E. Conclusions

This study has shown that Pb_2SiO_4 melts contain silicate anions larger than SiO_4^{4-} monomers. The anionic species that are present and their relative proportions have been shown to depend on the thermal history of the melt. These observations require that some of the oxygen in the melt not be bound to Si (i.e. oxygen anions exist in the melt). That ionic oxygen exists in Pb_2SiO_4 melts and that those melts are structurally similar to Fe_2SiO_4 melts (Kusabiraki and Shiraishi, 1981) can be taken as implying that ionic oxygen may exist in all orthosilicate melts. The results also show that NBO/T for Pb_2SiO_4 melts is less than 4 and that NBO/T depends on the thermal history of the melt.

V. The Oxidation State of Iron in Silicate Melts: New Data for Basaltic Melts

A. Introduction

The relationship between the oxidation state of iron in natural rock melts and the bulk composition, temperature and oxygen fugacity has been investigated by a number of workers in recent years (Kennedy, 1948; Fudali 1965; Thornber *et al.*, 1980; and Sack *et al.*, 1980). Other workers including Paul and Douglas (1965), Mysen and Virgo (1978), and Dickensen and Hess (1981) have investigated the same relationship for iron in simple synthetic silicate melts. The volume of work on synthetic melts far surpasses that for natural melts. The result is that, except for the equation presented by Sack *et al.* (1980), there is no way to predict the iron redox equilibria in natural melts for given conditions. Furthermore, much of the work on natural melts was done at low oxygen fugacities (10^{-4}-10^{-8} bars). Only Kennedy reports data determined at high oxygen fugacity (0.21 bar). In addition, only Kennedy (1948) has done experiments on a single composition at more than two temperatures. Consequently, while the relationship presented by Sack *et al.* (1980) has a diverse compositional base (143 data sets extending from nephelinitic to granitic compositions), the range of oxygen fugacities is quite limited and the data were determined at only 3 or 4 different temperatures. Therefore, this study was undertaken

to expand upon the data base used by Sack *et al.* (1980) by providing new data for basaltic melts at high oxygen fugacity and over a range of temperatures.

The results of 27 experiments on three basaltic compositions are presented in this paper. The bulk of the experiments were done in air and span the temperature range 1250-1437°C. The new data were combined with those of Kennedy (1948), Fudali (1965), Thornber *et al.* (1980), and Sack *et al.* (1980) and an equation, relating the ferric/ferrous ratio of the melt to temperature, oxygen fugacity, and bulk composition, was determined by multiple regression analysis of the data. The results presented in this paper expand the previous data base in terms of temperature and oxygen fugacity. This increases the validity of extrapolating the predictive equation outside the temperature and oxygen fugacity range of the data set. In addition, including 27 new data sets for basalts improves the accuracy of the method for basaltic liquids.

B. Experimental and Analytical

The experiments were done on three different "basaltic" melts. Those compositions are C-11 (a nephelinite), KR-13 (an alkali basalt), and 1921 Kilauea tholeiite. The sample of C-11 was provided by Dr. T. Fujii, the sample of KR-13 was provided by Dr. C.M. Scarfe, and the sample of 1921 Kilauea tholeiite was provided by Dr. I Kushiro. The starting materials were initially ground to powder in a

tungsten carbide swing mill. The powders were then fused in covered Pt crucibles in air at 1350°C for at least 2 hours. The experiments were done at both low ($\log fO_2$=-8.0) and high ($\log fO_2$=-0.68) oxygen fugacities in an electrically heated vertical tube furnace (Deltech DT-31VT) equipped with a gas-tight Al_2O_3 muffle tube. Oxygen fugacities were set either by leaving the furnace open to air, or by passing mixtures of CO and CO_2 through the furnace. The ratio of CO to CO_2 used in the low oxygen fugacity experiments was set with an oxygen fugacity probe of the type used by Arculus and Delano (1981). The low oxygen fugacities are estimated to be accurate to within ±0.25 log units of fO_2. The temperatures during the experiments were monitored with a $Pt\text{-}Pt_{.8}Rh_{.2}$ thermocouple which was calibrated against the melting point of Au (1064.5°C).

All but three of the experiments were done by the Pt wire loop method (Donaldson, 1975). The other three experiments were done as batch fusions in Pt crucibles. The samples were placed on the Pt loops as slurries with acetone. After the acetone evaporated from the slurry, the sample was lightly fused onto the loop with an oxy-acetylene torch. The low oxygen fugacity experiments were done in the same manner. Iron loss to the Pt loops was not thought to be a problem as the samples were analyzed after the experiments. Each experiment included several samples of the same basalt. Each sample was split into several pieces. One piece was used for bulk chemical analysis and the other

Figure 20. Calculated time required for equilibration in iron oxidation state experiments for a spherical 50 mg. sample with a density of 2.75 g/cm³. The method is explained in the text.

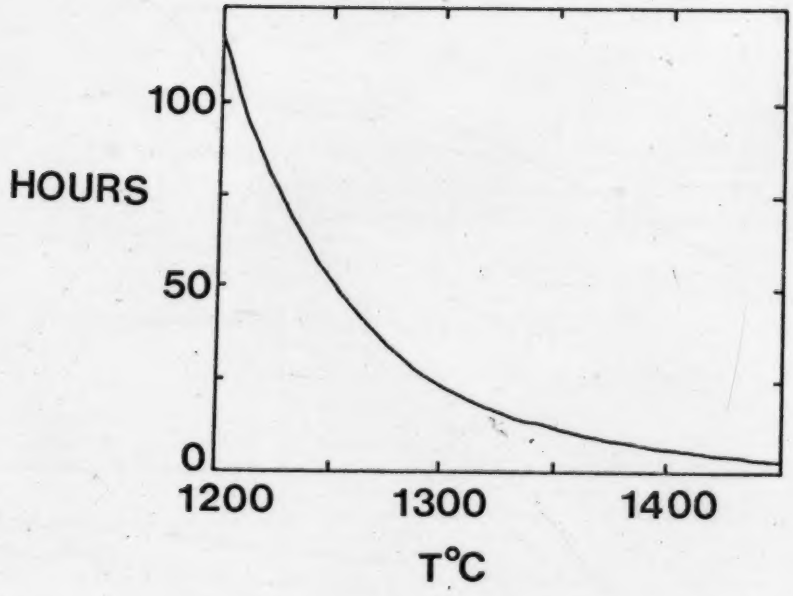

pieces were analyzed for FeO. In most cases the samples analyzed for FeO were also analyzed for total iron by atomic absorption using BCR-1 (Flanagan, 1973) as a standard.

The bulk chemical analyses were done on the University of Alberta ARL-SEMQ electron microprobe. Suitable standards were used to allow data reduction by the method of Bence and Albee (1968) using the alpha factors of Albee and Ray (1970). The FeO analyses were done by the method of Wilson (1960). Microsyringes were used for the titrations in the FeO analyses, thus allowing a precision of ±0.01 wt. % to be achieved for most of the analyses. The solutions used were frequently standardized against one another to assure that the ferrous ammonium sulphate solution had not become oxidized. The accuracy of the FeO analyses was checked by analyzing 25 aliquots of BCR-1 (Flanagan, 1973). The result of those analyses was 8.66±0.21 wt % as compared to the reported value of 8.80 wt. % (Flanagan, 1973). All of the experimental products produced in this study were totally glassy as determined by optical examination of the crushed samples.

If experiments of the type done in this study are to have any meaning, they must be equilibrium experiments. Thornber *et al*. (1980) argue, on the basis of a time study, that only 5-7 hours are required to reach equilibrium in wire loop experiments with samples of up to 100 mg. However, their replicate experiments all fail to produce the same Fe^{3+}/Fe^{2+} value for given conditions, but different

experimental durations. The rate of approach to equilibrium in iron oxidation experiments is controlled by the diffusion of oxygen either into or out of the sample (see chapter 6). Thus, measured oxygen diffusivities in silicate melts may be used to calculate the time required for equilibration in such experiments. Most of the experiments reported here were done on KR-13 alkali basalt. The zero pressure oxygen diffusivity for that composition was determined in chapter 3 (Table 9) and is approximately 10^{-4}cm^2/sec at 1400°C. Assuming an activation energy of approximately 70 kcal (Table 8) the diffusion coefficient is approximately 3×10^{-7}cm^2/sec at 1300°C. That diffusion coefficient can be used in conjunction with eqn. 16:

$$r = (Dt)^{1/2} \qquad (16)$$

to calculate an equilibration time for wire loop experiments by letting r equal the radius of the sample, D equals the oxygen diffusion coefficient, and t equal the duration of the experiment. That was done, assuming a 50 mg. sample mass and a melt density of 2.75 g/cm^3. The results are presented in fig. 20 in which equilibration time is plotted as a function of experimental temperature. Fig. 20 was used to determine the experimental durations used in this study.

C. Results and discussion

The experimental results are given in Table 12. Sack *et al*. (1980) used the technique of multiple regression to derive an equation of the form:

Table 12. Analyses of experimental products. Analyses were done by electron microprobe. FeO was determined by the method of Wilson (1960). Fe_2O_3 was determined by difference from total iron determined either by electron microprobe or by atomic absorption.

Exp. #	15	16	17	18	19	20
fO_2	air	air	air	air	air	air
T°C	1262	1278	1300	1300	1300	1300
t(hr)	91	70	23	82	48	144
SiO_2	47.20	47.90	49.14	46.20	46.90	47.60
TiO_2	2.50	2.40	2.14	2.80	2.70	2.50
Al_2O_3	15.20	15.80	16.14	14.90	15.30	15.60
MgO	5.70	6.00	5.99	6.00	5.80	5.90
CaO	9.60	10.00	9.60	9.40	9.50	9.50
FeO	1.49	1.76	2.05	1.84	1.92	2.11
Fe_2O_3	10.24	10.16	9.22	12.07	10.54	10.70
MnO	n.a.	n.a.	n.d.	n.a.	n.a.	n.a.
Na_2O	3.60	3.40	4.03	3.10	3.40	3.10
K_2O	1.11	1.02	1.23	0.87	0.95	0.61
P_2O_5	n.a.	n.a.	0.41	n.a.	n.a.	n.a.
Total	97.63	99.44	99.94	98.37	98.12	98.57

Exp. #	21	22	25	26	27	28
fO_2	air	air	air	air	air	air
T°C	1305	1320	1321	1340	1350	1360
t(hr)	81	17	64	48	47	24
SiO_2	47.00	47.80	47.20	50.40	47.70	51.42
TiO_2	2.50	2.28	2.60	2.11	2.40	2.32
Al_2O_3	14.80	16.00	15.60	15.64	15.50	16.05
MgO	5.80	5.82	5.80	6.05	5.90	5.89
CaO	9.30	9.54	9.60	9.82	9.40	9.57
FeO	2.01	1.91	2.08	2.37	2.40	2.62
Fe_2O_3	10.88	11.91	10.45	8.68	9.94	9.06
MnO	n.a.	0.14	n.a.	0.19	n.a.	n.d.
Na_2O	3.30	3.68	3.30	3.73	3.40	3.53
K_2O	0.78	1.18	0.84	0.96	0.86	0.97
P_2O_5	n.a.	0.36	n.a.	0.14	n.a.	0.21
Total	97.47	100.63	98.59	100.09	97.50	101.64

n.d. - not detected.
n.a. - not analyzed.

Table 12. Analyses of experimental products (cont.).

Exp. #	29	30	31	32	33	34
fO_2	air	air	air	air	air	air
T°C	1380	1380	1400	1400	1420	1420
t(hr)	18	27	20	23	23	26
SiO_2	46.32	47.10	49.24	47.70	47.30	47.20
TiO_2	3.57	2.50	2.26	2.50	3.20	2.70
Al_2O_3	14.78	15.20	16.27	15.30	15.46	15.50
MgO	5.95	5.90	6.11	5.80	6.01	5.90
CaO	8.82	10.70	9.67	9.50	9.17	9.30
FeO	3.28	2.93	3.51	2.66	2.88	3.16
Fe_2O_3	13.18	10.34	7.63	9.69	13.80	10.57
MnO	n.d.	n.a.	0.15	n.a.	0.13	n.a.
Na_2O	3.32	3.20	3.65	3.50	3.10	3.00
K_2O	0.90	0.95	1.10	1.05	0.75	0.85
P_2O_5	0.23	n.a.	0.17	n.a.	0.04	n.a.
Total	100.35	98.82	99.67	97.70	101.84	98.18

Exp. #	35	39	41	43	93	94
fO_2	air	-8.18	-8.30	-8.15	air	air
T°C	1438	1250	1300	1350	1350	1400
t(hr)	21	91	61	45	45	24
SiO_2	48.70	47.60	49.40	49.60	41.36	39.63
TiO_2	2.57	2.80	2.50	2.60	2.93	2.97
Al_2O_3	15.81	15.60	16.70	16.50	12.37	12.59
MgO	5.93	6.20	6.10	6.40	9.38	9.48
CaO	9.13	9.90	10.50	10.40	13.04	12.80
FeO	2.41	10.63	9.00	8.24	2.19	2.65
Fe_2O_3	10.65	0.96	0.79	0.66	14.57	13.75
MnO	n.d.	n.a.	n.a.	n.a.	0.25	0.27
Na_2O	4.75	3.00	2.90	2.30	3.34	3.63
K_2O	1.10	0.95	0.94	0.79	0.76	0.91
P_2O_5	0.02	n.a.	n.a.	n.a.	0.72	0.82
Total	100.14	97.69	98.83	97.49	100.91	99.50

n.a. - not analyzed.
n.d. - not detected.

Table 12. Analyses of experimental results (cont.)

Exp. #	C-11	KR-13	1921
fO_2	air	air	air
T°C	1350	1400	1350
t(hr)	24	43	23
SiO_2	37.77	49.63	48.08
TiO_2	2.75	2.43	2.97
Al_2O_3	12.00	14.63	12.11
MgO	9.29	5.91	11.30
CaO	12.59	9.38	9.44
FeO	2.08	2.26	2.44
Fe_2O_3	13.46	10.10	10.05
MnO	0.22	0.21	0.18
Na_2O	4.29	4.06	2.25
K_2O	2.17	1.25	0.51
P_2O_5	2.37	0.50	0.28
Total	98.99	100.36	99.68

n.a. - not analyzed.
n.d. - not detected.
Experiments 15-43 were done on KR-13, experiments 93 and 94 were done on C-11.

$$ln\{X(Fe_2O_3)/X(FeO)\} = a\,lnf(O_2)+b/T+c+\sum_i d(i)X(i) \qquad (17)$$

where X(i) is the mole fraction of oxide component i in the melt and a, b, c, and d are coefficients determined from the multiple regression analysis. In their analysis Sack *et al.* (1980) excluded the oxides TiO_2, MnO, Cr_2O_3, and P_2O_5 on the basis that those oxides can have very low concentrations in silicate melts and are frequently not reported in analyses. The oxides TiO_2, MnO, and P_2O_5 were included in the analysis reported here because examination of the data set showed, that while the proportions of the oxides are generally low,

there was considerable variation in their concentrations. Cr_2O_3 was excluded from the analysis for the same reasons given by Sack *et al*. (1980).

The multiple regression analyses were done using the program MULTR (Davis, 1973) (translated into basic). The program was modified to allow the multiple regression coefficients to be standardized. The regression coefficients were standardized using equation 18

$$b = d\{(\text{std. dev. I})/(\text{std. dev B})\} \qquad (18)$$

where B is the dependent variable, I is an independent variable, d is the multiple regression coefficient of variable I, and b is the standardized multiple regression coefficient of variable I. Standardizing the regression coefficients allows direct comparison of the regression coefficients in order to determine which of them accounts for more of the variance of the dependent variable (Davis, 1973).

The multiple regressions were done incrementally as different groups of analyses were added to the data set. The grouping of analyses for the multiple regressions was: (A) the 27 analyses presented in this study (Table 12); (B) the 57 analyses presented by Sack *et al*. (1980); (C) the combination of A and B above; (D) the results of Thornber *et al*. (1980) plus C above; and (E) the results of Kennedy (1948) and Fudali (1965) plus D above (150 analyses). The results of the multiple regression analyses are presented in Table 13. The largest data set (E) is not significantly

Table 13. Results of multiple regression analyses. The columns are labelled according to the cases defined in the text.

Variable	A	B	C	D	E
$lnfO_2$	0.207	0.297	0.231	0.230	0.228
1/T	6344	25124	12415	11535	11676
Const.	-103.24	-34.93	-12.46	-56.35	0.16
SiO_2	100.21	22.44	106.74	50.88	-5.78
TiO_2	77.94	20.37	103.30	49.00	-5.65
Al_2O_3	97.94	10.34	94.25	42.75	-13.35
MgO	99.61	18.09	102.26	46.43	-10.29
CaO	93.08	25.93	109.11	53.18	-3.59
FeO	112.22	18.45	107.92	52.30	-4.44
MnO	148.34	60.32	69.29	46.67	-13.00
Na_2O	119.54	31.90	119.13	57.46	0.48
K_2O	18.00	30.53	115.92	59.31	1.87
P_2O_5	199.50	13.72	112.58	56.56	2.61
r^2	0.99	0.54	0.97	0.96	0.96

r^2 is the goodness of fit from the regression analyses.

larger than that analyzed by Sack *et al.* (1980) due to the rather more stringent equilibrium criteria applied in this study. Table 14 lists the variables in order of the relative proportion of the variance attributable to the variable for each of the cases above.

The regression coefficients for the complete data set (case E) compare favorably with those determined by Sack *et al.* (1980) except that the sign of the coefficient for CaO is negative in this study, while it was positive in Sack's study. The coefficients for $lnf(O_2)$, $X(Na_2O)$, $X(K_2O)$, and $X(P_2O_5)$ are all positive. Thus, an increase in any of those

components can be expected to coincide with an increase of Fe^{3+} in the melt. However, it is of interest to note that all of the regression coefficients are positive for cases A, B, C, and D. Only in case E are there any negative regression coefficients. Standardizing the regression coefficients (Table 14) shows that the fraction of the variance of the dependent variable attributable to any given independent variable is dependent on the variance of all the variables in the data set. In other words, if an independent variable varies greatly in the data set, then it will have a proportionately large fraction of the variance of the dependent variable attributed to it. Therefore, multiple regression analysis, while providing a useful way of determining a predictive model, provides little or no insight into the real relationships between the dependent and independent variables.

D. Applications

Sack *et al.* (1980) have demonstrated that their multiple regression equation reproduces measured oxidation states of iron in natural melts quite well. Rather than go through the exercise of making the same comparisons as were made by Sack *et al.* (1980), the results of the equation determined for case E were compared directly with the results produced by Sack's equation. The comparison was made for two diverse melt compositions (BCR-1 - Flanagan, 1973 and average rhyolite - Nockolds, 1954) as a function of both

Table 14. Variables ranked according to the relative fraction of the total variance attributable to them (#1 = highest). The columns correspond to the cases described in the text.

Rank	A	B	C	D	E
1	SiO_2	SiO_2	SiO_2	SiO_2	$lnfO_2$
2	MgO	CaO	CaO	CaO	SiO_2
3	FeO	MgO	MgO	MgO	MgO
4	$lnfO_2$	FeO	FeO	1/T	1/T
5	CaO	K_2O	Al_2O_3	FeO	Al_2O_3
6	Al_2O_3	Na_2O	K_2O	K_2O	CaO
7	Na_2O	1/T	$lnfO_2$	Na_2O	FeO
8	P_2O_5	$lnfO_2$	Na_2O	Al_2O_3	TiO_2
9	TiO_2	TiO_2	TiO_2	TiO_2	K_2O
10	1/T	al_2O_3	1/T	$lnfO_2$	MnO
11	MnO	MnO	P_2O_5	P_2O_5	Na_2O
12	K_2O	P_2O_5	MnO	MnO	P_2O_5

temperature (fig. 21) and oxygen fugacity (fig. 22). Fig. 21 was calculated for an oxygen fugacity of 10^{-8} bar. The results for BCR-1 show that the equation determined in this study agrees quite well with that from Sack *et al.* (1980) for basaltic liquids. However, the agreement is not as good for the rhyolite composition, particularly at low temperatures. Fig. 22 shows that the two equations give virtually the same results as a function of oxygen fugacity at 1250°C. All four curves fall within the stipled area in fig. 22. Figs. 21 and 22 also illustrate that the effects of temperature and oxygen fugacity on the oxidation state of iron in the melt are large when compared to the effects of bulk composition.

Figure 21. The relationship between temperature and the oxidation state of iron at an oxygen fugacity of 10^{-8} bars in silicate melts calculated from the case E regression equation (Table 13) for BCR-1 (a) and average rhyolite (b). The results calculated from the equation of Sack *et al.* (1980) for BCR-1 (dashed line) and the average rhyolite (dotted line) are shown for comparison.

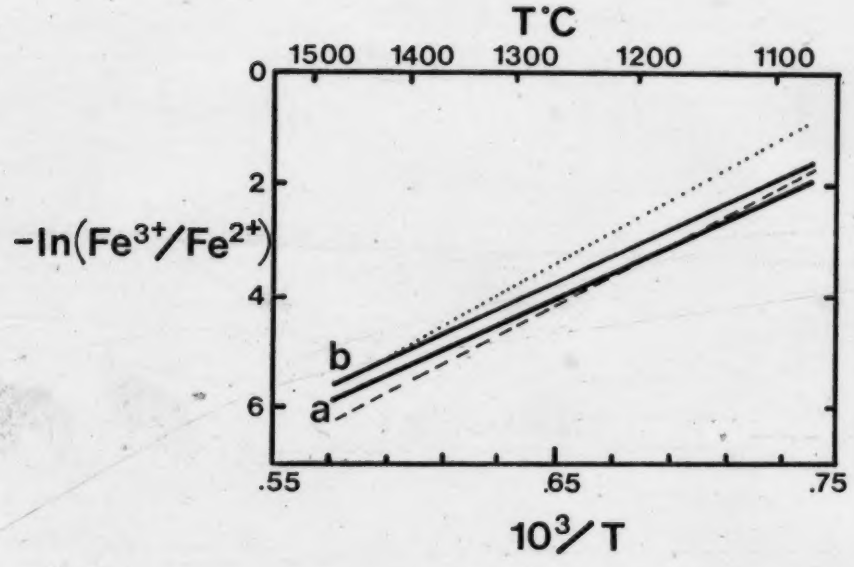

Figure 22. The relationship between the oxidation state of iron in silicate melts as calculated at 1250°C from the case E regression equation and the equation of Sack *et al.* (1980) for BCR-1 and average rhyolite. The results for both compositions and both equations are included within the stipled area.

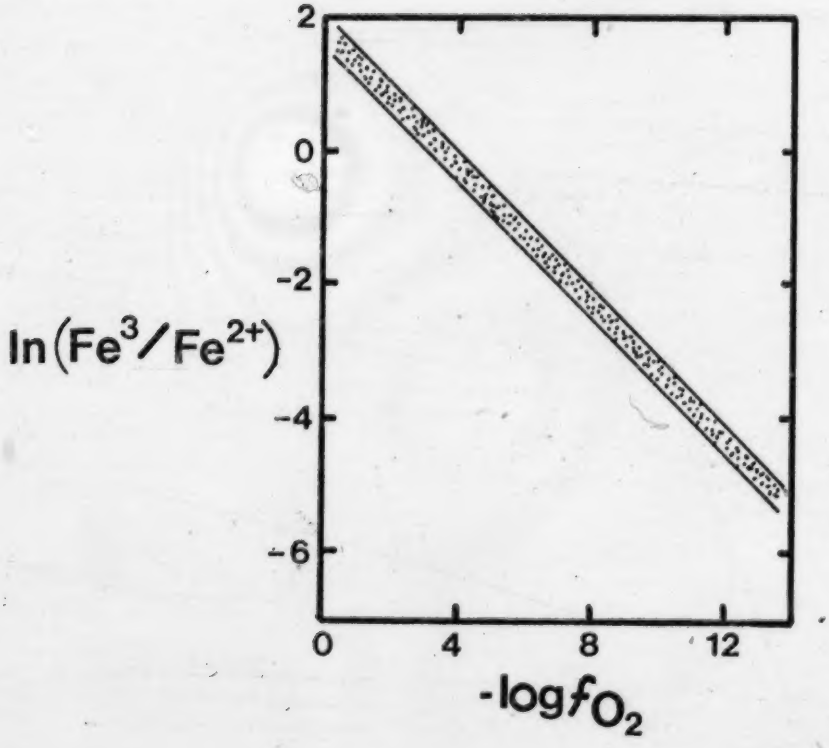

The multiple regression coefficient modifying the variable 1/T gives the enthalpy change of the reaction (Fudali, 1965):

$$FeO_{1.5} \rightleftharpoons FeO + 1/4O_2 \qquad (19)$$

which describes the redox equilibrium of iron in silicate melts. This study yields an enthalpy change of 23200 cal for reaction 19. The value determined from the equation of Sack *et al.* (1980) is 26200 cal. These results can be compared with the enthalpy change calculated by Kennedy (1948) of 18500 cal for a basaltic liquid. The differences between Kennedy's result and those calculated from the results of Sack *et al.* (1980) and this study most likely reflect the failure of the low temperature experiments done by Sack *et al.* (1980) to reach equilibrium, particularly for the more silicic compositions. This may be seen by comparing the experimental durations employed by Sack *et al.* (1980) with those calculated from oxygen diffusion data (fig. 20) for a temperature of 1300°C and a basaltic composition. The diffusivity of oxygen decreases as the silica content of the melt increases and as the temperature decreases (Dunn, 1982). Thus, fig. 20 shows that most of the low temperature experiments done by Sack *et al.* (1980) were unlikely to have reached equilibrium. Because the experiments of Sack *et al.* (1980) were done under reducing conditions, the failure to achieve equilibrium will result in an erroneously high ratio of Fe^{3+} to Fe^{2+} being incorporated into the data set. Furthermore, since it is most likely that equilibrium was

not achieved at the lower temperatures, such erroneous data will tend to increase the apparent magnitude of the temperature dependence of the oxidation state of iron when it is expressed as the ratio of ferric to ferrous iron. Correspondingly, as the enthalpy change of reaction 19 is given by (bR) where b is the regression coefficient modifying the variable 1/T and R is the gas constant, the calculated enthalpy change will be too large.

The observation that the regression coefficient modifying 1/T may be too large limits the range of temperatures over which the regression equations determined both in this study and by Sack *et al.* (1980) may be applied. Use of the equation at temperatures much below 1200°C will result in erroneously high fractions of Fe_2O_3 being calculated. The temperature coefficient determined in this study is smaller than that determined by Sack *et al.* (1980). Therefore, the equation determined here seems to be a better choice if an extrapolation below 1200°C is required.

E. Conclusion

Three different basaltic liquids have been equilibrated in terms of iron oxidation state at various temperatures from 1262 to 1437°C, either in air (24 experiments), or at an oxygen fugacity of approximately 10^{-8} bars (3 experiments). The 27 experimental data points have been added to the data base used by Sack *et al.* (1980) and the entire data set analyzed by multiple regression to yield a

predictive equation for the oxidation state of iron in silicate melts.

The predictive equation is quite similar to that determined by Sack *et al.* (1980). However, the temperature dependencies of both equations are probably too large. Consequently, extrapolation to low temperatures will yield erroneously high Fe^{3+}/Fe^{2+} ratios. In that respect, the equation determined in this study appears to be preferable as its temperature dependence is the smaller of the two.

While little can be said about the relative magnitudes of the effects of changes in the various oxide components on the iron oxidation state of the melt, it was observed that the effect of bulk composition is small relative to the effects of either temperature or oxygen fugacity.

VI. Oxygen Activity in an Alkali Basalt as a Function of Temperature

A. Introduction

The chemical and physical properties of iron-bearing silicate melts are strongly affected by the prevailing oxygen fugacity. Recently, Tran and Brungs (1980b) and Loh *et al.* (1981) have used oxygen activity probes similar to those described by Sato (1971) to directly measure the activity of oxygen in sodium disilicate and soda-lime silica melts, respectively. Their results show that the oxygen activity in simple silicate melts containing polyvalent cations can change very sharply with changes in temperature. Their results prompted this study of the feasibility of using oxygen activity probes to directly measure the activity of oxygen in natural rock melts.

This study reports the results of oxygen activity measurements in an alkali basalt melt over the temperature range 1257-1373°C. The oxygen potential measurements were made with an Y_2O_3 doped ZrO_2 electrolyte cell (Arculus and Delano, 1981). The half cell reactions upon which cells of this type are based are:

$$2O^{2-} \rightleftharpoons O_2(ref) + 4e^- \qquad (20)$$

at the reference electrode and:

$$O_2(melt) + 4e^- \rightleftharpoons 2O^{2-} \qquad (21)$$

at the measuring electrode. The overall reaction is:

$$O_2(melt) \rightleftharpoons O_2(ref) \qquad (22)$$

The free energy change for reaction 22 is:

$$\triangle G(rxn) = \triangle G^{\circ}(rxn) + RT\ln(aO_2(ref)/aO_2(melt)) \quad (23)$$

The half reaction which occurs in the melt is given by reaction 21. As four electrons are transferred in the reaction the relationship between the half cell potential and the free energy change of the reaction is:

$$\triangle G(rxn) = -4FE \quad (24)$$

where E is the cell *emf* and F is the Faraday constant. Substituting eqn. 24 into eqn. 23, and noting that $\triangle G^{\circ} = -4FE^{\circ}$ (where E° is the standard half cell potential at unit activity which goes to zero for a pure oxygen reference), gives:

$$E = RT\ln(aO_2(ref)/aO_2(melt)) \quad (25)$$

Eqn. 25 holds in the absence of ionic conduction in the electrolyte cell.

B. Experimental procedure

The experiment was done on a 20 gram batch of alkali basalt from Kettle River B.C. (KR-13; Table 15). A sample of the rock was crushed in a tungsten carbide swing mill and a split of the rock powder was placed in a Pt crucible and fused for 48 hours at 1300°C in air. The resultant glass was crushed (several chips were mounted for microprobe analysis), returned to the Pt crucible, mounted on a pedestal, and raised into the hot zone of an electrically heated vertical tube furnace (Deltech DT-31VT). The sample was held at 1250°C for 20 hours prior to starting the

Figure 23. Schematic drawing of the experimental configuration, showing the oxygen electrolyte cell and the position of the sample melt.

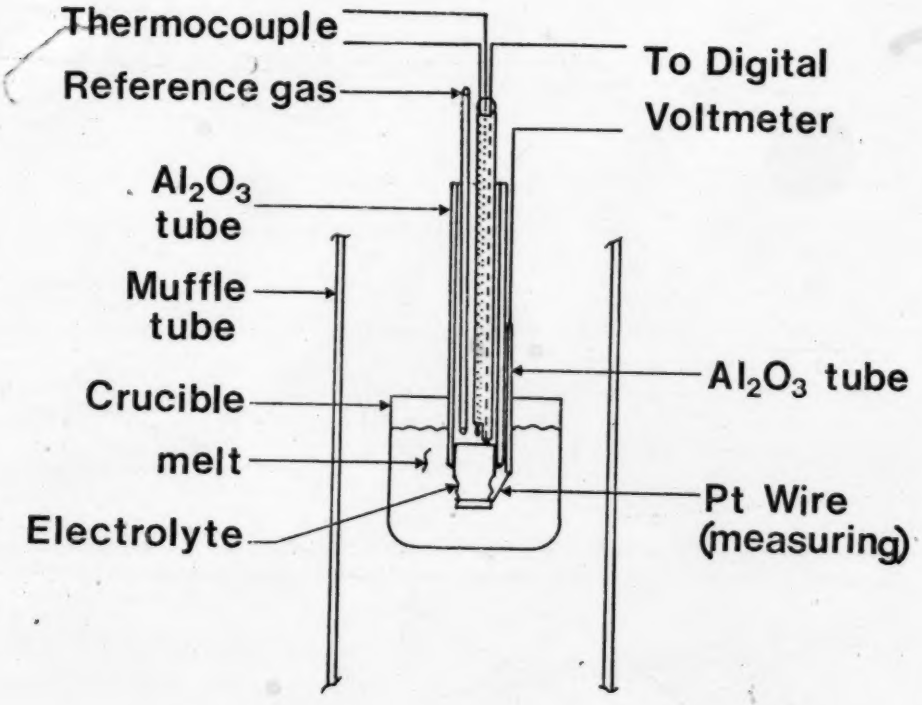

Table 15. Composition of the alkali basalt. Wt. % oxide determined by electron microprobe analysis of glass chips.

SiO_2	48.39
TiO_2	2.41
Al_2O_3	15.91
MgO	5.96
CaO	9.62
FeO'	11.35
MnO	0.25
Na_2O	3.98
K_2O	1.22
P_2O_5	0.51
Total	99.60

' - Total iron as FeO

experiment to assure oxidative equilibrium in the melt.

The microprobe analysis was done on the University of Alberta ARL-SEMQ electron microprobe using wavelength dispersive methods. Suitable standards were used to allow reduction of the raw data by the method of Bencé and Albee (1968) using the alpha factors of Albee and Ray (1970). The analysis of the starting material is given in Table 15.

The oxygen probe used in this study was the same as those used by Arculus and Delano (1981). However, several modifications were made to the experimental configuration. Only one probe was used and oxygen gas was used to provide the reference. The measuring electrode consisted of a Pt wire with a 6 cm length of high purity Al_2O_3 tube sintered onto it approximately 3 cm from one end. The exposed end of the Pt wire was attached directly to the zirconia/yttria electrolyte (fig. 23). The Al_2O_3 tube extends into the melt

when the probe is in use, preventing the establishment of the triple junction Pt-air-melt. This assures that the oxygen activity in the melt rather than at the melt/gas interface is measured. Tran and Brungs (1980b) noted that, for conventional Sato type oxygen probes (Sato, 1971), diffusion of oxygen through the electrolyte resulted in anomalously high oxygen potentials near the oxygen probe. To alleviate that problem they separated the measuring electrode from the the oxygen probe. That configuration was not used in this study because it was thought highly unlikely that any oxygen would diffuse through the one centimeter length of electrolyte in the probe used. Temperatures were measured with a Pt-$Pt_{.7}Rh_{.3}$ thermocouple placed inside the oxygen probe (fig. 23).

The *emf* output of the electrolyte cell was measured with both a digital voltmeter (10 megaohm input impedance) and a chart recorder (8 megaohm input impedance). All of the *emf*'s reported here were measured with the digital voltmeter. The digital voltmeter was also used in an attempt to measure the cell current. No measurement was obtained on the most sensitive scale (200 microamps full scale), thus satisfying the requirement that the cell current be zero.

The experiment was initiated by placing the electrolyte cell into the melt. The melt was then stepped to 1257°C and held at that temperature until the cell *emf* appeared to stabilize. The melt temperature was then increased by steps to 1373°C. The intermediate temperatures were 1286, 1316,

and 1345°C. At each step, the melt was held until the cell *emf* appeared to stabilize. After reaching 1373°C the system was cooled back to 1257°C using the same temperature steps. After the system appeared to stabilize at 1257°C another heating cycle was begun, but was only carried to 1316°C where the experiment was terminated.

At the end of the experiment the electrolyte cell was withdrawn from the melt. Examination of the cell showed that, except for a thin coating of basalt melt, the cell was apparently unaffected by its 76 hours immersion in the basalt melt. However, the lack of a visibly obvious reaction does not mean that the cell did not react with the melt to a limited extent. The evidence for limited reaction between the electrolyte cell and the melt is presented below.

C. Results and discussion

The results of the experiment are summarized in Table 16 and shown graphically in figs. 24 and 25. At the initiation of the experiment the *emf* of the electrolyte cell stabilized within 10 minutes. The temperature was then abruptly increased to 1257°C. As soon as the temperature of the system began to increase, the cell *emf* began to decrease reaching a minimum after 8 to 10 minutes, when the system temperature reached a maximum. After the temperature stabilized, the cell *emf* began a slow asymptotic approach to its final (equilibrium) value (fig. 24). Similar behavior was observed for each temperature increase. Apparent

Figure 24. Plot of the *emf* output of the oxygen electrolyte cell as a function of time. Two cooling (a and b) steps and one heating step (c) are shown. The temperature stabilized at the new setting within 10 minutes after each step.

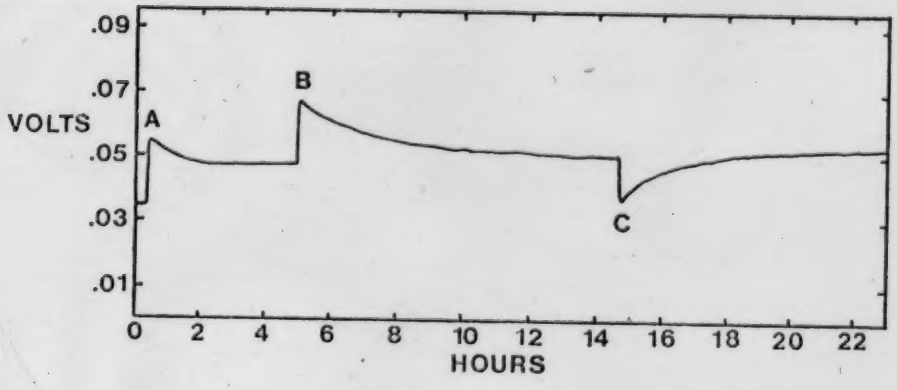

Figure 25. Plot of $\ln a(O_2)$ *versus* 1000/T (K) showing the experimental brackets and the best fit line to the data (eqn. 27). The solid triangles are values used to determine the best fit line. Open triangles are data points which were not used. The reasons for excluding those points are discussed in the text.

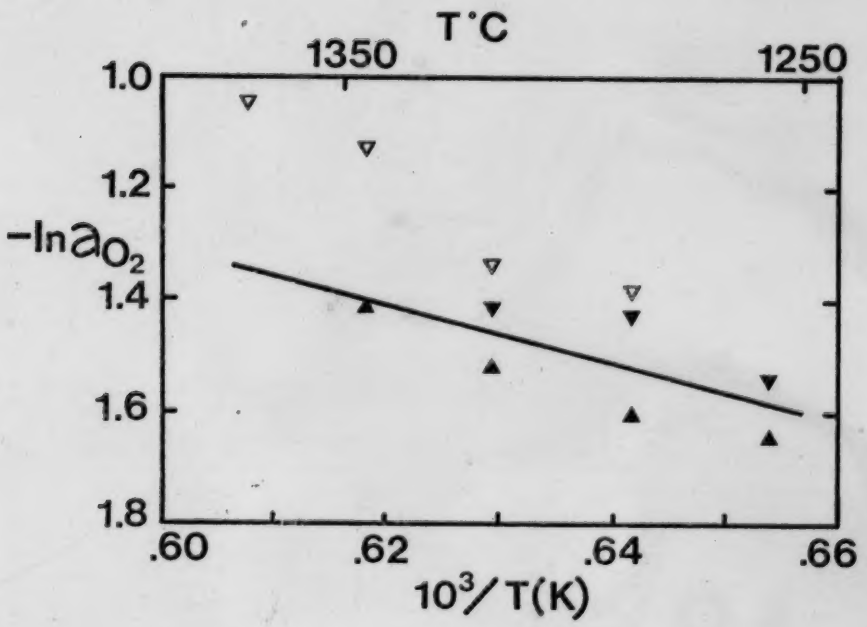

Table 16. Oxygen probe readings after apparent stabilization and calculated oxygen activities.

T°C	Mode	t(hr)	*emf*(v)	aO_2
1257	H	1.6	0.0501	0.216
1257	C	16.0	0.0540	0.194
1286	H	2.2	0.0465	0.251
1286	C	7.5	0.0541	0.200
1286	H	10.0	0.0480	0.240
1316	H	3.5	0.0458	0.263
1316	C	9.5	0.0516	0.220
1316	H	16.3	0.0483	0.244
1345	H	2.5	0.0392	0.325
1345	C	4.5	0.0491	0.245
1373	H	2.3	0.0371	0.351

Mode - Indicates whether the temperature was approached by heating (H) or cooling (C) the melt.

stabilization times ranged from as little as 6 to longer than 16 hours and were not systematically related to the system temperature. The cell response was the same, but in the opposite sense, when the temperature was decreased. When the melt temperature was decreased the cell *emf* rapidly increased, passed through a maximum at the minimum temperature and then asymptotically approached equilibrium (fig. 24). The maxima and minima observed in the cell *emf* correspond to oxygen activities as low as 0.1 and as high as 0.6. Those are significant variations relative to the equilibrium value of 0.21. While the magnitude of the changes to be expected at low oxygen fugacity is unknown, if those changes are of the same relative magnitude as they are

at high oxygen fugacities, the redox equilibria in the melt could be greatly affected.

Eqn. 25 shows that the oxygen activity in the melt is inversely related to the electrolyte cell *emf*. Thus the decrease in the cell *emf* upon heating corresponds to an increase in oxygen activity, and the *emf* increase upon cooling indicates a decrease in oxygen activity. Such sharp changes in oxygen activity upon heating and cooling (fig. 24) can be attributed to rapid oxidation/reduction reactions in the melt (Loh *et al.*, 1981).

The only cation present in significant proportions in basaltic melts which undergoes a valence change under the conditions of the experiment, is iron. The oxidation/reduction behavior of iron in silicate melts can be expressed by equation 26 (Fudali, 1965 and Sack *et al.*, 1980):

$$FeO_{1.5} \rightleftharpoons FeO + 1/4\ O_2 \qquad (26)$$

where $FeO_{1.5}$ is ferric iron and FeO is ferrous iron. Equation 26 shows that the reduction of ferric iron produces oxygen and thus causes an increase in the activity of oxygen in the melt. Conversely, the oxidation of ferrous iron consumes oxygen and decreases the activity of oxygen. Many workers (e.g. Sack *et al.*, 1980; Thornber *et al.*, 1980; Fudali, 1965, and Kennedy, 1948) have observed that the proportion of ferrous iron in basaltic liquids increases with

increasing temperature. Thus, it is reasonable to equate the abrupt increase in oxygen activity observed with increasing temperature with the production of oxygen through the reduction of Fe^{3+} to Fe^{2+} and *vice versa* for decreasing temperature. The abrupt nature of the change in oxygen activity with changes in temperature, indicates that the oxidation/reduction of iron in silicate melts is fast. Similarly, Semkow *et al.* (1982) have observed that oxidation/reduction reactions for Ni, Co, and Zn in diopside composition melts are rapid.

The slow decrease in the activity of oxygen (increase in cell *emf*) following a temperature increase is due to the diffusion of oxygen (produced by the reduction of ferric iron) out of the system. The reverse is the case following a temperature decrease. The time required for the system to reach the equilibrium oxygen activity is dependent on the geometry and dynamics (whether or not the system is convecting) of the system. Thus, it seems unlikely that equilibrium was achieved at any time during the course of the experiment.

Fig. 25 is a plot of the log of the oxygen activity, determined with the probe after stabilization, *versus* 1/T. The brackets determined during the heating and cooling cycles are shown. The line in fig. 25 is a least squares fit to the data points shown as solid triangles. Data points shown as open triangles were not included in the regression analysis because their inclusion caused the line to fall

outside one or more of the experimental brackets. The principle criterion used to exclude those points is that the process responsible for the non-equilibrium behavior has a simple exponential temperature dependence over the temperature interval studied. In that case the line shown in fig. 25 must be a straight line. The equation of the line in fig. 25 is:

$$\ln a(O_2) = (1.71\pm1.46)-(5030\pm2300)/T \quad r^2=0.49 \quad (27)$$

The non-zero slope of the line given in equation 27 shows that the oxygen probe measured anomalously high oxygen activities relative to the imposed oxygen fugacity at higher temperatures. That observation can be explained by permeation of oxygen through either the electrolyte or the alumina tube portions of the probe. Tran and Brungs (1980b) report similar behavior, but only when highly reduced melts were examined. Due to the design differences between the oxygen probes used by Tran and Brungs (1980b) and those used in this study (fig. 23) and the fact that an oxidized melt was studied, it is likely that the anomolous activities observed are not due to the permeation of oxygen through the probe walls. It seems likely, that at the higher temperatures there was some solution of the Al_2O_3 from the alumina tube into the melt. Solution of Al_2O_3 would promote polymerization of the melt (Mysen *et al.*, 1980d), thus increasing the activity of oxygen in the vicinity of the probe. That problem does not have a significant effect on the conclusions of this study, but must be taken into

consideration if oxygen probes of the type used in this study are to be used for quantitative studies in natural rock melts.

D. Petrologic implications

This study has shown that, upon heating and cooling, the oxidation state of iron in the melt changes very rapidly either releasing (upon the reduction of iron) or consuming (upon the oxidation of iron) oxygen in the process. The release or consumption of oxygen rapidly changes the oxidation state of the melt. When a melt cools, the iron in the melt becomes increasingly oxidized in response to the temperature change (Kennedy, 1948; Fudali, 1965; and Sack *et al.*, 1980). Simultaneously, the activity of oxygen in the melt decreases, creating disequilibrium conditions. In an open system, oxygen can diffuse into the melt from the surroundings and increase the oxygen activity back to the equilibrium value. Open system conditions of this sort exist in gas buffered experiments. If sufficient time is allowed for oxygen diffusion to restore the equilibrium oxygen activity, then the equilibrium iron oxidation state in the melt is attained. In crystallization experiments, the samples are generally cooled from superliquidus temperatures to the run temperature. That will cause the oxygen activity to be depressed below the equilibrium value for the conditions. Such kinetically-imposed reducing conditions may induce the crystallization of phases which will not be in

equilibrium when the oxygen activity in the melt equilibrates. If such crystalline phases do not dissolve back into the melt, they can only reach equilibrium with the melt through solid state diffusion.

Heating or cooling a melt under closed system conditions (relative to oxygen transfer) also increases or decreases the oxygen activity in the melt. However, in the closed system case, oxygen cannot diffuse into or out of the system. The result, upon cooling, is that the oxygen activity becomes increasingly reducing. If the melt was originally quite reduced, it is conceivable that the system could autoreduce itself into the Fe^{2+} or even the Fe^{0} field. Such a situation could lead to the crystallization of phases enriched in Fe^{2+}, relative to the composition expected from the bulk composition and estimated equilibrium oxygen fugacity of the melt. In extreme conditions, this process could even lead to the precipitation of metallic iron from the melt as is observed for lunar basalts (Levinson and Taylor, 1971). Closed system conditions of this sort are easy to conceive of for natural melts. The case of a basalt erupted onto the surface of the earth is one instance where the melt is rapidly cooled and closed system conditions may be provided by the chilled margin of the flow.

Autoreduction of the melt by the process described above may also affect the volatile phase speciation in the melt. If a melt is cooled quickly over a large temperature range, as is the case for sea floor basalts, it is

conceivable that some of the CO_2 dissolved in the melt could be reduced to CO or even to graphite (which could then precipitate). A large decrease in the activity of oxygen in the melt would also promote the dissociation of water to H_2 and O_2, thus lowering the apparent water content of the melt (if the H_2 diffuses out of the system). This process can account for the presence of elemental carbon in sea floor basalts (Mathez and Delaney, 1981) as well as for the low water contents observed for some sea floor basalts (Muenow *et al.*, 1979). Furthermore, because of this effect, the iron oxidation state of quenched basalts may not be a good indicator of the prevailing oxygen fugacity in the melt prior to eruption.

E. Conclusion

This study has shown that the oxidation state of a basaltic melt changes rapidly in response to temperature changes. Cooling of a melt results in an immediate decrease in the activity of oxygen as a consequence of the rapid oxidation of Fe^{2+} to Fe^{3+}. In a system closed to oxygen transfer, the decrease in oxygen activity may result in the quenched melt being out of oxidative equilibrium with the crystalline phase assemblage. Consequently, the oxidation state of quenched melts (glasses) may not reflect the oxidation state of the magma from which the glass was quenched.

VII. Conclusion

A. Summary of conclusions

The five studies presented in this thesis illustrate the value of studying oxygen in silicate melts. Chapter 2 showed that the principal species contributing to the diffusivity of oxygen is no larger than the SiO_4^{4-} monomer, even in melts which are thought of as highly polymerized. It was also observed that oxygen conforms to the compensation law for cationic diffusion in silicate melts. That observation suggests that the diffusing species is "cation-like" (O^{2-}). The magnitude of oxygen diffusivity was found to be similar to the magnitudes of divalent cation diffusivity, which further supports the suggestion that oxygen diffusivity receives a significant contribution from O^{2-} anions.

Chapter 3 showed that the relationship between oxygen diffusion in basaltic liquids and pressure is not at all like the pressure dependences observed for cations in silicate melts. Furthermore, the observation of negative activation volumes for oxygen diffusion argues strongly that variations in the diffusivity of oxygen with pressure are not related to changes in the free volume of the melt. The correspondence between abrupt changes in oxygen diffusivity and changes in the liquidus mineralogy of the melts studied, suggests that the pressure dependence of oxygen diffusion is related to changes in the anionic speciation of the melt.

The pressure dependence of oxygen diffusion is not related to the pressure dependence of viscosity for the melts studied. Therefore, the correspondence between viscous flow and oxygen diffusivity suggested by Oishi *et al.* (1975) and Yinnon and Cooper (1980) may be fortuitous. Oxygen diffusivities in basaltic liquids are of the same magnitude as divalent cation diffusivities. Therefore, in cases of diffusion controlled or slower crystal growth, crystals will not be out of oxidative equilibrium with the body of the melt.

Chapter 4 demonstrated that the structure of Pb_2SiO_4 melts depends on thermal history. The melts become increasingly polymerized (NBO/T decreases) with either decreasing cooling rate, or increasing duration of isothermal soaking. The presence of silicate anions larger than SiO_4^{4-} in lead orthosilicate melt requires a corresponding proportion of O^{2-} anions in the melt.

Chapter 5 presents an improved predictive equation for calculating either the oxidation state of iron in a melt (given the temperature and the oxygen fugacity), or the oxygen fugacity of a melt (given the iron oxidation state and the temperature). The oxidation state of iron in silicate melts was shown to depend much more on temperature and oxygen fugacity than on bulk composition.

Chapter 6 presented new data on the change of the oxidation state of a basaltic melt with changing temperature. The oxygen activity of a basalt melt was shown

to decrease rapidly on cooling in response to oxidation of Fe^{2+}. Reequilibration of the oxygen activity then occurred by the diffusion of oxygen into the melt from the surroundings. In the case of a system closed to oxygen transfer, this process provides a possible explanation for the occurrence of reduced phases in an otherwise apparently more oxidized system.

B. Concluding remarks

The results presented in chapters 2, 3, and 4 suggest that O^{2-} is present not only in orthosilicate melts, but also in much more polymerized melts. That observation requires that models of silicate melt structure which do not incorporate the O^{2-} anion be reassessed. The presence of O^{2-} in relatively polymerized silicate melts allows the presence of a greater variety of anionic species in the melt than is the case if O^{2-} is not present. Furthermore, Mysen *et al.* (1980d) argue that NBO/T, as they calculate it, is definitive of the structure of the melt and depends only on bulk composition. The results presented here do not agree with that assertion. The presence of oxygen anion (O^{2-}) in silicate melts and the suggestion that it participates in reactions with anionic polymers (chapter 3) implies that the structure of the melt is dependent on oxygen fugacity. Finally, the results of this thesis have shown that oxygen can act as a very sensitive probe into the structure of silicate melts.

Bibliography

Albee, A.L. and Ray, L. (1970). Correction factors for electron microprobe microanalysis of silicates, oxides, carbonates, phosphates, and sulphates. *Anal. Chem.* **42**,1408-1414.

Arculus, R.J. and Delano, J.W. (1981). Intrinsic oxygen fugacity measurements: techniques and results for spinels from upper mantle peridotites and megacryst assemblages. *Geochim. Cosmochim. Acta* **45**, 899-914.

Bence, A.E. and Albee, A.L. (1968). Empirical correction factors for the electron microanalysis of silicates and oxides. *J. Geol.* **76**, 382-403.

Billhardt, H.W. (1969). Synthesis of lead pyrosilicate and other barysilite-like compounds. *Am. Mineral.* **54**, 510-521.

Birge, R.T. (1932). The calculation of errors by the method of least squares. *Phys. Rev.* **40**, 207-227.

Birle, J.D.; Gibbs, G.V.; Moore, P.B.; and Smith, J.V. (1968). Crystal structures of natural olivines. *Am. Mineral.* **53**, 807-824.

Bockris, J.O'M.; Kitchener, J.D.; Ignatowicz, S,; and Tomlinson, J.W. (1948). The ecectrical conductivity of silicate melts: systems containing Ca, Mn, Al. *Discuss. Faraday Soc.* **4**, 281-286.

Bond, W.L. (1951). Making small spheres. *Rev. Sci. Instrum.* **22**, 344-345.

Bottinga, Y.; Weill, D.; and Richet, P. (1982). Density calculations for silicate liquids. I. Revised model for aluminosilicate compositions. *Geochim. Cosmochim. Acta* **46**, 909-919.

Bowen, N.L. (1913). The melting phenomena of the plagioclase feldspars. *Am. J. Sci.* **35**, 577-599.

Bowen, N.L. (1915). The crystallization of haplobasaltic, haplodioritic and related magmas. *Am. J. Sci.* **40**, 161-185.

Boyd, F.R. and England, J.L. (1960). Apparatus for phase equilibrium measurements at pressures up to 50 kilobars and temperatures up to 1750°C. *J. Geophys. Res.* **65**, 741-748.

Brown, R.G. and Ross, S.D. (1972). The vibrational spectra of some condensed tetrahedral anions $(X_2O_7)^{n-}$. *Spectrochim. Acta* **28A**, 1263-1274.

Bues, W.; Buchler, K.; and Kuhnle, P. (1963). Raman-Spektren von Diphosphat, Diarsenat und deren Gemische in der Schmelze. *Z. Anorg. Allg. Chem.* **325**, 8-14.

Burns, R.G. and Huggins, F.E. (1972). Cation determinative curves for Mg-Fe-Mn olivines from vibrational spectra. *Am. Mineral.* **57**, 976-985.

Carmichael, I.S.E.; Nicholls, J.; Spera, F.J.; Wood, B.J.; and Nelson, S.A. (1977). High temperature properties of silicate liquids: applications to the equilibration and ascent of basic magma. *Phil. Trans. Roy. Soc. London*, **A 286**, 373-431.

Chandrasekhar, S. (1961). *Hydrodynamic and Hydromagnetic Stability*. Clarendon Press, Oxford.

Clayton, R.N. and Mayeda, T. (1963). The use of bromine pentafluoride in the extraction of oxygen from oxides and silicates for isotopic analysis. *Geochim. Cosmochim. Acta* 27, 43-52.

Davis, J.C. (1973). *Statistics and Data Analysis in Geology*, Wiley, New York, NY.

deBerg, K.C. and Lauder, I. (1980). Oxygen tracer diffusion in a potassium silicate glass above the transformation temperature. *Phys. Chem. Glasses* 21, 106-109.

deBerg, K.C. and Lauder, I. (1978). Oxygen tracer diffusion in lead silicate glass above the transformation temperature. *Phys. Chem. Glasses* 19, 78-82.

De Jong, B.H.W.S. and Brown, G.E. (1980). Polymerization of silicate and aluminate tetrahedra in glasses, melts, and aqueous solutions - I. Electronic structure of $H_4Si_2O_7$, H_4SiAlO_7, $H_4Al_2O_7$. *Geochim. Cosmochim. Acta* 43, 61-77.

Dickenson, M.P. and Hess, P.C. (1981). Redox equilibria and the structural role of iron in aluminosilicate melts. *Contrib. Mineral. Petrol.* 78, 352-357.

Donaldson, C.H. (1975). A sample holding techniquep for study of crystal growth in silicate melts. *Am. Mineral.* 60, 324-326.

Doremus, R.H. (1960). Diffusion of oxygen from contracting bubbles in molten glass. *J. Am. Ceram. Soc.* 43, 655-661.

Dunn, T. (1982). Oxygen diffusion in three silicate melts

along the join diopside-anorthite. *Geochim. Cosmochim. Acta* **46**, 2293-2299.

Eggler, D.H. and Rosenhauer, M. (1978). Carbon dioxide in silicate melts II. solubilities of CO_2 and H_2O in $CaMgSi_2O_6$ (diopside) liquids and vapors at pressures to 40 kb. *Am. J. Sci.* **278**, 64-94.

Eggler, D.H.; Mysen, B.O.; and Hoering, T.C. (1979). Gas species in sealed capsules in solid-media, high-pressure apparatus. *Carnegie Inst. Wash. Yearbk. 73*, 228-232.

Ernst, W.G. (1960). The stability relations of magnesioriebeckite. *Geochim. Cosmochim. Acta* **19**, 10-40.

Eugster, H.P. and Wones, D.R. (1962). Stability relations of the ferruginous biotite annite. *J. Petrol.* **3**, 82-125.

Flanagan, F.J. (1973). 1972 values for international geochemical reference samples. *Geochim. Cosmochim. Acta* **37**, 1189-1200.

French, B.M. and Eugster, H.P. (1965). Experimental control of oxygen fugacities by graphite-gas equilibrium. *J. Geophys. Res.* **70**, 1529-1539.

Fudali, R.F. (1965). Oxygen fugacities of basaltic and andesitic magmas. *Geochim. Cosmochim. Acta* **29**, 1063-1075.

Fujii, T. and Kushiro, I. (1977). Density, viscosity, and compressibility of basaltic liquid at high pressures. *Carnegie Inst. Wash. Yearbk. 76*, 419-424.

Furukawa, T.; Brawer, S.A.; and White, W.B. (1979). Raman and IR spectroscopic studies of the crystalline phases

in the system Pb_2SiO_4-$PbSiO_3$. *J. Am. Ceram. Soc.* **62**, 351-356.

Furukawa, T.; Brawer, S.A.; and White, W.B. (1978). The structure of lead silicate glasses determined by vibrational spectroscopy. *J. Mat. Sci.* **13**, 268-282.

Glasstone, S.; Laidler, K.J.; and Eyring, H. (1941). *The Theory of Rate Processes.* McGraw-Hill, New York.

Gotz, J.; Hoebbel, D.; and Wieker, W. (1975a). Die Konstitution der Silicatanionen im kristallinen $2PbO.SiO_2$. I. *Z. Anorg. Allg. Chem.* **416**, 163-168.

Gotz, J.; Hoebbel, D.; and Weiker, W. (1975b). Die Konstitution der Silicatanionen im kristallinen $2PbO.SiO_2$. II. *Z. Anorg. Allg. Chem.* **418**, 29-34.

Gotz, J.; Hoebble, D.; and Wieker, W. (1976). Silicate groupings in glassy and crystalline $2PbO.SiO_2$. *J. Non-Cryst. Solids* **20**, 413-425.

Gotz, J.; Hoebbel, D.; and Wieker, W. (1980). The influence of cooling rate of a $2PbO.SiO_2$ melt on the constitution of silicate anions. *J. Non-Cryst. Solids* **37**, 367-380.

Hamann, S.D. (1965). The influence of pressure on electrolytic conduction in alkali silicate glasses. *Aust. J. Chem.* **18**,1-8.

Harris, D.M. (1981). The microdetermination of H_2O, CO_2, and SO_2 in glass using a 1280°C microscope vacuum heating stage, cryopumping, and vapor pressure measurements from 77 to 273 K. *Geochim. Cosmochim. Acta* **45**, 2023-2036.

Harris, D.C. and Bertolucci, M.D. (1978). *Symmetry and*

Spectroscopy, Oxford Press, New York, NY.

Hess, P.C. (1971). Polymer model of silicate melts. *Geochim. Cosmochim. Acta* 35, 289-306.

Hess, P.C. (1975). $PbO-SiO_2$ melts: structure and thermodynamics of mixing. *Geochim. Cosmochim. Acta* 39, 671-687.

Hess, P.C. (1977). Structure of silicate melts. *Can. Mineral.* 15, 162-178.

Hofmann, A.W. and Magaritz, M. (1977). Diffusion of Ca, Sr, Ba, and Co in a basalt melt: implications for the geochemistry of the mantle. *J. Geophys. Res.* 82, 5432-5440.

Hofmann, A.W. (1980). Diffusion in natural silicate melts: A critical review. In *Physics of Magmatic Processes*, (ed. R. Hargraves), Princeton Press, Princeton, NJ.

Ishikawa, T. and Akagi, S. (1978). Structures of glasses in the system $SnO-SiO_2$. *Phys. Chem. Glasses* 19, 111-114.

Jost, W. (1960). *Diffusion in Solids, Liquids, and Gases.* Academic Press, New York, NY.

Karsten, J.L.; Holloway, J.R.; and Delaney, J.R. (1982). Ion microprobe studies of water in silicate melts: temperature dependent water diffusion in obsidian. *Earth Planet. Sci. Lett.* 59, 420-428.

Kennedy, G.C. (1948). Equilibrium between volatiles and iron oxides in igneous rocks. *Am. J. Sci.* 246, 529-549.

Kirkpatrick, R.J.; Kuo, L-C; and Melchior, J. (1981). Crystal growth in incongruently-melting compositions:

programmed cooling with diopside. *Am. Mineral.* **66**, 223-241.

Koros, P.J. and King, T.B. (1962). The self-diffusion of oxygen in a lime-silica-alumina slag. *Tran. Met. Soc.* **AIME 224**, 299-306.

Kozu, S. and Kani, K. (1935). Viscosity measurements of the ternary system diopside-albite-anorthite. *Imperial Acad. Japan (Tokyo) Proc.* 11, 383 385.

Kusabiraki, K. and Shiraishi, Y. (1981). The IR spectrum of vitreous fayalite. *J. Non-Cryst. Solids* **44**, 365-368.

Kushiro, I. (1976). A new furnace assembly with a small temperature gradient in solid-media, high-pressure apparatus. *Carnegie Inst. Wash. Yearbk. 75*, 832-833.

Kushiro, I. (1980). Viscosity, density, and structure of silicate melts at high pressures, and their petrological applications. In *Physics of Magmatic Processes* (ed. R. Hargraves), Princeton Press, Princeton, NJ.

Kushiro, I.; Yoder H.S. Jr.; and Mysen, B.O. (1976). Viscosities of basalt and andesite at high pressures. *J. Geophys. Res.* 81,6351-6356.

Levinson, A.A. and Taylor, M.P. (1971). *Moon Rocks and Minerals*, Pergammon Press.

Loh, I.; Frey, T.; and Schaeffer, H.A. (1981). Continuous determination of the oxidation state in a soda-lime-silica glass melt during refining. *Comm. Am. Ceram. Soc.*, 168-169.

Masson, C.R.; Smith, I.B.; and Whiteway, S.G. (1970).

Activities and ionic distributions in liquid silicates: application of polymer theory. *Can. J.. Chem.* 48, 1456-1464.

Mathez, E.A. and Delaney, J.R. (1981). The nature and distribution of carbon in submarine basalts and peridotite nodules. *Earth Planet. Sci. Lett.* 56, 217-232.

May, H.B.; Lauder, I.; and Wollast, R. (1974). Oxygen diffusion coefficients in alkali silicates. *J. Am. Ceram. Soc.* 57, 197-200.

Morimoto, N.; Tokanami, M.; Watanabe, M.; and Koto, K. (1974). Crystal structures of three polymorphs of Co_2SiO_4. *Am. Mineral.* 59, 475-485.

Muehlenbachs, K. and Kushiro, I. (1974). Oxygen isotope exchange and equilibration of silicates with CO_2 and O_2. *Carnegie Inst. Wash. Yearb.* 73, 232-236.

Muenow, D.W.; Graham, D.G.; Liu, N.W.K.; and Delaney, J.R. (1979). The abundance of volatiles in Hawaiian tholeiitic submarine basalts. *Earth Planet. Sci. Lett.* 42, 71-76.

Mysen, B.O. and Virgo, D. (1978). Influence of pressure, temperature, and bulk composition on melt structures in the system $NaAlSi_2O_6$ $NaFe^{3+}Si_2O_6$. *Am. J. Sci.* 278, 1307-1322.

Mysen, B.O. and Virgo, D. (1980). Solubility mechanisms of carbon dioxide in silicate melts: a Raman spectroscopic study. *Am. Mineral.* 65, 885-899.

Mysen, B.O.; Ryerson, F.J.; and Virgo, D. (1980a). The influence of TiO_2 on the structure and derivative properties of silicate melts. *Am. Mineral.* **65**, 1150-1165.

Mysen, B.O.; Ryerson, F.J.; and Virgo, D. (1980b). The structural role of phosphorus in silicate melts. *Am. Mineral.* **65**, 106-117.

Mysen, B.O.; Seifert, F.E.; and Virgo, D. (1980c). Structure and redox equilibria of iron bearing silicate melts. *Am. Mineral.* **65**, 867-884.

Mysen, B.O.; Virgo, D.; and Scarfe, C.M. (1980d). Relations between the anionic structure and viscosity of silicate meltsA Raman spectroscopic study. *Am. Mineral.* **65**, 690-711.

Mysen, B.O.; Virgo, D.; and Kushiro, I. (1981). The structural role of aluminum in silicate melts - a Raman spectroscopic study at 1 atmosphere. *Am. Mineral.* **66**, 678-701.

Mysen, B.O.; Finger, L.W.; Virgo, D.; and Seifert, F.E. (1982a). Curve-fitting of Raman spectra of silicate glasses. *Am. Mineral.* **67**, 686-695.

Mysen, B.O.; Virgo, D.; and Seifert, F.A. (1982b). The structure of silicate melts: Implications for chemical and physical properties of natural magma. *Rev. Geophys. Space. Phys.* **20**, 353-398.

Nakamoto, K. (1978). *Infrared and Raman Spectra of Inorganic and Coordination Compounds.* Wiley-Interscience, New

York, NY.

Nockolds, S.R. (1954). Average chemical compositions of some igneous rocks. *Bull. Geol. Soc. Am.* **65**, 1007-1032.

Oishi, Y.; Terai, R.; and Ueda, H. (1975). Oxygen diffusion in liquid silicates and relation to their viscosity. In: *Mass Transport Phenomena in Ceramics*, (eds. A. Cooper and A. Heuer), Plenum Press, New York, NY.

Oishi, Y,; Nanba, M.; and Pask, J. (1982). Analysis of liquid interdiffusion in the system $CaO-Al_2O_3-SiO_2$ using multiatomic ion models. *J. Am. Ceram. Soc.* **65**, 247-253.

Paul, A. and Douglas, R.W. (1965). Ferrous-ferric equilibria in binary alkali silicate glasses. *Phys. Chem. Glasses.* **6**, 207-211.

Petter, W.; Harnik, A.B.; and Keppler, U. (1971). Die Kristallostruktur von Blei-Barysilit, $Pb_3Si_2O_7$. *Z. Kristallogr.* **133**, 445-458.

Richet, P. and Bottinga, Y. (1980). Heat capacity of liquid silicates: new measurements on $NaAlSi_3O_8$ and $K_2Si_4O_9$. *Geochim. Cosmochim. Acta* **44**, 1535-1541.

Roziere, J.; Pascal, J-L.; and Potier, A. (1973). Calcul du champ de force de l'anhydride perchlorique a partir de l'approximation des vibrations de groupe. *Spectrochim. Acta* **29A**, 169-175.

Sack, R.O.; Carmichael, I.S.E.; Rivers, M.; and Ghiorso, M.S. (1980). Ferric-ferrous equilibria in natural silicate liquids at 1 bar. *Contrib. Mineral. Petrol.* **75**, 369-376.

Sasabe, M. and Goto, K.S. (1974). Permeability, diffusivity, and solubility of oxygen gas in liquid slag. *Met. Tran.* 5, 2225-2233.

Sato, M. (1971). Electrochemical measurements and control of oxygen fugacity and other gaseous fugacities with solid electrolyte sensors. In: *Research Techniques for High Pressure and High Temperature.* (ed. G. Ulmer), Springer-Verlag, New York, NY.

Scarfe, C.M. (1981). The pressure dependence of the viscosity of some basic melts. *Carnegie Inst. Wash. Yearbk. 80*, 336-339.

Scarfe, C.M.; Mysen, B.O.; and Virgo, D. (1979). Changes in viscosity and density of melts of sodium disilicate, sodium metasilicate, and diopside composition with pressure. *Carnegie Inst. Wash. Yearbk.* 78, 547-551.

Scarfe, C.M.; Cronin, D.J.; Wenzel, J.T.; and Kauffman, D.A. (1980). Viscosity temperature relationships at 1 ATM in the system diopside-anorthite. *Carnegie Inst. Wash. Yearb.* 79, 315-318.

Schreiber, H.D.; Lauer, H.V.; and Thanyasiri, T. (1980). The redox state of cerium in basaltic magmas: an experimental study of iron-cerium interactions in silicate melts. *Geochim. Cosmochim. Acta* **44**, 1599-1612.

Seifert, F.E.; Mysen, B.O.; and Virgo, D. (1981). Structural similarity of glasses and melts relevant to petrological processes. *Geochim. Cosmochim. Acta* **45**, 1879-1884.

Semkow, K.W.; Rizzo, R.A.; Haskin, L.A.; and Lindstrom, D.J.

(1982). An electrochemical study of Ni^{2+}, Co^{2+}, and Zn^{2+} ions in melts of composition $CaMgSi_2O_6$. *Geochim. Cosmochim. Acta* **46**, 1879-1889.

Sharma, S.K.; Virgo, D.; and Mysen, B.O. (1978). Structure of glasses and melts of Na_2OxSiO_2 (x=1, 2, 3) composition from Raman spectroscopy. *Carnegie Inst Wash. Yearb.* 77, 649-652.

Smart, R.M. and Glasser, F.P. (1978). Silicate anionic constitution of lead silicate glasses and crystals. *Phys. Chem. Glasses* **19**, 95-102.

Smith, D.G.W. and Gold, C.M. (1979). EDATA2 a Fortran IV computer program for processing wavelength- and energy-dispersive electron microprobe analyses. *Proc. 14th Ann. Conf. Microbeam Anal. Soc. (San Antonio, TX, 1979)* (ed. by D. Newbury), 273-278, San Francisco Press.

Sweet, J.R. and White, W.B. (1969). Study of sodium silicate glasses and liquids by IR spectroscopy. *Phys. Chem. Glasses* **10**, 246-251.

Takahashi, E. (1980). Melting relations of an alkali-olivine basalt to 30 kbar, and their bearing on the origin of alkali basalt magmas. *Carnegie Inst. Wash. Yearbk. 79*, 271-276.

Tarte, P. (1963). Etude infra-rouge des orthosilicates et des orthogermanates - II. Structures du type olivine et monticellite. *Spectrochim. Acta* **19**, 25-47.

Taylor, M. and Brown, G.E. (1979). Structure of mineral glasses. I. The feldspar glasses $NaAlSi_3O_8$, $KAlSi_3O_8$,

and $CaAl_2Si_2O_8$. *Geochim. Cosmochim. Acta* **43**, 61-77.

Thornber,C.R.; Roeder, P.L.; and Foster, J.R. (1980). The effect of composition on the ferric-ferrous ratio in basaltic liquids at atmospheric pressure. *Geochim. Cosmochim. Acta* **44**, 525-532.

Towers, H. and Chipman, J. (1957). Diffusion of calcium and silicon in a lime-alumina-silica slag. *Trans.* **AIME 299**, 769-773.

Tran, T. and Brungs, M.P. (1980a). Applications of oxygen electrodes in glass melts. Part 1. Oxygen reference electrode. *Phys. Chem. Glasses* **21**, 133-140.

Tran, T. and Brungs, M.P. (1980b). Applications of oxygen electrodes in glass melts. Part 2. Oxygen probes for the measurement of oxygen potential in sodium disilicate glass. *Phys. Chem. Glasses* **21**, 178-183.

Tyburczy, J.A. and Waff, H.S. (1982). Electrical conductivity of molten basalt and andesite to 25 kilobars pressure: Geophysical significance and implications for charge transport and melt structure. *J. Geophys. Res.*, (In press).

Waff, H.S. (1975). Pressure induced coordination changes in magmatic liquids. *Geophys. Res. Lett.* **2**, 193-196.

Watson, E. B. (1979). Calcium diffusion in a simple silicate melt to 30 kbar. *Geochim. Cosmochim. Acta* **43**, 313-322.

Watson, E. B. (1981). Diffusion in magmas at depth in the earth: the effects of pressure and dissolved H_2O. *Earth Planet. Sci. Lett.* **53**, 291-301.

Watson, E. B. and Bender, J.F. (1980). Diffusion of Cesium, Samarium, Strontium, and Chlorine in molten silicate at high temperatures and pressures. *Geol. Soc. Am. Abstracts with Programs* **12** , p545.

Watson, E. B.; Sneeringer, M.; and Ross, A. (1982). Diffusion of dissolved carbonate in magmas: Experimental results and applications. *Earth Planet. Sci. Lett.*, (In press).

Weill, D.F.; Hon, R.M.; and Navrotsky, A. (1980). The igneous system $CaMgSi_2O_6$-$CaAl_2Si_2O_8$-$NaAlSi_3O_8$: Variations on a classic theme by Bowen. In: *Physics of Magmatic Processes* (ed. R. Hargraves), Princeton Press, Princeton, NJ.

Wendlandt, R.F. (1980). Oxygen diffusion in basalt and andesite melts. *Trans. Am. Geophys. Union* **EOS 61**, p1142.

Whittaker, E.J.W. and Muntus, R. (1970). Ionic radii for use in geochemistry. *Geochim. Cosmochim. Acta* **34**,945-957.

Wilson, A.D. (1960). The microdetermination of ferrous iron in silicate minerals by a volumetric and colorimetric method. *Analyst* **85**, 823-827.

Winchell, P. (1969). The compensation law for diffusion in silicates. *High Temperature Science 1*, 200-215.

Winchell, P. and Norman, J.H. (1969). A study of the diffusion of radioactive nuclides in molten silicates at high temperatures, in *High Temperature Technology*, Third International Symposium Asilomar 1967, 479-492.

Wing, R. and Callahan, P. (1969). The characterization of

metal-oxygen bridge systems. *Inorg. Chem.* 8,871-874.

Worrell, C.A. and Henshall, T. (1978). Vibrational spectroscopic studies of some lead silicate glasses. *J. Non-Cryst. Solids* 29, 283-299.

Yinnon, H. and Cooper, A.R. (1980). Oxygen diffusion in multicomponent glass forming silicates. *Phys. Chem. Glasses* 21, 204-211.